2006

Ignition by air injection (CIBAI) for controlled auto-ignition in a CFR engine

Fernando Echavarria
West Virginia University

Ignition by Air Injection (CIBAI) for Controlled Auto-Ignition in a CFR Engine

Fernando Echavarria

Dissertation submitted to the College of Engineering and Mineral Resources
at West Virginia University
in partial fulfillment of the requirements
for the degree of

Doctor of Philosophy
in
Mechanical Engineering

John Loth, Ph.D., Chair
Gary Morris, Ph.D.
Nigel Clark, Ph.D.
John Zondlo, Ph.D.
Scott Wayne, Ph.D.

Department of Mechanical and Aerospace Engineering

Morgantown, WV
2006

Keywords: Compression by Air Injection, Combustion, Controlled Auto-Ignition, Pre-Ignition, Compression Ignition, Homogeneous Charge Compression Ignition

Abstract

Ignition by Air Injection (CIBAI) for Controlled Auto-Ignition in a CFR Engine

Fernando Echavarria

Compression ignition by air injection (CIBAI) has been successfully achieved in a modified single cylinder, four-stroke, spark ignition cooperative fuel research (CFR) engine. The CIBAI cycle was invented by Professor John Loth and Professor Gary Morris, US patent No's: 6,994,057 Feb. 7, 2006 and 6,899,061 May 31, 2005. This new revolutionary combustion concept has the potential to become an alternative to traditional (SI) spark ignited and compression ignited (CI) diesel engines.

A CIBAI engine consists of two or more even numbers of adjacent cylinders that work in synchronization. One cylinder normally contains a conventional air-fuel mixture at a compression ratio limited by fuel auto-ignition properties while the second cylinder contains air-only at high compression ratio. Only during the compression stroke are these cylinders separated with a closed cylinder-connecting valve (CCV). The CCV valve normally opens near the top dead center (TDC) to allow transfer of high-pressure air from the air-only cylinder into the air-fuel mixture cylinder. Mixing air with pre-evaporated fuel with hot high-pressure air causes rapid two-step pressure rise, first by air addition and second by combustion compression. Ignition by air injection provides high ignition energy allowing very lean mixtures to be ignited for low emissions. Expanding combustion gases in both cylinders results in increased expansion ratio and thus thermal efficiency.

The objective of this dissertation was to demonstrate experimentally the viability of achieving ignition by air injection (CIBAI) for controlled auto-ignition in a CFR engine. This experimental work involved the development of an air injection model, and the design, assembly, and testing of a highly specialized air injection and timing equipment. These experiments were designed to substitute CIBAI ignition for one cycle in a spark ignition engine. The CIBAI engine cycle analysis is included, followed by an analytical model of the air injection process. A controller for the air injection and timing system had been designed, built and tested under different operating conditions until a satisfactory experimental procedure was developed for testing using the CIBAI concept. Based on the measured pressure-time history a numerical modeling code was developed to analyze power and combustion parameters (indicated net work, indicated mean effective pressure (IMEP), net heat release, net heat release rate, mass fraction burned (MFB), temperature history, combustion duration, and ignition delay). Finally, a parametric study was conducted to determine the effect of compression ratio, intake temperature, air-fuel ratio, air preheated charging pressure, and air-injection timing on CIBAI combustion.

Experimental and numerical model results indicated that ignition is readily achieved by air injection (CIBAI) in a CFR engine using the proper air injection system and proper air injection timing strategy.

Dedication

To my lovely wife—for her love, patience, support, and encouragement during this long journey.

Acknowledgments

I would like to express my sincere gratitude to my research advisor, Dr. Loth, for his teaching, guidance, and support during this research. He has not been only my mentor, teacher, and advisor, but also a person who has taught me to approach engineering from a different perspective.

I would also like to thank Dr. Gary Morris, a member of my committee, for introducing me to the world of microcontrollers and for his valuable contribution to this research. I would like also to thank the remaining members of my committee, Dr. Nigel Clark, Dr. Scott Wayne, and Dr. John Zondlo, with their expertise in engine research, for giving me suggestions, and their interest in this project.

I would like to thank Dr. Jacky Prucz and Dr. Ever Barbero for their support and timely advices during my graduate program, and for allowing me to teach at West Virginia University (WVU). It was a great experience.

My sincere appreciation to all my professors who encouraged me to pursue higher education. I would like to thank Dr. Gorli Harish, Director and Founder of Mahantech Corporation, for his financial support during these three years of graduate school at WVU.

I would like to thank Pat Browning for helping me with the experimental set-up and data acquisition unit. I would also like to thank Mr. Cliff Judy and Mr. Chuck Coleman for their support in the MAE shop, and Mrs. Debbie Willis for her timely information regarding matters related to the MAE department.

Finally, I would like to thank all of my officemates, especially Alejandro Posada and Julio Noriega, for helping me with some of my courses. Thanks to all of you.

Table of Contents

List of Figures

List of Tables

Nomenclature and Symbols

A^*	=	Effective choked flow area
A_e	=	Orifice area
AKI	=	Anti-knock index
A_o	=	Orifice cross-sectional area
A_p	=	Area piston
AR	=	Activated radical
ATAC	=	Active thermo-atmosphere combustion
aTDC	=	After top dead center
ASTM	=	American society for testing and materials
b	=	Cylinder bore diameter
BDC	=	Bottom dead center
BSFC		Brake specific fuel consumption
bTDC	=	Before top dead center
CAI	=	Controlled auto-ignition
CAS	=	Crank angle sensor
cc	=	Cubic centimeter
CCV	=	Cylinder-connecting valve
CFR	=	Cooperative fuel research
CI	=	Compression ignition
CIBAI	=	Compression ignition by air injection
CIHC	=	Compression ignited homogeneous charge
CN	=	Cetane number
CO	=	Carbon monoxide
C.R	=	Compression ratio
DAQ	=	Data Acquisition
DME	=	Dimethyl-ether
EGR	=	Exhaust gas recirculation
E.R	=	Equivalence Ratio
EVC	=	Exhaust valve closing

f	=	Actual fuel-air ratio
F	=	Fuel-air ratio
FD-LI	=	Photon detonation laser ignition
FFT	=	Fast Fourier Transform
F.L	=	Fuel level
FS	=	Fuel sensitivity
f_s	=	Stoichiometric fuel-air ratio
g_c	=	Conversion factor
GDI	=	Gasoline direct injection
h	=	Specific enthalpy (absolute)
H_2	=	Hydrogen
HC	=	Hydrocarbon
HCCI	=	Homogeneous charge compression ignition
IAPAC	=	Injection assistee par air comprime (French)
IC	=	Internal combustion
ICADE	=	Isolated combustion and diluted expansion
ID	=	Ignition delay
IMEP	=	Indicated mean effective pressure
IVO	=	Intake valve opening
J	=	Joule
l	=	Connecting rod length
M	=	Total mass
MAE	=	Mechanical and Aerospace Engineering
M_a	=	Mass of air
M_f	=	Mass of fuel
MFB	=	Mass fraction burned
MIE	=	Minimum ignition energy
M_i	=	Cylinder mass before injection
MON	=	Motor octane number
n	=	Revolutions per engine cycle (rev/cycle)
N	=	Engine speed

NC	=	Normal closed contact
NETL	=	National Energy Technology Laboratory
NG	=	Natural gas
NO	=	Normal open contact
NO_x	=	Oxides of nitrogen
NPT	=	National pipe thread
ON	=	Octane number
P	=	Pressure (absolute)
P_1	=	Initial Pressure
P_a	=	Air cylinder pressure
P_{af}	=	Air-fuel cylinder pressure
PCCI	=	Premixed charge compression ignition
PM	=	Particular matter
P_{prod}	=	Products pressure
PRF	=	Primary reference fuels
PT	=	Pressure transducer
q	=	Specific heat transfer
Q	=	Heat transfer
r	=	Crank radius
R	=	Gas constant
r_c	=	Combustion induced temperature ratio
r_m	=	Air-fuel mixture mass ratio
RON	=	Research octane number
r_p	=	Instantaneous pressure ratio
$r_{pcritical}$	=	Critical pressure
RPM	=	Revolutions per minute
r_{va}	=	Air compression ratio
r_{vaf}	=	Fuel-air compression ratio
t	=	Time
T	=	Temperature (absolute)
T_1	=	Initial Temperature

T_a	=	Air cylinder temperature
T_{af}	=	Air-fuel cylinder temperature
TDC	=	Top dead center
T_{prod}	=	Products temperature
s	=	Stroke
SC	=	Solenoid close
SCFM	=	Standard cubic feet per minute
SI	=	Spark ignition
SO	=	Solenoid opening time
u	=	Specific internal energy (absolute)
U	=	Total internal energy (absolute)
UAV	=	Unmanned aerial vehicles
V	=	Total volume
V_a	=	Air cylinder volume
V_{af}	=	Air-fuel cylinder volume
V_c	=	Clearance volume
V_d	=	Displacement volume
V_{dact}	=	Actual displacement volume
VCT	=	Variable camshaft timing
V_{heater}	=	Volume heater
V_n	=	Laminar burning velocity
VVT	=	Variable valve timing
V_s	=	Flame speed
X_{stroke}	=	Distance traveled by the piston (at θ) measured from TDC ($\theta = 0$)
W	=	Work
WVU	=	West Virginia University
β	=	Cut-off ratio
γ	=	Specific heat ratio
η_{Cibai}	=	CIBAI thermal efficiency
η_{Diesel}	=	Diesel thermal efficiency

η_{Otto}	=	Otto thermal efficiency
η_v	=	Volumetric efficiency
θ	=	Engine crank angle (radians measured from TDC)
Φ	=	Equivalence ratio
3D	=	Three dimensions
ΔU	=	Change in internal energy
ΔH	=	Change in internal enthalpy
Δt	=	Injection duration
^{o} CA	=	Crank angle degree
^{o} CA bTDC	=	Crank angle degree before top dead center
dm/dt	=	Rate of air injection
°F	=	Degree Fahrenheit
°R	=	Degree Rankine

Chapter 1: Introduction

Intensive research to increase engine fuel efficiency and reduce emissions is driven by the increase in worldwide oil demand and stringent emissions control regulations. As a result, a wide range of internal combustion (IC) engine cycle modifications have being developed and implemented to achieve complete combustion of lean fuel-air mixtures for low NO_X, while maximizing combustion compression for high thermal efficiency.

This research effort has resulted in the application of new emission control techniques (i.e. exhaust gas recirculation (EGR), variable valve timing, and NO_x dilution), the use of new alternative fuels in internal combustion engines (i.e. natural gas (NG), alcohols, and hydrogen), the design of new power train configurations (i.e. fuel cells technology and hybrid vehicles), and the use of new ignition and combustion strategies (i.e. compression ignition by air injection (CIBAI), gasoline direct injection (GDI), photon detonation laser ignition (FD-LI), controlled auto-ignition (CAI), homogeneous charge compression ignition (HCCI), and stratified charge engines).

Internal combustion engines (IC) are primarily classified into spark ignition (SI) and combustion ignition (CI) engines. SI engines start the combustion process by using a high-voltage electrical discharge from a spark plug in each combustion cycle. CI engines start the combustion process when the fuel-air mixture self-ignites due to high temperature in the combustion chamber, caused by high compression. SI engines have higher power density, but are less efficient at part load because of losses associated with throttling [1]. CI engines avoid throttling and thus are more efficient at part load;

however CI engines usually produce high particulate matter and oxides of nitrogen (NO_x) emissions under high load.

Modern SI and CI engines have reached significant improvements in emissions reduction, and performance. However, their indicated thermal efficiencies are still in the range of 40% to 50% [2]. The thermal efficiency of spark ignition (SI) engines is limited by compression ratio, fuel octane number (ON), and knock, while the thermal efficiency of compression ignition (CI) engines is limited by fuel cetane number (CN), and exhaust emissions. In addition, an important factor limiting the thermal efficiency is the low flame speed associated with combustion, initiated by a spark or by a spray of diesel fuel [3].

In recent years controlled auto-ignition (CAI) has been extensively studied as an alternative to traditional spark ignition (SI) and compression ignition (CI) engines [4]. Controlled auto-ignition (CAI) is defined in the literature as a combustion process, which involves the auto-ignition and simultaneous combustion of a homogeneous air-fuel mixture. This ignition system allows burning very lean mixtures for more efficient operation at reduced power levels. Some additional benefits of CAI ignition over SI and CI ignition are: lower NO_x emissions at part load, leaner mixture operation, reduced cycle-to-cycle variation, and lower soot emissions. However, its application in a production engine has been limited due to high peak pressures, high HC and CO emissions, the difficulty in timing of the auto-ignition, and heat release rate over the entire engine operational range.

Loth and Morris [3,5] patented a new thermodynamic cycle for piston type internal combustion (IC) engines called “Compression Ignition by Air Injection

(CIBAI)." The CIBAI cycle offers an IC engine capable of an increased thermal efficiency, operating over a wide range of fuels, rapid ignition of very lean fuel-air mixtures, and reduced NO_x. The researchers indicated that CIBAI cycle could be more efficient than the Otto or Diesel cycle, and simpler, since it does not require high maintenance items like spark plug ignition systems, or high pressure diesel type fuel pump and fuel injectors.

Recently, researchers at the National Energy Technology Lab (NETL) reported obtaining laser-spark ignition of an ultra lean mixture using a Ricardo Proteous, single-cylinder, four-stroke, spark-ignited natural gas engine [6]. CIBAI and laser-spark ignition offer an alternative to traditional spark and compression ignited engines with their above-average ignition energy achieving faster combustion of lean fuel-air mixtures for low NO_x, while maximizing combustion compression for high thermal efficiency.

The objective of this dissertation was to demonstrate experimentally the viability of achieving ignition by air injection (CIBAI) for controlled auto-ignition using a CFR engine. This experimental work mainly involved the development of an air injection model, the construction of specialized air injection and timing equipment, the collection of experimental data, the implementation of a numerical modeling program code, and the execution of a parametric study to determine the effect of operating parameters on CIBAI combustion. The specific tasks accomplished during this dissertation are presented next.

Chapter 2: Objectives

The objective of this dissertation was to demonstrate experimentally the viability of achieving ignition by air injection (CIBAI) for controlled auto-ignition in a CFR engine. This concept was originally proposed by Professor Loth and Professor Gary Morris [3,5] and is based on theoretical concepts related to combustion, auto-ignition, and chemical kinetics. This objective was accomplished through the following tasks:

- A literature review was conducted to determine the combustion characteristics and engine operating parameters for controlled auto-ignition (CAI).
- Existing auto-ignition modeling techniques were reviewed.
- A simple, yet reliable, numerical model was developed and implemented to theoretically predict the influence of air injection, design parameters and operation variables in the compression ignition by air-injection (CIBAI) combustion.
- Multiple air-injection systems were designed, assembled, and tested to determine the optimal air-injection strategy.
- A microcontroller was designed, assembled, and tested to control the air-injection timing and operate the CFR engine safely during the air injection. Specialized control systems were needed to assure that the air injection occurred at the desired crank angle and the desired amount of air was injected all at once without additional air transfer after ignition occurred.
- Several cylinder-connecting valves (CCV) were designed, built, and tested to simulate the CIBAI combustion process using the CFR engine.

- A suitable data acquisition system was assembled to be able to compare the CFR engine performance with spark ignition and with air-injection ignition.
- Multiple tests were carried out and recorded for different engine operating conditions while the CFR was motored, fired, and operated under the CIBAI cycle to determine experimentally the optimal operating conditions for CIBAI combustion.
- Experimental CIBAI combustion testing was performed to collect the empirical input data necessary to complete the numerical, parametric study, and to evaluate the effects of operating parameters on CIBAI combustion.
- A parametric study was conducted to study the effect of compression ratio, intake temperature, air-charged pressure, air-fuel ratio, and air-injection timing on CIBAI combustion.
- A computer code (Appendix A) was developed and integrated within a graphical user interface (GUI) to analyze the CIBAI cycle, implement the numerical model, and perform the parametric study.
- Model results were compared with experimental data to validate the ability of the numerical model to predict the effect of operating parameters on CIBAI combustion.
- Air-injection design recommendations, and conclusions were provided based on the results obtained through CIBAI experimentation and modeling.

Chapter 3: Literature Review

Auto-Ignition

In SI engines auto-ignition is defined as the ignition of the air-fuel mixture during the compression stroke before the spark plug fires. Auto-ignition increases the combustion chamber temperature and under certain conditions leads to a knock or detonation reducing the power output and efficiency. The knock appears as a spontaneous and excessive pressure rise rate within the cylinder chamber. It has been found to be related to octane number, degree of mixing, and compression ratio. Fuels with low octane number have more propensity to the knock. SI Engines operating with high compression ratios need to use high octane number fuel to prevent the knock.

The mechanisms of auto-ignition and subsequent knock phenomena have been the subject of intensive research since the beginning of the automotive industry. Studies in the auto-ignition of hydrocarbons are normally done using constant-volume bombs, rapid compression machines, shock tubes, and cooperative fuel research CFR engines. Ricardo [7] and Erren and Campbell [8] indicated the importance of detecting and eliminating abnormal combustion phenomenon for a smooth operation of an IC engine. Experiments carried out by King [9], and King and Rand [10] indicated that “hot spots,” such as spark plugs, exhaust valves, and the formation of deposits in the combustion chamber as the result of pyrolysis of lubricating oil could cause auto-ignition.

Obert [11] stated that the factors controlling auto-ignition or spontaneous chemical reaction are: temperature, pressure, ignition delay (ID), air-fuel ratio, the presence of inert gases, and in some cases turbulence. He used the auto-ignition model illustrated in Figure 3.1 to explain the correlation among those factors. Line AB’C

represents a homogeneous air-fuel mixture with a particular condition of pressure, temperature, and air-fuel ratio. This mixture has been rapidly compressed at a certain compression ratio and held at high pressure and temperature, but has not been able to self-ignite; it rather cooled down after a short period of time. Lines AB"C'D' and AB"'C"D" represent the same mixture, but compressed at a higher compression ratio. This mixture is held at higher pressure and above its self-ignition temperature, reaching self-ignition after a short induction time (ignition delay). The ignition delay is shown to be shorter for mixtures compressed at higher temperature.

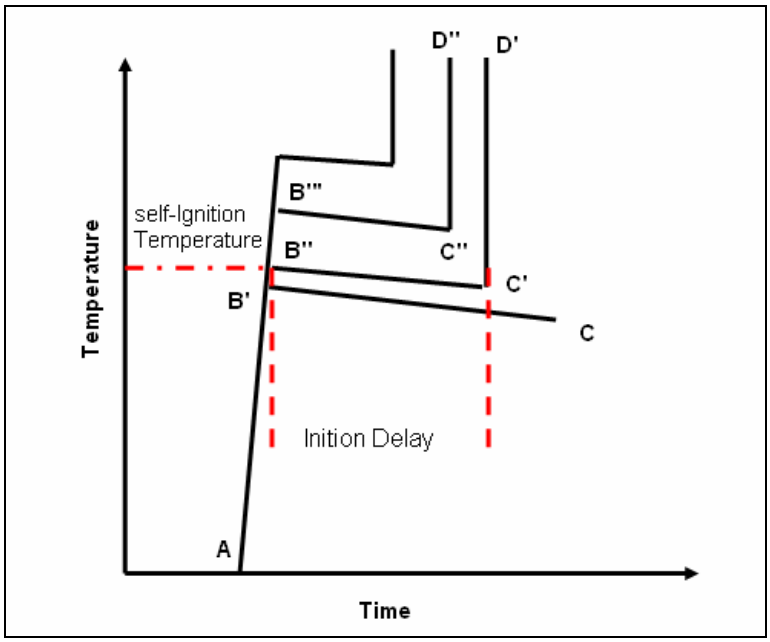

Figure 3.1 Ignition delay and the self-ignition temperature [11]

Miller [12], and Haskell and Bame [13] have proposed a detonation wave as a mechanism for auto-ignition. This shock wave is assumed to travel through the combustion chamber at supersonic velocity, compressing the unburned mixture at pressures and temperatures where auto-ignition occurs almost instantaneously [11].

Controlled Auto-Ignition (CAI)

Overview

Controlled auto-ignition (CAI) is defined in the literature as a combustion process which involves the auto-ignition and simultaneous combustion of a homogeneous air-fuel mixture [4]. This chemical kinetics process is characterized by the absence of flame propagation, the near simultaneous oxidation of the entire cylinder charge, rapid heat release rates, small cyclic pressure variations, and very low NO_x emissions [14]. CAI combustion combines features of both SI and CI combustion since the fuel is exposed to conditions of compression heating suitable for auto-ignition, yet the air-fuel mixture is homogeneous.

In recent years, CAI combustion has emerged as an alternative to SI and CI combustion due to the decrease in exhaust emissions and improvement in fuel economy. CAI produces extremely low NO_x emissions and almost zero PM emissions due to the absence of high temperature regions and nonexistence of localized fuel-rich regions [15]. Its fuel economy can approach the level of conventional diesel engines due to the fast burning rate, lean combustion, absence of throttling, and the removal of knock tendency [14].

However, its application in a production engine has been limited due to high-peak pressures, high HC and CO emissions, and the difficulty in timing of the auto-ignition and heat release rate over the entire engine operational range [16].

Researchers have given different names to controlled auto-ignition (CAI), including: active thermo-atmosphere combustion (ATAC) [14], activated radical (AR) combustion [17], injection assistee par air comprime (IAPAC) [18], homogeneous charge

compression ignition (HCCI) [19], compression-ignited homogeneous charge (CIHC) combustion [20], premixed charge compression ignition (PCCI) [21], and compression by air injection (CIBAI) [3,5]. The most relevant of those CAI combustion processes are described next.

Earlier Research

One of the first reported works in CAI is attributed to Onishi et al. [14]. They developed a new technique, called "Active Thermo-Atmosphere Combustion (ATAC)." They studied lean combustion of two-stroke spark-ignition engines and found that abnormal combustion and auto-ignition could be used effectively to control combustion of lean mixtures without a need of an initial ignition source such as an electrical spark. ATAC combustion ignites a homogeneous air-fuel mixture by controlled auto-ignition relatively early in the compression stroke (30^o CA bTDC - 70^o CA bTDC), as compared to conventional two-stroke engines (20^o CA bTDC - 45^o CA bTDC). They reported significant reduction of NO_x emissions, stable combustion using lean mixtures at part-throttle operation, smooth combustion with a little cycle-to-cycle variation, and improvement in thermal efficiency. Onishi et al. [14] stated that the conditions to achieve stable auto-ignition include uniform air-fuel mixture from cycle to cycle, high-combustion chamber temperature, and the proper ratio of a new mixture to residual gases.

Najt and Foster [20] from the University of Wisconsin-Madison conducted extensive research in a CAI technique, termed "Compression Ignited Homogeneous Charge (CIHC)." The objective of this research was to evaluate the impact of changes in the operating parameters in the ignition and energy-release processes. The experiments were conducted using a single-cylinder four-stroke cycle Waukesha CFR engine with a

pressurized fuel intake and exhaust systems. These systems allowed control of the intake temperature and the mixing of fresh air and exhaust products. Their experimental results indicated high-compression-ratios advanced ignition and drastically increased energy-release rates. Satisfactory ignition and a smooth energy release were obtained with a compression ratio of 7.5:1. They also observed that variations in the air-fuel ratio from the fuel-lean limit to stoichiometric advanced the point of ignition and produced a rapid increase in the energy-release rate. Suitable ignition and smooth-combustion operation were obtained with an air-fuel ratio of 0.8. On the other hand, they stated that increase in the engine speed reduces the time available for the low-temperature (below 1200 ^{o}F) oxidation kinetics which lead to spontaneous ignition to occur, and thus ignition becomes delayed or unattainable. Exhaust-gas recirculation (EGR) was used to increase the temperature of the intake mixture, but it was found that the chemical species in the exhaust gas did not have any significant role in the ignition process. This is due to the increase in the mass of inert gases in the combustion chamber and the subsequent decrease in the combustion temperature. Finally, the authors concluded that variations in the type of the fuel used modifies the CIHC combustion process by changing the low-temperature (below 1200 ^{o}F) oxidation kinetics, but it did not affect the high-temperature (above 1300 ^{o}F) heat-release process since similar CO and H_2 oxidation reactions prevail for all fuel types.

Fundamentals of CAI Combustion

Controlled auto-ignition (CAI) combustion is considered a pure, chemical-kinetics process marked by a homogeneous oxidation of an air-fuel mixture and gas, residual products. This statement has been supported by earlier research conducted by

Onishi et al. [14], Najt and Foster [20], Haskell [22], and Noguchi et al. [23]. Flow visualization techniques such as Schlieren photographs used on some of those experiments have not shown any evidence of passing flame fronts, hot-spot ignition sources or particle-induced ignition.

Most of the literature on chemical kinetics agreed to classify the reaction route for alkene fuels into three distinct chain-branching regimes: low (<900 ^{o}F), intermediate (1000-1200 ^{o}F), and high (>1300 ^{o}F). For the low regime, the leading fuel reactions are chain-propagating steps, pertaining to oxygen molecules and producing a series of complex partial oxidized species [24]. For the intermediate regime, the main fuel reactions are still chain-propagating steps, pertaining to oxygen molecules, but producing conjugate alkenes and HO_2 radicals [25]. For the high regime, the principal fuel reactions included thermal decomposition by C-C bond-breakage, forming alkenes and smaller radicals [26].

Similarly, Najt and Foster [20] indicated that CAI combustion is controlled by two distinct kinetics mechanisms: a low-temperature (below 1200 ^{o}F) kinetics mechanism, which controls the first stage of ignition, and a high-temperature (above 1300 ^{o}F) mechanism, which controls the start of the main ignition and the energy-release process. Their findings have been supported by numerous experimental studies including the work of Westbrook [27,28], and Halstead and Kirsch Kelly [29].

This research focuses on producing an overall understanding of the basic mechanisms involved in compression ignition by air injection (CIBAI) in a CFR engine and does not concentrate on providing a detailed evaluation of the specific chemical species and reactions involved.

Modeling CAI Combustion

Until recently, the majority of the studies on CAI combustion have been limited to experimental work due to the complexity of the chemical reactions. However, with the advent of high-speed computers and with a better understanding of the hydrocarbon chemistry, new theoretical formulations have been presented to describe the CAI combustion. CAI combustion models are mainly divided into single-zone models and multi-zone models.

Single-zone models have been used by Fiveland and Assanis [30] to simulate a four-stroke natural gas HCCI engine, Goldsborough and Van Blarigan [31] to model a hydrogen HCCI engine, Xu et al. [32] to study the characteristics of HCCI combustion in a four-stroke automotive engine, and by Dec [33] to investigate combustion emission in a HCCI engine. These models can predict ignition timing, heat release rates, and exhaust emissions.

In a multi-zone model the combustion chamber is divided into a specific number of zones that have particular mixture composition and initial pressure and temperature prescribed. Multi-zone models have been used by Najt and Foster [20] to evaluate the response of a CIHC engine to changes in operating parameters, Aceves et al. [34] to predict HCCI combustion and emissions, and by Easley et al. [35] to explore the effects of temperature stratification, heat loss and crevice volume on the HCCI combustion process and exhaust emissions.

Recent Research in CAI Combustion

During the last decade research in CAI Combustion has moved from research institutes and universities to the automotive industry. This new research effort has been

focused on achieving stable CAI combustion and controllable heat-release rate over the entire engine operational range. This research has been primarily conducted in two areas: variations in the thermo-chemical properties of the mixture and changes in the engine operation parameters.

The first area of research includes modification of the reactivity of the air-fuel mixture by altering its thermo-chemical properties. To this aim, several techniques have been used. These include changes in the intake temperature, variation of the air-fuel mixture, exhaust gas recirculation (EGR), and the use of additives and fuel modifications. Aceves et al. [34], Griffiths et al. [36], and Curran et al. [37] have indicated that higher intake temperature increases the heat release rate, advances the start of the first stage of ignition, and reduces the ignition delay.

Christensen et al. [38] studied the characteristics of CAI combustion using isooctane, ethanol, and natural gas (NG), and compared their results with SI operation. Experiments were carried out using a 1.6 liter single cylinder engine with a fixed compression ratio of 21:1 in CAI operation and 12:1 in SI operation. Stable CAI combustion was achieved for all three fuels with the same compression ratio. CAI combustion was obtained for isooctane ran unthrottled without heating. The intake temperatures of 170 ^{o}F and 250 ^{o}F were required to achieve CAI combustion for Ethanol and natural gas (NG) respectively.

Ishibashi [39], Christensen et al. [40,41], and Flowers et al. [42] have demonstrated the influence of the mixture composition in the CAI timing. They reported that rich mixtures tend to increase the ignition delay while lean mixtures tend to decrease

the ignition delay. This may be explained by the changes in the specific heat ratios (γ) that directly affect the quantity of disposable compression heating in the charge [4].

Law and Allen [43] and Law et al. [44] investigated the effects of exhaust gas recirculation (EGR) and/or trapped residuals in CAI combustion. They developed and implemented a two-exhaust valve control strategy in a single cylinder four-stroke engine. Their objective was to separate the thermal and chemical effect of EGR by injecting nitrogen and oxygen as a substitution. Nitrogen was heated to the same temperature of the exhaust residual gas and injected in the intake manifold. They found that nitrogen, due to its chemical inert nature, has the ability to delay combustion and smooth the heat-release rate. Oxygen injection was found to have a direct effect on the start of the ignition for intake temperatures greater than 250 ^{o}F and produce unmanageably high pressures similar to the knock phenomena. This was attributed to the oxygen's chemical nature.

Fuel modifications and additives have been used to accelerate or reduce the start of the ignition and control the heat-release rate. Flowers et al. [42] added dimethyl-ether (DME) while conducting experiments with a CFR engine running with methane fuel. They improved CAI combustion and heat-release rate by adding 15% DME (by volume). Ryan III et al. [45], and Jeuland et al. [46] carried out experiments to determine the fuel requirements for CAI combustion. They concluded that the fuel formulation plays a very important role in determining the operation range of CAI combustion and engine efficiency.

Water injection, a dilution technique normally used in hydrogen IC engines to reduce backfire and pre-ignition problems, was used by Christensen et al. [47] to affect

the start of the ignition and heat release rate. They observed an increase in the ignition delay, a reduction of the heat-release rate, and an increase in HC and CO emissions.

The second area of research includes changes in the engine-operation parameters. The objective of this approach is to control auto-ignition (CAI) and obtain smooth heat-release rate by affecting the time-temperature history of the mixture, for several engine-operation conditions. Changes in compression ratio, engine speed, variable valve timing (VVT), and supercharging have been extensively studied.

The effect of compression ratio on CAI combustion has been widely discussed in the literature. A higher compression ratio increases the thermal efficiency, and the temperature of the air-fuel mixture, and thus advances the start of the ignition [3,5,40,41,45,48,49,50]. Najt and Foster [20] earlier indicated that the engine speed did not affect the CAI combustion.

Variable valve timing (VVT) technique has been implemented by Law and Allen [43] and Law et al. [44]. They designed a special engine with a digitally-controlled, electro-hydraulic variable train system, which allowed changes in the valves opening profiles. Researchers indicated that this new technology has the potential for controlling CAI combustion and reducing NO_x emissions.

Kontarakis et al. [51] demonstrated the HCCI concept using a single cylinder four-stroke SI engine with modified valve timing. They obtained stable CAI combustion for a compression ratio of 10.3:1 by applying a late inlet opening, early exhaust valve, closing valve-timing strategy.

Ogura et al. [52] used an intake and exhaust continuous variable valve timing mechanism in a premixed gasoline engine to control HCCI combustion. They concluded

that it is possible to control the temperature in the cylinder during ignition timing by controlling early exhaust valve closing timing.

Supercharging has been used as a technique to increase the indicated mean effective pressure (IMEP) by increasing the mixture intake pressure. Christensen et al. [40,41] experimented with different compression ratios and boost pressures. They reported an increase in the IMEP and a broader CAI combustion operation range.

Yap et al. [53] used hydrogen addition on a natural gas HCCI combustion engine to lower the minimum intake temperature required for auto-ignition of natural gas. Authors reported a significant reduction on the intake temperature at part load due to hydrogen's lower auto-ignition temperature and minimum ignition energy (MIE), and wider flammability limits (4-75% by volume).

Recently, a number of studies have been done on controlled auto-ignition (CAI) combustion of gasoline engines. Oakley et al. [54] experimented with a four-stroke gasoline engine operating at 900 rpm with a compression ratio of 11.5:1 and using unleaded gasoline with an anti knock index (AKI) of 90. They obtained stable CAI combustion for an intake temperature of 600 ^{o}F, and air-fuel ratio in excess of 80:1 with a maximum EGR rate of 60%. They obtained very low NO_x emissions at full load, and very high levels of HC and CO emissions at part load.

Zhao et al. [55] obtained stable CAI combustion at part load without intake charge heating or increasing compression ratio in a production 1.7 Liter Zetec SE 16 valve four-stroke, four-cylinder port fuel injection gasoline engine, with a compression ratio of 10.3:1. They used a mechanical variable camshaft timing (VCT) system as presented by Lavy et al. [15]. They increased the amount of the residue through the extended valve

overlap by a combination of the early intake valve opening (IVO) and the retarded exhaust valve closing (EVC). They reported a reduction of almost 99% in NO_x emissions and a significant improvement in brake specific fuel consumption (BSFC) and CO emissions.

Hiraya et al. [56] conducted studies on a gasoline-fueled, compression-ignition, single-cylinder engine under various compression ratios, intake temperatures, and intake-gas compositions. They found a strong correlation between the timing for the onset of HCCI combustion and the intake-air temperature, and between the combustion duration and the air-fuel mixture composition. For compression ratio of 15:1 and an engine speed of 1200 rpm, researchers obtained stable and moderate CAI combustion for air-fuel ratios between 40:1 to 80:1(by volume) and intake temperature between 350 and 550 ^{o}F.

Yamaoka et al. [57] studied the influence of fuel injection timing on the stability of CAI combustion. Researchers experimented with a four-stroke, four-cylinder gasoline engine with a compression ratio of 12:1 and an intake temperature of 90 ^{o}F. The engine was equipped with a controller and an electric variable valve actuator to control the valve events and timing, and with an in-cylinder direction system. They observed reduced torque variance that occurred due to combustion instability, and significant reduction of NO_x and HC emissions.

CAI combustion has been demonstrated to achieve stable heat release rate and reduced NO_x emissions at part load. However, the main challenge remains to obtain stable combustion and a smooth heat-release rate at full load. Olsson et al. [58] proposed the use of turbo-charging or a mechanically-driven compressor to force more mass into an HCCI engine to recover some of the power loss due to EGR dilution. Experiments

were conducted using a modified six-cylinder, turbo-charged diesel engine. The fuel selected for this study was a combination of heptane and ethanol because of the high octane number of the ethanol. After multiple boosting strategies, authors concluded that it is not possible to boost a HCCI engine to the maximum load of a present-day diesel engine.

Zhao et al. [55] proposed to adopt a hybrid engine operation of SI and CAI combustion in order to implement CAI technology in a production vehicle. They suggested using CAI combustion at part load to obtain maximum benefit of low NO_x emissions and lean combustion, and using SI combustion at full load to sustain its maximum power and torque output.

Leach et al. [59] carried out experiments intended to control CAI combustion through injection timing in a gasoline direct injection (GDI) engine with an air-assisted injector. These experiments were done using a four-stroke, single-cylinder, Ricardo-research engine, with a compression ratio of 9:1. This engine operated under CAI combustion by residual gas recirculation (EGR). Small quantities of compressed air were injected together with the fuel at approximately 100 psig. Air was injected at exhaust valve closure (EVC), intake valve opening (IVO) and BDC of the intake and compression strokes. Unleaded gasoline with a research octane number (RON) of 95 was used for all tests. The results of this study indicated that a proper air injection strategy has the potential to increase the operability range of CAI combustion, improve the fuel ignitability, advance the ignition timing, and reduce HC and CO emissions.

Chapter 4: Compression Ignition by Air Injection (CIBAI)

Overview

Loth and Morris [3,5] patented a new thermodynamic cycle for piston type internal combustion, which Loth named "Compression Ignition by Air Injection (CIBAI)." The CIBAI cycle offers an IC engine capability to increase thermal efficiency, operate with a wide range of fuels, ignite rapidly very lean, fuel-air mixtures, and reduce NO_x. They indicated that the CIBAI cycle can be more efficient than the Otto or Diesel cycle, and be simpler as it does not require high maintenance items like spark-plug ignition systems, or high-pressure, diesel-type fuel pump and fuel injectors. The CIBAI cycle offers an alternative to spark- and compression-ignited engines, with auto-ignition timing, controlled by a cylinder-connecting valve. When it opens, hot-high-pressure air is injected into the adjacent cylinder, which contains pre-mixed air and fuel.

Earlier Research

In 1993, Loth et al. [60] patented a new IC combustion engine, called "Isolated Combustion and Diluted Expansion (ICADE) piston engine. The ICADE engine is a piston-cylinder assembly, used for the compression of air and expansion of diluted combustion products. The authors indicate that improvement in thermal efficiency and exhaust-pollution reduction can be obtained in the ICADE engine because the piston motion is used as a valve to isolate a small-cylinder volume, in which fuel injection and combustion are induced by auto-ignition.

In the ICADE engine combustion products are injected tangentially into a doughnut-shaped chamber, formed by the piston-cylinder clearance. The vortex produced in this compartment, induced by the combustion pressure, creates rapid mixing and fast

cooling, preventing the NO_x formation reactions, and the generation of vortex kinetic energy reduces the combustion pressure peak acting on the piston surface. Other benefits reported include the rapid burning of lean mixtures, allowing low octane fuel, and the elimination of the engine throttle valve to control engine power output, which otherwise reduces the compression ratio, and thereby thermal efficiency.

CIBAI Concept

Loth and Morris [3, 5] explained the CIBAI cycle concept as follows:

"*The CIBAI cycle requires two or more adjacent cylinders to work in tandem. Typically one of the cylinders contains a conventional fuel-air mixture, except with double the usual fuel-air ratio and uses a conventional compression ratio in accordance to the fuel octane rating. The adjacent cylinder compresses only air, but to a much higher compression ratio, at least double, that in the air-fuel cylinder. At top dead center its compression volume is less than half that of the adjacent air-fuel cylinder. Only during the compression stroke are the two adjacent cylinder volumes separated from one-another by a valve. Near top-dead center, when this valve opens, most of the high-pressure air transfers into the other cylinder, thereby compressing, heating and producing controlled auto-ignition in the leaned fuel-air mixture. This allows complete combustion, even with very lean mixtures, while both pistons are near top dead center. The cylinder-connecting valve (CCV) remains open during the entire power stroke to equalize the pressure in both cylinders. The expansion ratio is then the mean value of the compression ratio in both cylinder pair. Both the high combustion compression by auto-ignition and high expansion ratio is what renders the CIBAI cycle more efficient than*

either the limited compression ratio spark ignition Otto cycle or the low combustion compression of the Diesel cycle with its ignition delay by fuel injection."

A four-stroke configuration of an engine operating on the CIBAI cycle is shown in Figure 4.1. Its only additionally component is a cylinder-connecting valve (CCV), required to first transfer hot, high-pressure air for ignition, and subsequently combustion products in the other direction. Auto-ignition timing is controlled by the opening of the CCV valve.

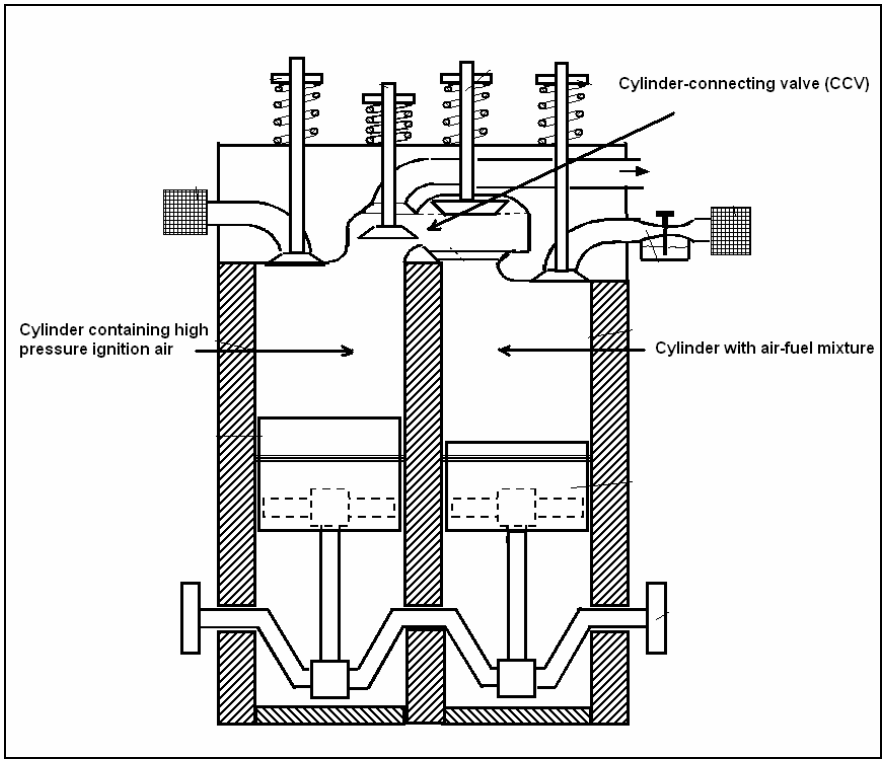

Figure 4.1 Four-stroke engine operating on the CIBAI cycle [3,5]

CIBAI Benefits and Applications

In addition to the high thermal efficiency, and the elimination of the need for a throttle valve, spark ignition, or high-pressure fuel injectors, Loth and Morris [3, 5] indicate that the CIBAI cycle has the potential to decrease NO_X emissions and exhaust

pipe loss due to the overall increase in expansion ratio in both cylinders. They pointed out five additional advantages of the CIBAI cycle:

1. Lower cost and increased reliability by reducing the components.
2. Avoiding the cold starting problem of the diesel engine because in CIBAI fuel-air mixture is fully mixed and pre-evaporated just like in the Otto cycle.
3. Applicable to any size engine, ranging from large ship engines to small engines such that of UAV's and lawn mowers, unlike the diesel engine, which requires a minimum displacement for accurate flow-metering during high-pressure fuel injection.
4. Capable of operating with low emissions in two-stroke engines by having two different cylinders, one only for air and fuel intake, while the other is only used for air intake and combustion product exhaust. This eliminates the possibility for unburned fuel to escape out of the exhaust port.
5. Increased safety is realized in a hydrogen engine as one cylinder compresses only hydrogen while the other only air, and these two gases only get to mix at the desired time of ignition when the CCV valve opens. Thus producing shaft power with hydrogen fuel in a CIBAI cycle is much safer than compressing a hydrogen-air mixture in a spark ignition engine because of its flammability limit (4-75% volume). Also the use of hydrogen is problematic in a fuel injected engine. Its low density increases the time required to inject sufficient fuel and also requires significant power to compress the hydrogen gas for cylinder injection.

In the second (CIBAI) patent Loth and Morris [5] listed the advantages of pre-heating and pressurizing a solid-oxide fuel cell with a CIBAI cycle engine. This allows extracting shaft power both during heating and pressurization, and also by using fuel cell

exhaust gas which still contains up to 20% hydrogen. Figure 4.2 shows a schematic diagram of the use of a CIBAI cycle engine in combination with a high temperature solid-oxide fuel cell to boost the overall conversion efficiency.

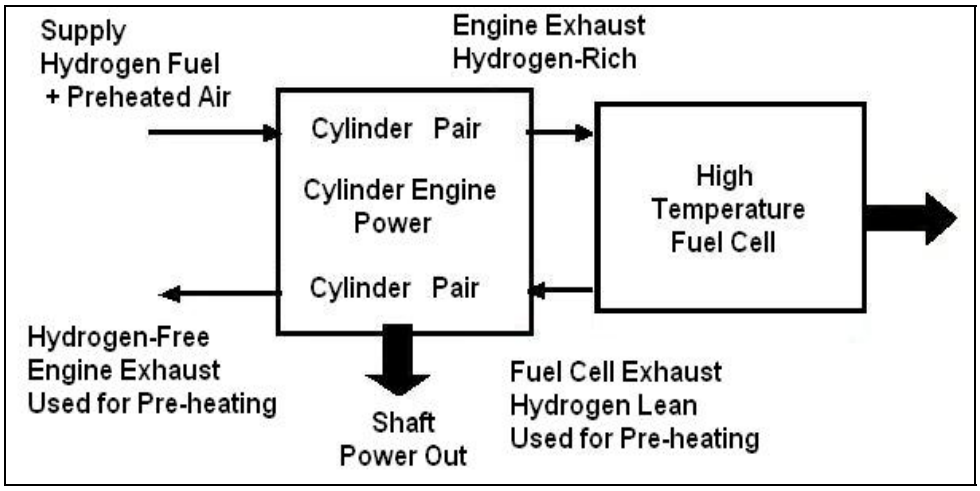

Figure 4.2 CIBAI engine in combination with a fuel cell [3,5]

Thermal Efficiencies Comparison

The cold-air standard thermodynamic theoretical efficiency for the three cycles: Otto, Diesel, and CIBAI cycles are shown for comparison in both the equation and graphical form (Figure 4.3)

Otto Cycle Thermal Efficiency:

$$\eta_{Otto} = 1 - \frac{1}{(C.R)^{\gamma-1}} \qquad (4.1)$$

Diesel Cycle Thermal Efficiency:

$$\eta_{Diesel} = 1 - \frac{1*(\beta^{\gamma}-1)}{(C.R)^{k-1}*\gamma*(\beta-1)} \qquad (4.2)$$

CIBAI Cycle Thermal Efficiency:

$$\eta_{Cibai} = \left[\frac{W_{out}}{Q_{in}} = \frac{r_{vaf}{}^{(\gamma-1)} - 1 + (r_{va}{}^{(\gamma-1)} - 1)*r_m}{(r_{vaf}{}^{(\gamma-1)} + r_{va}{}^{(\gamma-1)}*r_m)*r_c - 1)}\right] \qquad (4.3)$$

Thermal efficiency of the Otto cycle is only function of the compression ratio (C.R). As the compression ratio goes up, the thermal efficiency goes up. Thermal efficiency of the Diesel cycle is the function of the compression ratio (C.R) and cut-off ratio (β). Cut-off ratio is defined as the change in volume that occurs during combustion. Thermal efficiency of the CIBAI cycle is the function of the air compression ratio (r_{va}), fuel air compression ratio (r_{vaf}), air-fuel mixture mass ratio (r_m), and combustion induced temperature ratio (r_c). A complete derivation of the thermal efficiency of the CIBAI cycle is presented in references [3,5]. Theoretically, CIBAI cycle has a higher thermal efficiency than Otto and Diesel cycle due to its second stage compression, prior to auto-ignition (Figure 4.3).

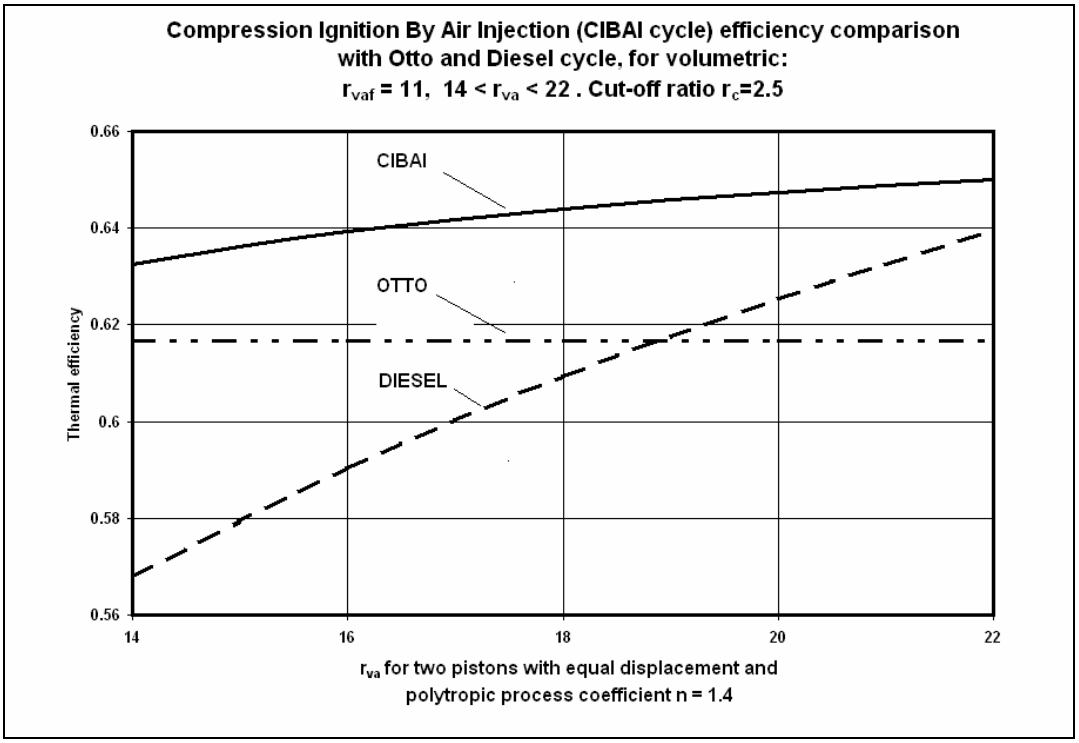

Figure 4.3 CIBAI cycle efficiency comparison with Otto and Diesel cycles [3,5]

Cold Air Standard CIBAI Cycle Analysis

The cold air-standard CIBAI cycle is an ideal cycle, which assumes that heat addition occurs instantaneously at constant volume while both pistons are at TDC. Such a CIBAI cycle is shown on the pressure ratio (P/P_1) and temperature ratio (T/T_1) vs. crank-angle diagrams of Figures 4.4 and 4.5 respectively. The following assumptions were made to evaluate the cold air-standard CIBAI cycle.

- The fuel-air mixture and combustion product properties are the same as air for the entire cycle.
- The combustion process was replaced with a heat addition term Q_{in} of equal energy value.
- Compression strokes and expansion strokes were approximated by isentropic processes (n=1.4).
- The exhaust process was replaced with a closed system heat rejection process Q_{out} of equal energy value.
- The combustion process was idealized by a constant-volume process.
- Air was treated as an ideal gas.

The CIBAI cycle consists of five processes in series. Process 1 is an isentropic compression process of the air as both pistons move from bottom dead center (BDC) to TDC (compression stroke). Process 2 is a constant volume process (combustion) which follows the opening of the cylinder-connecting valve (CCV). This valve allows the high-pressure air to enter the-low-compression-ratio cylinder to compress heat, and ignite its fuel-air mixture. This valve remains open during the power stroke.

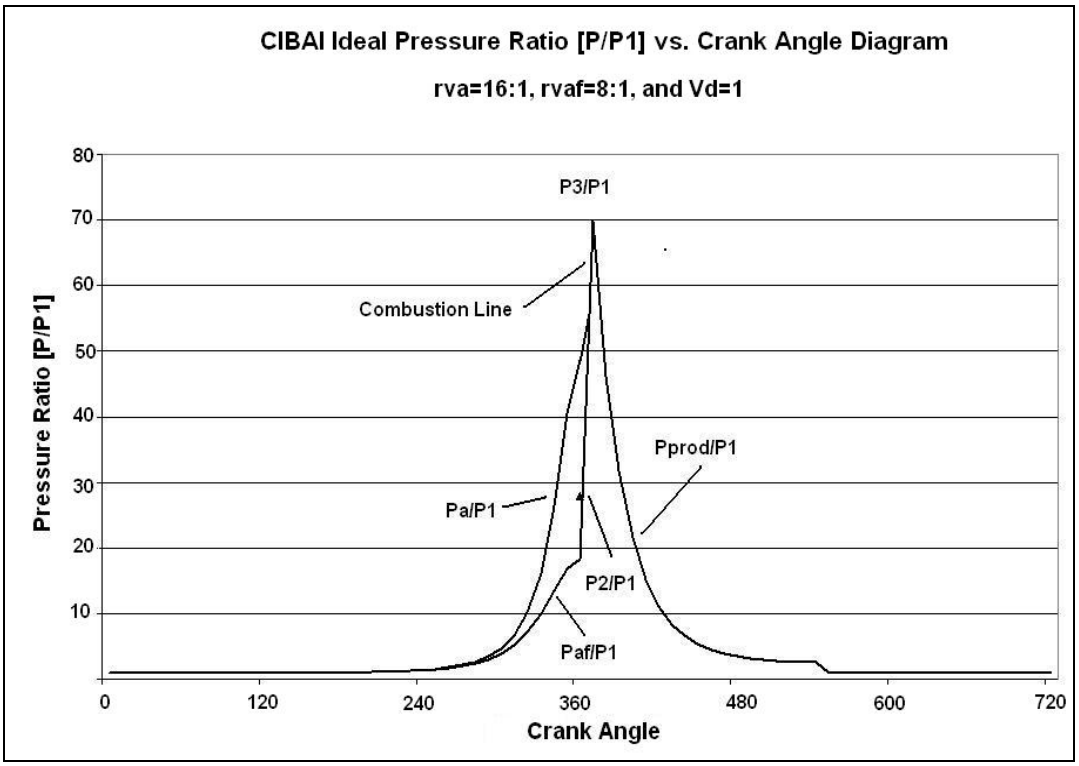

Figure 4.4 CIBAI cycle ideal pressure ratio (P/P_1) vs. crank angle

The vertical line represents constant-volume heat addition indicating the instantaneous auto-ignition of the fuel-air mixture at the top dead center (TDC). This is followed by an isentropic expansion (power stroke). The cycle is completed by a constant-volume process, in which heat is rejected from the air while the piston is at BDC. The exhaust and intake strokes are represented by horizontal lines on scale P/P_1= 1.0.

The set of equations for calculating the temperature and pressure ratios inside both cylinders (air-fuel and air-only) at any position during the expansion stroke are presented in references [3, 5].

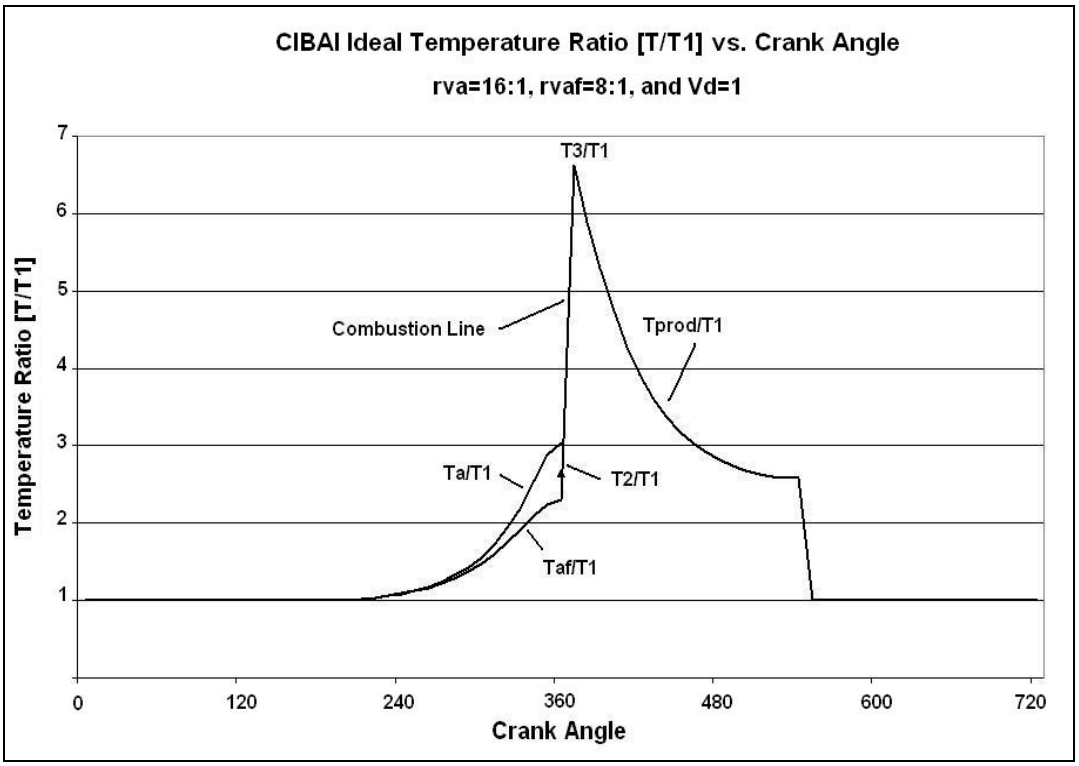

Figure 4.5 CIBAI cycle temperature ratio (T/T_1) vs. crank angle

Chapter 5: The Analytical Model

Overview

The objective of the analytical model presented here is the theoretical prediction of the influence of air-injection design parameters and operation variables in the compression ignition by the air-injection process. A cold-air-injection model is presented in chapter 6.

The thermodynamic cycle for controlled auto-ignition in a CFR engine is different from the CIBAI cycle above. The cold air from a bottle is pre-heated inside a pipe, placed inside the CFR engine exhaust. Its analytical model consists of two subsystems, a variable volume CFR engine combustion chamber and a fixed volume, containing hot, high-pressure air. These two compartments are normally isolated by a solenoid valve and a ball check valve, with an equivalent orifice-type, cross-sectional area A_o.

The combustion chamber and the air heater are modeled as separate thermodynamic systems with the outflow from the one, equal to the inflow into the other. This model is an extension of a model originally developed by El-Messiri [61], using a mathematical model developed by Borman [62], and thermodynamic properties obtained by Newhall and Starkman [63], using the data from the JANAF tables [64].

The solution to the model was used to generate the time histories of the air heater and combustion chamber thermodynamic properties throughout the cycle. Special attention is given to the combustion chamber pressure-time-volume history, which represents useful work produced per cycle. The schematic diagrams of the generalized thermodynamic model and the compression ignition by air injection model are shown in Figures 5.1, and 5.2 respectively.

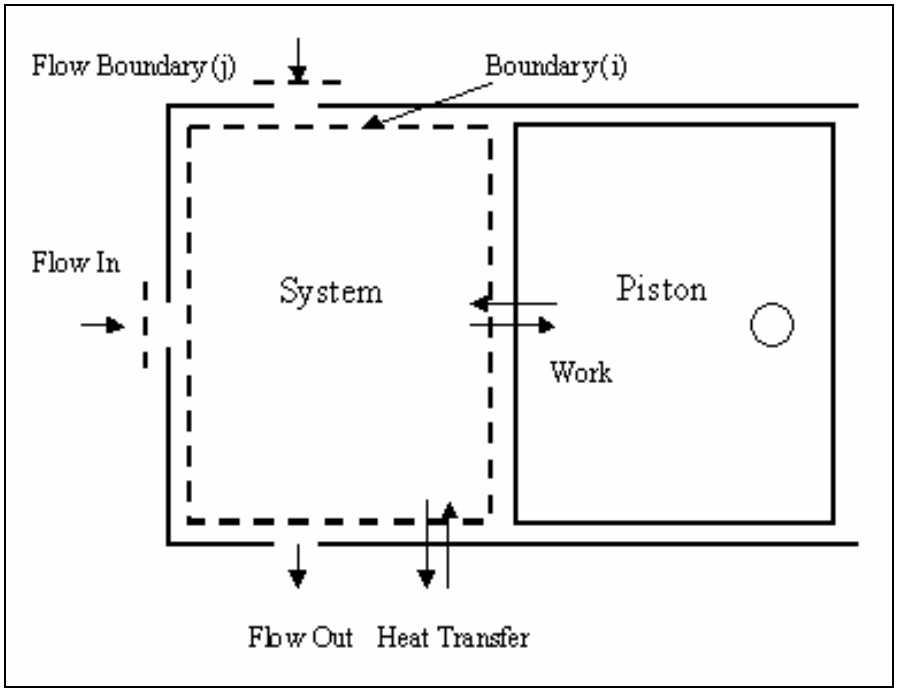

Figure 5.1 Generalized thermodynamic model [61]

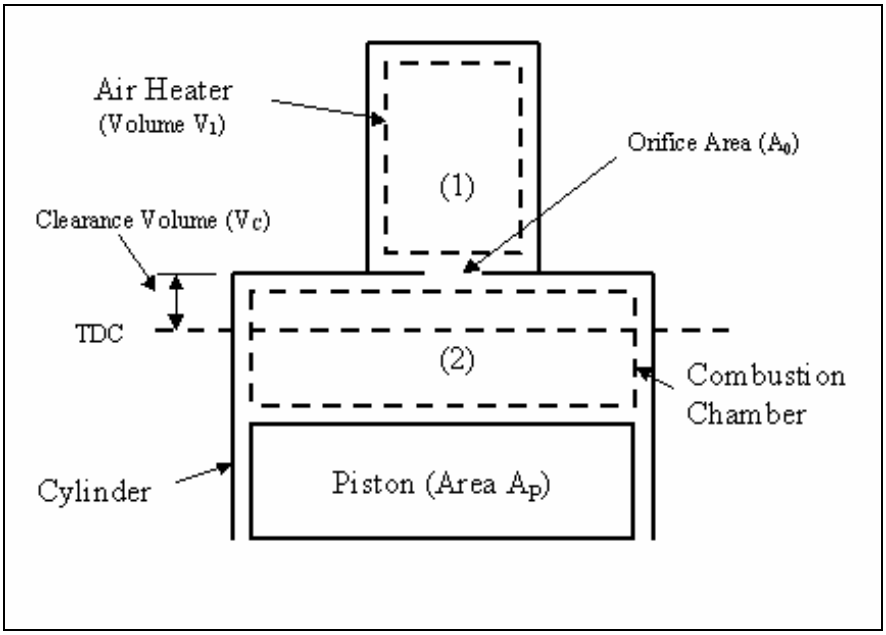

Figure 5.2 The compression ignition by air-injection (CIBAI) model

Assumptions

The ideal cycle analysis is based on the following assumptions:

1. The first stage of combustion is assumed to occur instantly at a constant volume, leading to formation of equilibrated combustion products.
2. The high-temperature air flowing from the air heater into the combustion chamber mixes instantly and completely with the contents of the combustion chamber (fuel-air mixture).
3. Each subsystem is considered as a homogeneous system of uniform temperature, pressure, and composition.
4. Combustion products are assumed to behave as the cold-air standard.
5. Heat transfer from the gases to cylinder walls is neglected.

Model Analysis and Governing Equations

The generalized model has been solved using the first law of thermodynamics (conservation of energy), the equation of mass continuity (conservation of mass), and the equation of state, together with the thermodynamic property equations relating equilibrium combustion product properties to time dependent values of temperature (T), pressure (P), and effective fuel-air ratio (F), as proposed by Borman [62]. The solution obtained for the generalized model will be applied to the combustion chamber and air heater systems.

Governing Equations

For the generalized thermodynamic system presented in Figure 5.1, the first law of thermodynamics (conservation of energy), the equation of mass continuity (conservation of mass), the equation of state, and the equilibrium combustion product equations are written as follows:

Conservation of Energy:

$$\dot{\overline{Mu}} = -P\dot{V} + \sum_i \dot{Q}i + \sum_j h_j \dot{M}_j \qquad (5.1)$$

Equation (5.1) is the time derivative version of the open-system energy balance. The left-hand side is the rate of change of the total energy of the system with time. The right-hand side consists of the work done due to the piston motion, the sum of the heat transfer rates across the boundaries of the system, and the sum of all energy flowing in and out of the system because of the mass transfer.

Conservation of Mass:

$$\dot{M} = \sum_j \dot{M}_j \qquad (5.2)$$

The Equation of State:

$$PV = MRT \qquad (5.3)$$

Equilibrium Combustion Products:

Borman [62] developed mathematical formulations to obtain the absolute internal energy (u) and gas constant (R) as a function of pressure, temperature, and fuel-air ratio. These formulations have the following forms:

$$u = u(T, P, F) \qquad (5.4)$$

$$R = R(T, P, F) \qquad (5.5)$$

Differential Equations for Temperature and Pressure:

The differential equations for temperature and pressure are obtained from equations (5.1) to (5.5). The approach is to derive the equations in terms of the dependent variables P, T, F, or related quantities that can be expressed in terms of these variables to facilitate the numerical solution. Time, t, will be treated as the only independent variable. The resulting differential equations are coupled and non-linear; therefore, a numerical integration technique needs to be used to obtain a reasonable solution. The mathematical procedure is described next.

Applying the product rule to the left-hand side of equation (5.1) gives

$$\dot{\overline{Mu}} = M\dot{u} + u\dot{M} \tag{5.6}$$

Using the chain rule of differentiation for equation (5.4) yields

$$\dot{u} = \frac{du}{dT}\dot{T} + \frac{du}{dP}\dot{P} + \frac{du}{dF}\dot{F} \tag{5.7}$$

Replacing (5.7) into (5.6), and the result equation into (5.1), and dividing equation (5.1) by mass (M), the following differential equation is obtained:

$$\frac{du}{dT}\dot{T} + \frac{du}{dP}\dot{P} + \frac{du}{dF}\dot{F} + U\frac{\dot{M}}{M} = -RT\frac{\dot{V}}{V} + \sum_j hj\frac{\dot{M}\,j}{M} \tag{5.8}$$

Equation (5.8) gives a relation between the pressure and temperature derivatives of the system. All other derivatives in equation (5.8) can be obtained in terms of the thermodynamic state variables, system geometry, and time. Another independent relation between the pressure and temperature derivatives is obtained by differentiating the equation of state (5.3) with respect to time as follows:

$$P\dot{V} + V\dot{P} = \dot{M}RT + M\dot{R}T + MR\dot{T} \tag{5.9}$$

Dividing equation 5.9 by PV yields the following equation

$$\frac{\dot{V}}{V}+\frac{\dot{P}}{P}=\frac{\dot{M}}{M}+\frac{\dot{R}}{R}+\frac{\dot{T}}{T} \tag{5.10}$$

Using the chain rule of differentiation for equation (5.5) yields

$$\dot{R}=\frac{dR}{dT}\dot{T}+\frac{dR}{dP}\dot{P}+\frac{dR}{dF}\dot{F} \tag{5.11}$$

Replacing (5.11) into (5.10) and rearranging terms gives the following differential equation

$$\frac{\dot{V}}{V}-\frac{\dot{M}}{M}-\frac{1}{R}\frac{dR}{dF}\dot{F}=\frac{\dot{T}}{T}\left(\frac{T}{R}\frac{dR}{dT}+1\right)+\frac{\dot{P}}{P}\left(\frac{P}{R}\frac{dR}{dP}-1\right) \tag{5.12}$$

Equation (5.12) gives a second relation between the pressure and temperature derivatives of the system. All other values, different from $\dot{T}$ and $\dot{P}$ in equation (5.12) can be obtained in terms of the thermodynamic state variables, system geometry, and time (t).

Equations (5.8) and (5.12) form a system of two independent, simultaneous, linear equations that can be solved together with the appropriate air-fuel ratio ($\dot{F}$), mass flow ($\dot{M}$), and volume change ($\dot{V}$) equations. The equilibrium thermodynamic properties of the products of combustion of C_nH_{2N} and air (u, and R and the six partial derivatives) can be calculated as proposed by [62].

Differential Equation for Air-fuel ratio (F):

By definition the fuel-air ratio (F) is the ratio of the actual fuel-air ratio (f) to the stoichiometric, or chemically correct, fuel-air ratio (f_s). The total mass at time (t) is equal to the sum of the mass of fuel (M_f) and the mass of air (M_a). These relations are shown in equations (5.13), (5.14), and (5.15) respectively.

$$F = \frac{f}{f_s} \tag{5.13}$$

$$f = \frac{M_f}{M_a} \tag{5.14}$$

$$M = M_f + M_a \tag{5.15}$$

where:

F=Fuel-air air-fuel ratio
f=Actual fuel-air ratio
f_s=Stoichiometric fuel-air ratio
M=Total mass
M_f=Mass of fuel
M_a=Mass of air.

Since the air-fuel ratio of the combustion chamber will be continuously changing during the air injection through the flow boundary j, an "effective" air-fuel ratio for the mixture needs to be calculated. Following the same methodology presented by Borman, [62] the differential equation for F was obtained.

$$\dot{F} = \frac{1}{M_a}\left(\sum_j \frac{\dot{M}_j F_j}{1+f_j}\right) - \frac{M_f}{M_a{}^2}\left(\sum_j \frac{\dot{M}_j}{1+f_j}\right) \tag{5.16}$$

Mass Flow Rate Through the Orifice:

Since the mass flow must enter through a restricted area, called here an orifice, the conservation of mass can be written as

$$\dot{M}_1 = -\dot{M} = -\dot{M}_2 \tag{5.17}$$

The mass flow rate, $\dot{M}$, through the orifice connecting the combustion chamber and the air heater system can be calculated from the quasi-steady compressible flow equation as follows:

$$\dot{M} = AeP_1\left[\frac{2\gamma}{\gamma-1}\frac{g_c}{R_1T_1}\left(\left(r_p\right)^{\frac{2}{\gamma}} - \left(r_p\right)^{\frac{\gamma+1}{\gamma}}\right)\right]^{\frac{1}{2}} \tag{5.18}$$

where:

$r_p = \frac{P_2}{P_1}$ (Instantaneous pressure ratio)
A_e = Orifice Area
g_c = Dimensional constant
γ = Specific heat ratio.

During the initial stages of injection and/or expansion, the flow through the orifice is likely to be the choked flow. In this case the pressure ratio (r_p) in equation (5.18) should be replaced by the critical pressure

$$r_p \Big|_{critical} = \left(\frac{2}{\gamma+1}\right)^{\frac{\gamma}{\gamma-1}} \tag{5.19}$$

Therefore, for the calculation of the mass flow rate using equation (5.18), the instantaneous pressure ratio (r_p) needs to be compared to the critical pressure ratio ($r_p \Big|_{critical}$). If r_p is less than then the critical pressure ratio, then $r_p \Big|_{critical}$ is used in equation (5.17) since then the pressure ratio and the calculated mass flow rate correspond to the choked flow.

The expression $\dot{M}/M$ appearing in equations (5.8) and (5.12) can be replaced by the following expression

$$\frac{\dot{M}}{M} = A_e\frac{P_1}{M_1}\left[\frac{2\gamma}{\gamma-1}\frac{g_c}{R_1T_1}\left(\left(r_p\right)^{\frac{2}{\gamma}} - \left(r_p\right)^{\frac{\gamma+1}{\gamma}}\right)\right]^{\frac{1}{2}} \tag{5.20}$$

Volume and Rate of Change of Volume for the Cylinder:

The volume (V) and the rate of change of volume ($\dot{V}$) for the cylinder is given by Lichty [65] in terms of engine geometry as follows:

$$V = VC + \pi B^2 X / 4 \tag{5.21}$$

in which

$$X = r\left[1 - \cos\theta + (L/r)(1 - Z)\right] \tag{5.22}$$

and

$$Z = [1 - (r/L)^2 \sin^2\theta]^{\frac{1}{2}} \tag{5.23}$$

$$\dot{V} = \frac{\pi}{4} B^2 r \left[\sin\theta + \frac{r}{2LZ}\sin 2\theta\right]\dot{\theta} \tag{5.24}$$

$$\dot{\theta} = 2\pi(N)/60 \tag{5.25}$$

The only independent variable in the system of equations is time (t). Therefore, an expression of θ (in radians) in terms of time (t) is required for the derivation of the differential equations of the system. This is obtained by integrating equation (5.25) between t=0 and t to give

$$\theta = \theta_0 + \frac{2\pi(N)}{60} t \tag{5.26}$$

The expression $\dot{V}/V$ appearing in equations (5.8) and (5.12) can be obtained at any instant of time (t) from equations (5.21) and (5.24).

Equations (5.8), (5.12), (5.16), (5.20), (5.21) and (5.24) completely characterize the generalized thermodynamic model. These equations constitute a system of coupled non-linear ordinary differential equations that need to be solved using numerical methods.

Application to the Air-Injection System

The equations derived in the previous section for the generalized thermodynamic model are applied to each subsystem (combustion chamber and air heater) to theoretically predict the influence of air-injection, design parameters and operation variables on the process of compression ignition by air injection. Denoting the air heater by subscript 1 and the combustion chamber by subscript 2, the equations for each subsystem are obtained as follows.

Air Heater

For the air-heater subsystem, the volume is constant. Therefore, the equations for this subsystem are obtained from equations (5.8), and (5.12) by replacing $\dot{V}_1 = 0$ and $\dot{F}_1 = 0$. Equation (5.8) is reduced to the following normalized form by dividing both sides by R_1T_1, making use of the equation of state (PV=MRT) and the definition of enthalpy (h=u +PV)

$$\frac{1}{R_1}\left(\frac{du}{dT}\right)_1 \frac{\dot{T}_1}{T_1} - \frac{\dot{M}_1}{M_1} + \left(\frac{P_1}{R_1T_1}\left(\frac{du}{dP}\right)_1 \frac{\dot{P}_1}{P_1}\right) = 0 \tag{5.27}$$

Equation (5.12) is reduced to:

$$\left[\frac{T_1}{R_1}\left(\frac{dR}{dT}\right)_1 - 1\right]\frac{\dot{T}_1}{T_1} + \frac{\dot{M}_1}{M_1} + \left[\frac{P_1}{R_1}\left(\frac{dR}{dP}\right)_1 - 1\right]\frac{\dot{P}_1}{P_1} = 0 \tag{5.28}$$

Combustion Chamber

For this subsystem, the volume as well as the fuel-air ratio are changing. The generalized equations (5.8), (5.12), (5.16), (5.20), (5.21), and (5.24) will be applied to

this subsystem and the expressions $\frac{\dot{M}_2}{M_2}$ and $\dot{F}$ will be expressed in terms of $\frac{\dot{M}_1}{M_1}$ to facilitate the solution by numerical methods.

From conservation of mass

$$M_1 + M_2 = M = \text{Constant}$$

differentiating both sides with respect to time (t)

$$\dot{M}_2 = -\dot{M}_1$$

and in terms of $\frac{\dot{M}_1}{M_1}$, the quantity $\frac{\dot{M}_2}{M_2}$ is expressed as

$$\frac{\dot{M}_2}{M_2} = -\frac{\dot{M}_1}{M - M_1} = \frac{1}{1-\left(\frac{M}{M_1}\right)}\frac{\dot{M}_1}{M_1} \tag{5.29}$$

Using equation (5.29) and dividing both sides of equation (5.8) by R_2T_2 yields

$$\left[\frac{1}{R_2}\left(\frac{du}{dT}\right)_2\right]\frac{\dot{T}_2}{T_2} + \left[\frac{P_2}{R_2T_2}\left(\frac{du}{dP}\right)_2\right]\frac{\dot{P}_2}{P_2} + \left[\frac{1}{R_2T_2}\left(\frac{du}{dF}\right)_2\right]\dot{F}_2 + \left[\frac{u_2 - u_1 - R_1T_1}{R_2T_2} * \frac{1}{1-\left(\frac{M}{M_1}\right)}\right]\frac{M_1}{M_1} = -\frac{\dot{V}_2}{V_2} \tag{5.30}$$

Applying equation (5.12) to the subsystem and by using equation (5.30), the following expression is obtained

$$\left[\frac{T_2}{R_2}\left(\frac{dR}{dT}\right)_2 + 1\right]\frac{\dot{T}_2}{T_2} + \left[\frac{P_2}{R_2}\left(\frac{dR}{dP}\right)_2 - 1\right]\frac{\dot{P}_2}{P_2} + \left[\frac{1}{R_2}\left(\frac{dR}{dF}\right)_2\right]\dot{F}_2 + \left[\frac{1}{1-\left(\frac{M}{M_1}\right)}\right]\frac{M_1}{M_1} = \frac{\dot{V}_2}{V_2} \tag{5.31}$$

Finally, an expression for the air-fuel ratio F_2 and its time derivative $\dot{F}_2$ is obtained from equations (5.13) through (5.16) and equation (5.31) as follows

$$\dot{F}_2 = \frac{(F_2 - F_1)M_1}{F_1 f_S M_{02} + M - M_1} * \frac{\dot{M}_1}{M_1} \tag{5.32}$$

In summary, equations (5.27) through (5.32) together with the properties given by equations (5.4) and (5.5) completely describe the thermodynamics of the compression by the air-injection model. The volume terms V_2 and $\dot{V}_2$ are prescribed by the geometry and operating speed of the engine mechanism and the mass flow term $\dot{M}_1$ by the appropriate fluid dynamic expressions. These equations constitute a system of coupled non-linear ordinary differential equations that need to be solved using numerical methods. A cold-air-injection model was used to determine the air-injection, initial conditions and the air-heater design parameters (see chapter 6).

Chapter 6: The-Cold-Air Injection and Thermodynamic Models

Overview

The cold-air-injection model proposed in this chapter uses thermodynamic concepts and fuel properties to determine the ideal operating conditions needed to reach auto-ignition by hot ,high-pressure air injection during one single CFR engine event. High-pressure air injection into the CFR is modeled by using a fixed container, connected by a solenoid valve and an injector ball-check valve to the cylinder-piston arrangement shown in Figure 6.1. The fixed container delivers a precise, controlled amount of hot-high-pressure air into the cylinder during one single engine cycle. The analysis of the model is done by using the conservation of mass and energy principles, the ideal gas law, and the CIBAI concept.

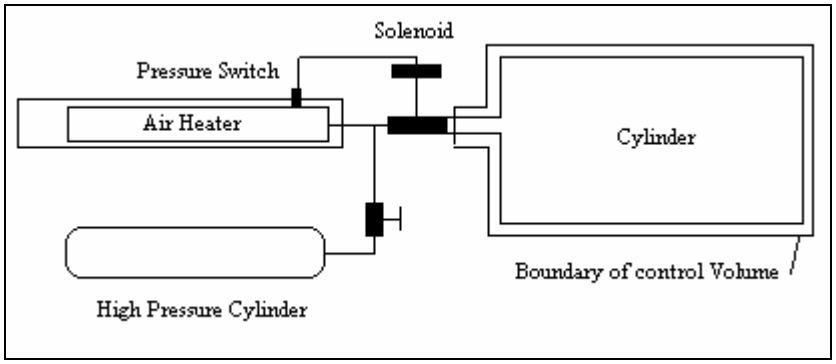

Figure 6.1 Air injection schematic model

As mentioned earlier, the new thermodynamic cycle for IC engines, CIBAI cycle, patented by Loth and Morris [3,5], indicates that it is possible to obtain a higher thermal efficiency than with the Otto or Diesel cycle by simply injecting compressed air into an air-fuel mixture cylinder. The higher thermal efficiency may be explained by the increase in combustion compression due to the use of a high energy ignition source in the form of hot-high-pressure air injection. However, this research is based on using a CFR engine

and therefore differs significantly from the CIBAI cycle. The conservation of mass and energy principles, and the ideal gas model are used to determine the final equilibrium temperature and pressure of the air in the cylinder after all the injected air has entered prior to auto-ignition. The second law of thermodynamics is used to determine the heat rejection during the combustion process. The derivation of the CFR engine air-injection process resulted in two models: the air-injection model, and the thermodynamic model. These models are described next.

Air-Injection Model

The schematic diagram shown on Figure 6.1 is used to simulate the hot high-pressure air injection into the CFR engine. High-pressure air from a compressed bottle is injected into the air heater at a known temperature and pressure. The air heater is located inside the flexible exhaust pipe of the CFR engine. Air is injected into the cylinder through an injector ball-check valve in series with a normally closed solenoid valve. This valve is operated by a microcontroller that receives and processes input signals from sensors added to the engine. The solenoid valve is closed at the moment that the pressure inside the heater reaches a pre-selected cut-off pressure. A detailed description of the instrumentation, data acquisition system, and the control system is included in the experimental set-up and procedure section of this paper (Chapter 8). The following assumption are needed for the analysis of the air injection model

Assumptions

1. Air injection occurs at TDC.
2. The ideal gas model for air is applied.
3. The P and T of the injected air remain constant prior to entering the cylinder.

4. The amount of air injected into the cylinder is limited to the actual displacement volume, Vd_{act}.

Analysis

The analysis of this model involves the steps needed to calculate the amount of air in the air heater and the amount of air injected into the CFR engine in one single cycle event. An analysis of the air-injection model is shown below.

The displacement volume (V_d) at sea level can be represented as a function of the engine bore (b) and stroke (s) values

$$V_d = \frac{\pi * b^2 * s}{4} \tag{6.1}$$

The actual volume displacement, V_{dact}, is a function of the CFR engine operating conditions

$$V_{dact} = \frac{\dot{V}}{\frac{N}{n}} \tag{6.2}$$

where:

$\dot{V}$ = Volumetric air flow rate
N= Revolutions per minute (RPM)
n = Revolutions per engine cycle (Rev/cycle).

The associated volumetric efficiency (η_{vol}) is given by

$$\eta_{vol} = V_{dact} / V_d \tag{6.3}$$

The required heater volume, V_{heater}, can be obtained from the conservation of mass principle

$$m_c - m_p = m_i \tag{6.4}$$

where:

m_c= Mass initially inside the heater at the maximum pressure and temperature
m_p= Mass remaining in the heater after the cut-off pressure
m_i= Mass injected into the cylinder.

V_{heater} and P_{cutoff} are designed in such a way that m_i equals the mass already present inside the CFR engine cylinder, prior to injection. Substituting into Eq. 6.4

$$\frac{P_{\max} * V_{heater}}{R * T_{\max}} - \frac{P_{cutoff} * V_{heater}}{R * T_{\max}} = \frac{P_{ref} * V_{dact}}{R * T_{ref}}$$

where:

P_{max} = Maximum pressure at which gas is injected into the air heater
P_{ref} = Pressure reference at sea level
P_{cutoff} = Cut-off pressure. This is the pressure value inside the air heater at which the solenoid valve is closed.
R = Gas constant
T_{max} = Maximum temperature air heater
T_{ref} = Temperature reference at sea level.

and solving the equation for V_{heater} results in:

$$V_{heater} = \frac{P_{ref} * V_{d\,act} * T_{\max}}{[p_{\max} - P_{cutoff}] * T_{ref}} \tag{6.5}$$

Finally, the hot, high-pressure air injected into the cylinder will have a volume at sea level conditions V_i, as calculated from the ideal gas law equation

$$V_i = \frac{m_i * R * T_{ref}}{P_{ref}} \tag{6.6}$$

Thermodynamic Model

The conservation of mass and energy principles is used to calculate the temperature and pressure in the cylinder at TDC before and after air injection for several compression ratios.

Derivation of the Temperature and Pressure Before Air Injection

The temperature and pressure inside the cylinder before the air injection are calculated using the air-standard, Otto-cycle analysis introduced previously, under the following assumptions.

Assumptions

1. The air in the piston-cylinder assembly is the closed system.
2. The compression and expansion processes are adiabatic.
3. All processes are internally reversible.
4. Air injection occurs at TDC.
5. The air-fuel mixture is modeled as an ideal gas.
6. Kinetic and potential energy effects are negligible.
7. Process 1-2 (adiabatic compression) of the air-standard Otto cycle is considered for the calculation of the temperature and pressure at TDC before the air injection.

Analysis

For an isentropic process:

pv^k = Constant with $k = c_p/c_v$

For process 1-2

$p_1 v_1^k = p_2 v_2^k$, m = constant

Therefore, the pressure p_2 before the air injection at TDC is given by the following equation:

$$p_2 = p_1 * \left(\frac{V_1}{V_2}\right)^K$$

$$p_2 = p_1 * (C.R)^k \tag{6.7}$$

where C.R = Compression ratio.

In the similar manner, the temperature T_2 before the air injection at TDC is obtained as follows:

$$\frac{v_1^{\,k}}{v_2^{\,k}} = \frac{p_2}{p_1} = \frac{\frac{RT_2}{v_2}}{\frac{RT_1}{V_1}} = \frac{T_2 * v_1}{T_1 * v_2}$$

$$\frac{v_1^{\,k} * v_2}{v_2^{\,k} * v_1} = \frac{T_2}{T_1}$$

$$\frac{T_2}{T_1} = \frac{v_1^{\,k-1}}{v_2^{\,k-1}} = \left(\frac{v_1}{v_2}\right)^{k-1}$$

Since m = constant, then

$$\frac{T_2}{T_1} = \left(\frac{v_1}{v_2}\right)^{k-1} = \left(\frac{V_1}{V_2}\right)^{k-1} = \left(\frac{V_{BDC}}{V_{TDC}}\right)^{K-1} = (C.R)^{k-1}$$

Thus, the temperature before the air injection in the cylinder at TDC is given by:

$$T_2 = T_1 * (C.R)^{(k-1)} \tag{6.8}$$

Derivation of the Temperature and Pressure After Air Injection

The following assumptions are considered to determine the final temperature and pressure after the air injection and prior to detonation.

Assumptions

1. Injection occurs at TDC.
2. The state of the injected air remains constant until it enters the cylinder.
3. There is no heat transfer with the surrounding, $\dot{W}_{cv} = 0$, and all kinetic and potential energy effects are ignored.
4. The ideal gas model applies assuming air.

Analysis

The control volume shown in Figure 6.1 has a single inlet and no exit. Therefore the mass rate balance takes the form

$$\frac{\partial m_{cv}}{dt} = \dot{m}_i \tag{6.9}$$

Similarly, the energy rate balance is

$$\frac{\partial E_{cv}}{dt} = \dot{Q}_{cv} - \dot{W}_{cv} + \dot{m}_i * (h_i + \frac{Vi^2}{2} + g * z_i) \tag{6.10}$$

With assumption 3, $\dot{Q}_{cv} = \dot{W}_{cv} = 0$, and all kinetic and potential energy effects can be neglected. Thus

$$\frac{\partial U_{cv}}{dt} = \dot{m}_i * h_i \tag{6.11}$$

Combining the mass and energy rate balances give

$$\frac{\partial U_{cv}}{dt} = h_i * \frac{dm_{cv}}{dt} \tag{6.12}$$

In accordance with assumption 2, the specific enthalpy of the air entering the control volume is constant: hi = h(T_i), where T_i is the temperature of the air within the air heater. Thus, on integration, the above equation becomes

$$\Delta U_{cv} = h(T_i) * \Delta m_{cv} \tag{6.13}$$

where ΔU_{cv} and Δm_{cv} denote, respectively, the changes in the internal energy and mass of the control volume. The change in the mass contained within the control volume equals the mass injected into the cylinder

$$\Delta m_{cv} = m_i \tag{6.14}$$

The change in internal energy is

$$\Delta U_{cv} = (m_c + m_i) * u(T) - m_c * u(T_c) \tag{6.15}$$

where:

m_c = Mass of the air initially in the cylinder
m_i = Mass of the air injected into the cylinder
T_c = Temperature of the air initially in the cylinder at TDC
T = Final temperature of the air within the cylinder after the air injection and prior to detonation
$u(T_c)$ = Specific internal energy as a function of T_c
u(T) = Specific internal energy as a function of T.

Grouping equations (6.13), (6.14), and (6.15) and solving them gives the specific internal energy at T temperature

$$u(T) = \frac{m_c * u(T_c) + m_i * h(T_i)}{m_c + m_i} \tag{6.16}$$

Using the ideal gas properties of air tables from Moran and Shapiro [66], and interpolating with the value of the specific internal energy obtained from equation (6.16), the final temperature T of the air in the cylinder after the air injection and prior to auto-ignition is obtained.

The final pressure P of the cylinder at TDC after the air injection and prior to auto-ignition is found by using the ideal gas equation of state

$$P = (m_c + m_i) * R * T / V \tag{6.17}$$

The volume (V) of the cylinder at TDC can be obtained from the ideal gas equation of state, and it is equal to the clearance volume (V_c). It can be calculated using equation 6.18.

$V = V_c$

$$V = m_c * R * T_c / P_c \tag{6.18}$$

where P_c and T_c are the pressure and temperature of the air initially in the cylinder before the air injection. Combining equations 6.17 and 6.18 the final pressure p after the air injection and prior to auto-ignition is found.

$$P = \frac{(m_c + m_i) * R * T}{(m_c * R * T_c / P_c)} = P_c * \frac{T}{T_c} * \left(\frac{m_c + m_i}{m_c} \right) \tag{6.19}$$

The air-injection model developed in this section was used to quantitatively evaluate the benefits of ignition by hot, high-pressure air injection on a CFR engine during one single engine cycle (Appendix B). The results of this analysis were used as the primary design criteria for the design of the air-injection system presented in Chapter 8 of this dissertation.

Chapter 7: Preliminary Designs

Overview

The air-injection model developed in Chapter 6 was used to quantitatively evaluate the benefits of ignition by hot, high-pressure air injection on a CFR engine during one single engine cycle. The results of this analysis were used as the primary design criteria for the design of the air-injection system. Safety considerations were also important in the selection of materials, equipment, and operating procedures.

Based on the results obtained through the implementation of the air-injection model presented in the previous chapter, and the CIBAI fundamentals proposed by Loth [3], the following design criteria were chosen for the air-injection system:

1) The amount of hot, high-pressure air injection was limited to 437 cc of standard air.
2) A maximum air-charge pressure of 1000 psig and minimum of 700 psig were chosen.
3) A maximum exhaust temperature of 1100 ^{o}F and a minimum of 600 ^{o}F were selected to pre-heat the air charge prior to injection.
4) The injector ball type check valve, downstream of the solenoid valve was set to open at 500 psig. This means that this valve would open for a charging pressure greater than or equal to 500 psig.
5) A compression ratio (C.R) limit of 8:1 was selected for the initial CIBAI combustion test. However, the system would allow working with higher compression ratios if needed.
6) An intake mixture temperature of 70 °F was chosen for the first set of experiments.
7) A maximum air-injection time of 20 ms was chosen to assure that most of the air injected would have entered the cylinder prior to reaching TDC.

8) Test repeatability was determined to be paramount.

9) Digitalized data acquisition was chosen to store the large amount of data.

10) Synchronization between air-injection timing, data acquisition, and engine operation was essential in the data acquisition phase.

In order to fulfill the design requirements presented above for the air-injection system, several conceptual and physical designs were proposed, and analyzed during the course of this research. These designs are discussed next.

Conceptual Designs

Conceptual designs are defined as those that were proposed, and evaluated, but never built. However, they provided valuable information about the functionality and feasibility of the CIBAI engine. Conceptual designs included 3D models of a four-stroke and two-stroke CIBAI engines, a CIBAI combustion bomb, and an air-gun rapid-compression machine.

3D Models

Two four-stroke CIBAI engines were modeled using a 3D software package. A 1000 cc two-cylinder engine (Figures 7.1) and a 2000 cc four-cylinder engine (Figure 7.2) were evaluated. The aim of this modeling was to gain understanding of the challenges to implement the CIBAI concept in a commercial engine. It demonstrated the importance of the correct location and size of the cylinder-connecting valve (CCV), as described by Loth and Morris [3,5], to make an engine operate on the CIBAI cycle.

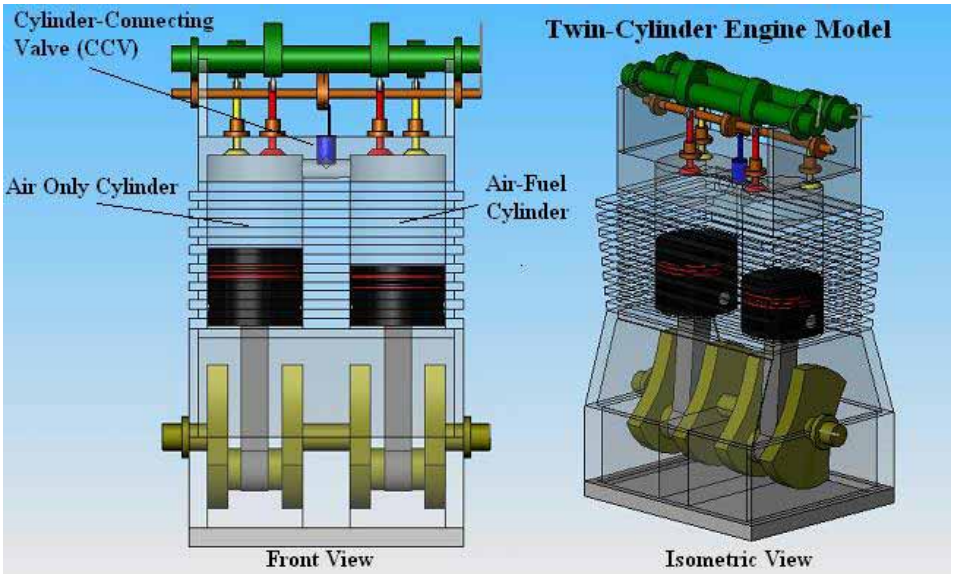

Figure 7.1 Twin-cylinder CIBAI engine 3D model

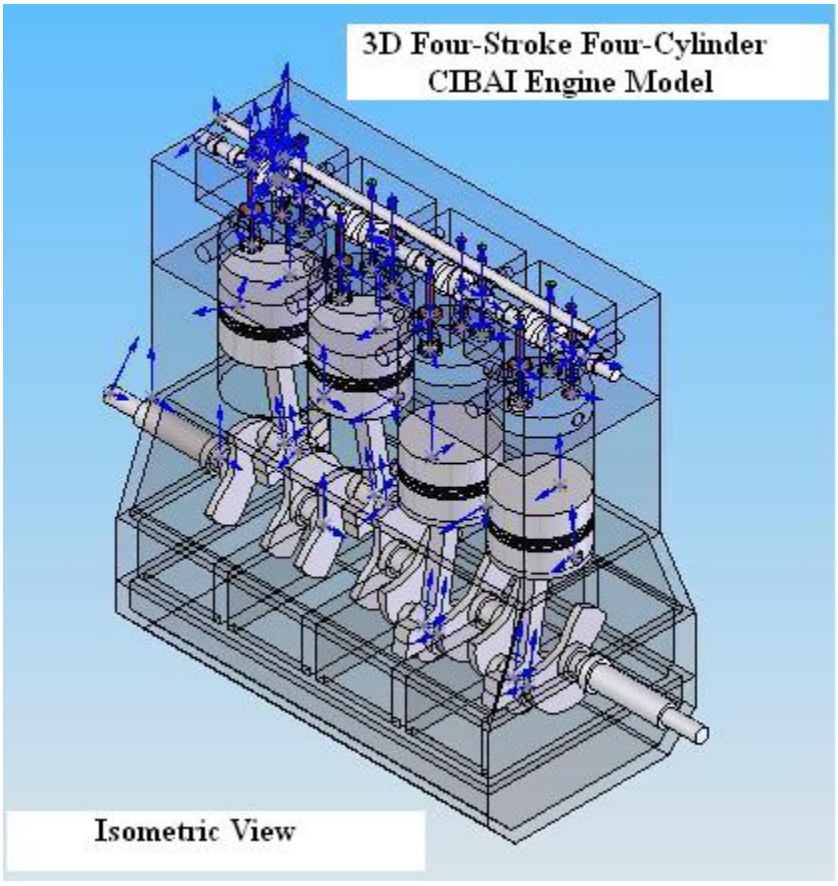

Figure 7.2 Four-stroke four-cylinder CIBAI engine 3D model

The need for the modification of the crankshaft, cylinder head, and camshaft are clearly evident in these 3D models. This is the reason why the concept of Compression Ignition By Air Injection (CIBAI) was studied in an available CFR engine, which was easily converted to ignition-by-air injection to prove the concept.

CIBAI Combustion Bomb

Most of the earlier studies done on auto-ignition were carried out using rapid compression machines, pulse combustors, shock tubes, and combustion bombs. Combustion bombs have been a very useful tool to understand the phenomena occurring in the combustion chamber, and allowed advanced engine concepts to be explored in search of higher efficiency, lower emissions, and greater fuel flexibility. This type of device is relatively simple in concept, although, in order to reach auto-ignition conditions, it is necessary to use high pressures and temperatures. A single-event, constant-volume combustion bomb could have been used to simulate the CIBAI combustion process, without the need of the moving parts of traditional reciprocating engines.

The design of the CIBAI combustion bomb was completed with several major objectives in mind. The design strategy for the CIBAI combustion bomb was to produce a simple and flexible research apparatus that would be inexpensive to build and operate. Therefore, off-the shelf components were proposed to be used. For example, a solenoid activated valve could be used to simulate the cylinder-connecting valve (CCV), and the container could be welded together using standard pipes and flanges. As a research device, it was deemed necessary to make adequate provisions for the CIBAI combustion bomb to be highly instrumented. Therefore, sensor ports, and optical observation

windows would be needed in the bomb design. Additional design considerations would be needed to assure the safe operation of the combustion bomb, due to the unique hazards of this type of device. For example, a reliable pressure relief valve would be needed, and test procedures would have to be specified. The bomb was designed for a temperature and pressure before ignition of 500^{o} F and 700 psig, respectively.

Figure 7.3 shows a cross-sectional diagram of the CIBAI combustion bomb proposed for this study. It was designed particularly for gaseous fuel experiments, but could be used for gasoline and diesel fuel combustion with minor changes in the fuel supply system. The gaseous fuel and compressed air are supplied to the combustion bomb from high-pressure cylinders through a system of control valves and meters.

The CIBAI combustion bomb consists of an outer casing, incorporates a 1" stainless steel ball valve (4000 psi 150^{o} F) to simulate the cylinder-connecting valve (CCV), two tubes of 1" diameter schedule 40 stainless steel pipe of 12" and 40" long sections act as dual combustion chambers for the air and fuel respectively, a heating element, insulation materials, two 1" quartz windows, different fittings for air and fuel filling, a pressure transducer, a thermocouple probe, and exhaust and relief valves. The outer casing consists of a 1" stainless steel box of a 10" x 10" x 4" with a 1" base plate of 10" x 6", and a 1" removable top cover. The volumes of the air and fuel chambers are 35 cc and 70 cc respectively for a volume ratio of 2.

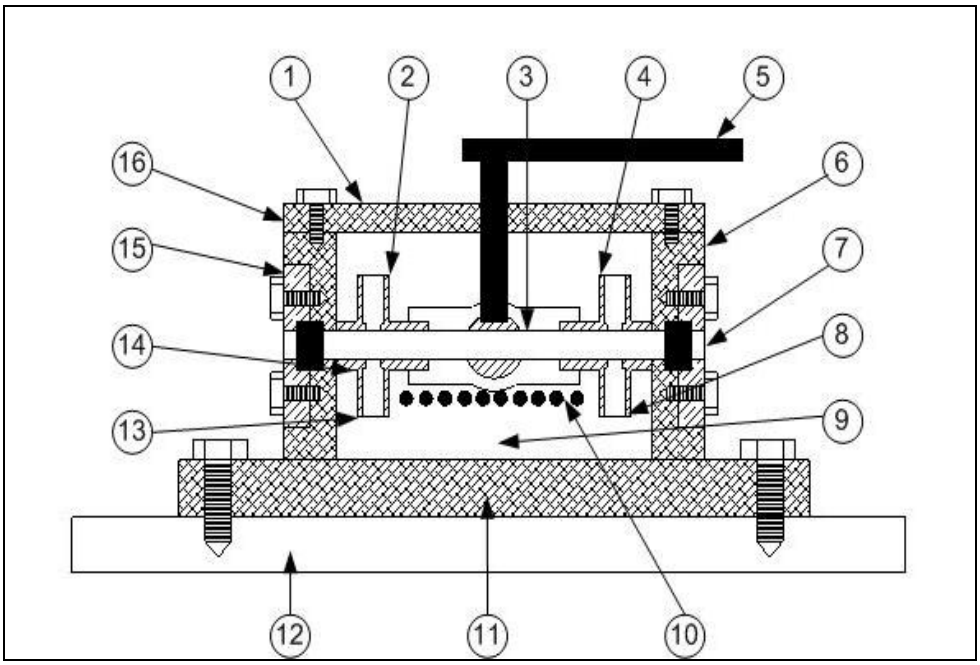

Figure 7.3 Cross-sectional diagram of the CIBAI combustion bomb

1. CIBAI Combustion bomb. 2. Pressure Transducer Port. 3. Cylinder-connecting valve (CCV). 4. Thermocouple Port. 5. Valve Actuator. 6. Lateral Outer Casing. 7. Quartz Observation Window. 8. Air Intake Port. 9. Insulation Blanket. 10. Electrical Resistance Heater. 11. Bottom Outer Casing. 12. Concrete Pad. 13. Fuel Intake Port. 14. Stainless Steel Pipe. 15. Observation Window Flange. 16. Top Outer Casing. 17. Relief Valve (Back). 18. Exhaust Valve (Back). 19. Injector Port (Front – Optional). 20. Spark Plug Port (Front- Optional).

Since the CIBAI combustion bomb has no moving parts, such as the piston of the internal combustion engine, used to compress the inlet cold air and fuel to auto-ignition, an electrical resistance heater located at the bottom of the chamber was proposed in order to raise the temperature of the air and fuel to the required level. To achieve the pre-ignition pressure conditions, the combustion chamber is pressurized with air and filled with an air-fuel mixture fuel to theoretical pressures normally obtained during the compression stroke in a reciprocating engine. To minimize the heat loss through the walls, the combustion bomb and the outer casing are wrapped with ceramic fiber blankets, which can withstand continuous usage at very high temperatures. The CIBAI

combustion bomb design is fully instrumented and equipped with a trigger system to provide the proper synchronization between the start of the combustion event, and the beginning of the data acquisition.

Even though, a CIBAI combustion bomb as described here was never built, it provided valuable insights in the design necessary to obtain auto-ignition under a controllable environment.

Air-Gun Rapid Compression Machine

An air-gun rapid compression machine was proposed to simulate the CIBAI combustion process in a single cylinder four-stroke CFR engine. The air gun consists of a ½" inside diameter glass tube with a Teflon piston, a 2000 psig ¼" NPT carbon steel check valve, a 2000 psig ¼" NPT stainless steel three-way ball valve, and a 2000 psig 1/8" NPT 115VAC brass solenoid valve. Four hundred and thirty seven (437) cc of sea level air at an average of 700 psig would be injected into the glass tube cylinder-piston assembly from a 2000 psig compressed bottle. This air is injected into the CFR engine through the normally closed solenoid valve at a mass flow rate of 0.0404 kg/s, for a discharged time of 6.72 ms or 36 crank angle degree at 900 rpm.

This design indicated the importance of a rapid response mechanism to inject the air into the CFR engine. This design did not provide a way to pre-heat the air before injection into the CFR engine, which is a critical factor to obtain auto-ignition for the CIBAI concept.

Physical Designs

The designs discussed in this section were built and tested under different operating conditions. The objective at this stage was to build a simple air-injection

system capable to simulate the combustion process in a CIBAI engine. Special attention was given to the safety of the system and operator, time response of the system, accuracy of the data, and repeatability of the results. In order to achieve these objectives a piston-cylinder assembly, air injectors, and cylinder-connecting valves (CCV) were designed, built, and extensively tested. In addition, some complementary components were built to support some of the preliminary experiments. These designs are discussed next.

Piston-Cylinder Assembly Design

One of the objectives of this piston-cylinder assembly was to simulate the initial conditions occurring in a CIBAI engine prior to combustion. Another objective was to determine the time response of the solenoid valve to changes in the amount of air injected, charged pressure, amplified pressure, and back pressure. Finally, the purpose was to incorporate the piston-cylinder assembly in a more complex experimental set-up to study the compression ignition by air injection (CIBAI) in a CFR engine for a single cycle event as proposed by Loth and Morris [3,5].

The piston-cylinder assembly is shown in Figure 7.4. It consisted of a CFR simulator, pressure amplifier, and a pressure charger. The CFR simulator resembled the air-fuel cylinder of the CIBAI engine. Physically, it simulated a clearance volume of 77 cc of a 500 cc single-cylinder four stroke CFR engine with a compression ratio (C.R) of 8:1 at TDC in the compression stroke. Back pressure was adjusted by way of a pressure regulator connected to either a 200 psig pressurized air tank or a 2000 psig compressed air bottle (Appendix C). A 1000 psig Omega pressure transducer (Appendix D) installed in the upper right side of the CFR simulator was used to obtain the time-pressure history inside the clearance chamber.

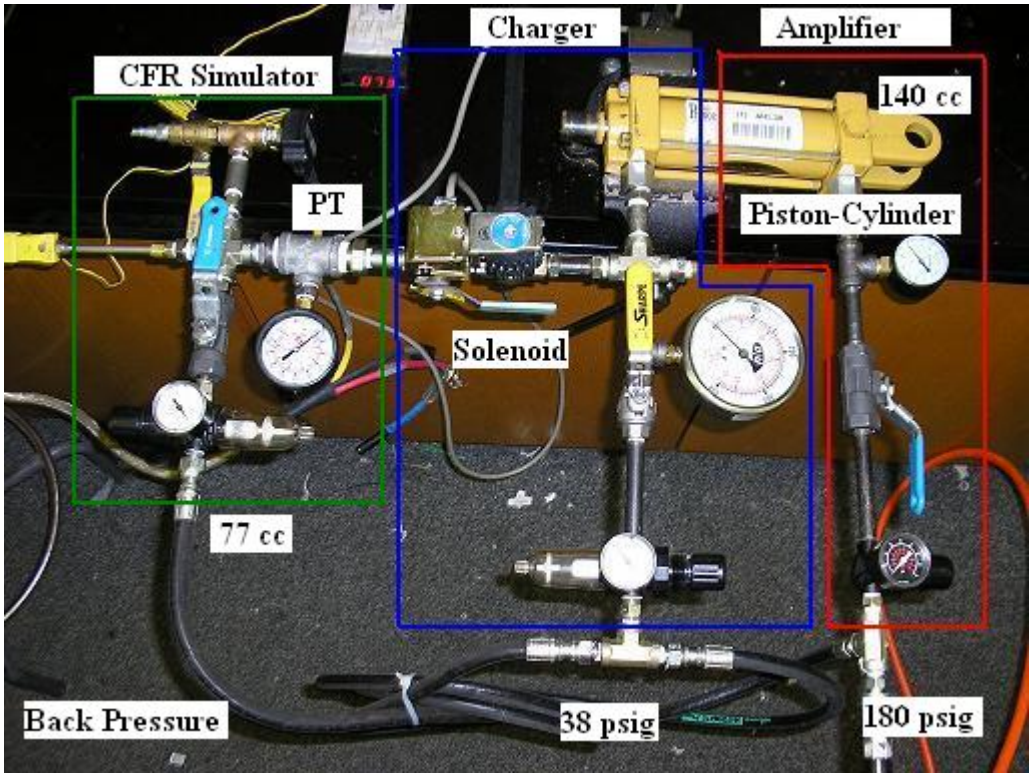

Figure 7.4 Piston-cylinder assembly

The pressure charger and pressure amplifier simulated the air-only cylinder paralleled to the air-fuel cylinder of the CIBAI engine. The pressure charger controlled the amount of air injected into the CFR simulator by isothermally compressing the air, at 38 psig into a volume of 140 cc, located in the piston-cylinder rod compartment, which is equivalent to 500 cc of the standard air. By actuating the 1/8" brass 115 VAC solenoid valve (Appendix E), located between the CFR simulator and piston-cylinder assembly, the mass of air was then injected into the CFR simulator, at a pressure of 600 psig by the action of the pressure amplifier. The solenoid valve simulated the cylinder-connecting valve (CCV), which joins the air-fuel mixture cylinder together with the air only cylinder at nearly constant volume at TDC in the CIBAI engine. Charging pressure was supplied from a 200 psig pressurized air tank.

The pressure amplifier consisted of a 2500 psig double acting tie-rod hydraulic cylinder (Appendix F), an air pressure regulator, a bleed valve, a pressure gauge, and plumbing. Pressure amplification up to 3.16 can be obtained from the area ratio between the piston and the piston rod areas. Amplified pressure was supplied from either a 200 psig-pressurized air tank or a 2000 psig-compressed air bottle. To prevent damage to the cylinder-piston assembly during air injection, a 1/8" rubber O-ring was installed to cushion the impact of the piston with the plug at the end of the cylinder.

By injecting an additional 500 cc of standard air into the CFR engine, the in-cylinder pressure is increased to an approximate value of 500 psig, which is equivalent to polytropic compressed air (γ=1.35) from an initial intake pressure of 12.2 psig at a compression ratio (C.R) of 16:1. If auto-ignition conditions are met (temperature, pressure, and air-fuel ratio), then suddenly doubling the CFR engine air mass will cause the homogeneous air-fuel mixture to auto-ignite, or CIBAI combustion to occur, as proposed by Loth and Morris [3,5].

The piston-cylinder assembly was tested over a wide range of pressures ranging from 0 to 100 psig. Charging pressures ranged from 30 to 100 psig, and amplified pressures ranged from 0 to 400 psig. The time-pressure history of the clearance chamber and the corresponding volumetric values were collected and verified.

Several important findings were obtained from this experimental work. The discharged time ranged between 40 ms for high pressure charged to 150 ms for low pressure charged. The piston movement was slow due to friction and the cylinder-piston assembly was considered unsuitable for experiments with ignition by air injection (CIBAI) in a CFR engine running at 900 rpm, and completing a thermodynamic cycle in

133 ms. The low response time of the cylinder-piston assembly was attributed to high friction between the cylinder and piston surface, and to large masses of the piston, and solenoid valve actuator, which required a minimum of 20 ms to open fully.

Lower than expected pressures in the clearance chamber were observed for most of the tests. This was attributed to additional plumbing volume outside the cylinder-piston assembly, which could not be pressurized by the piston during air injection.

Finally, the pressure amplification was not consistent for most of the tests, possibly because of leakages in the system.

Air-Injector Design

After the decision was made to use the CFR engine as the main apparatus for experiments with controlled auto-ignition by air injection, the design of an air injector was initiated taking under consideration the engine space constraints and the need for access ports for the pressure transducer (PT), solenoid valve, and pressure relief valve. The first design (Figure 7.5) was a multifunctional air injector that operated partially as a CCV while air injection was controlled by a solenoid valve and pressure relief configuration.

This design consisted of a two-piece element: a 7/8” OD diameter by 2-47/64” long carbon steel rod with two 3/16” diameter holes and two 1/8” NPT ports for the pressure transducer (PT), an air injection access port, and a 1-3/8” OD by 7/8” ID carbon steel bushing by 7/8” long with two lateral 1/8” NTP ports 90 degrees apart to connect the pressure-relief valve and the solenoid valve connections. The steel bushing had two 1/8” by 3/16” grooves for two high temperature rubber O-rings to prevent leakage from

inside the combustion chamber. The air injector was flush-mounted on the cylinder head in place of the original CFR engine 7/8" detonation pick-up.

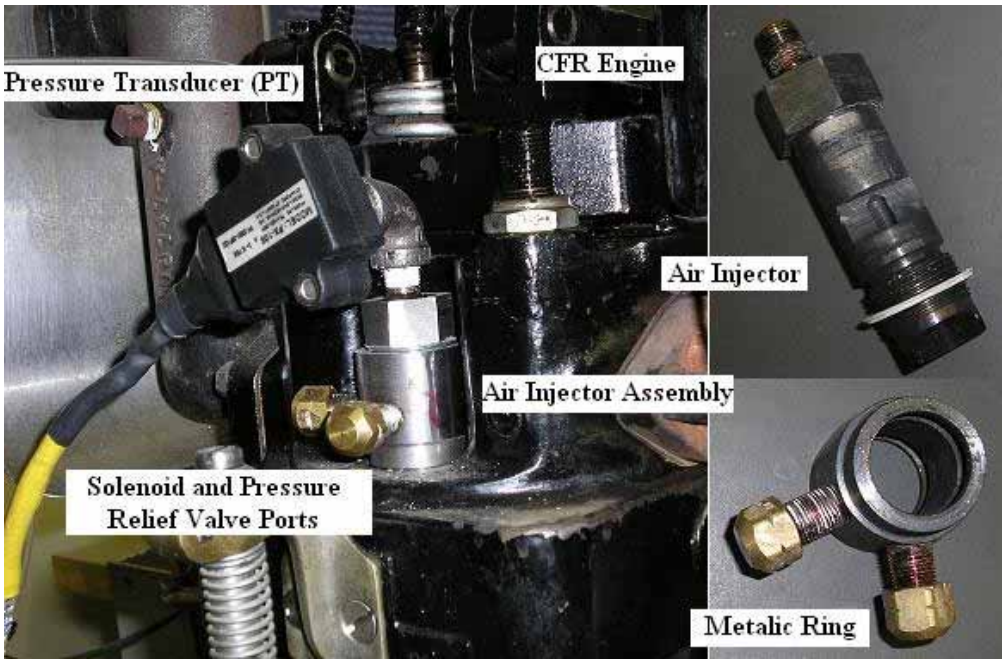

Figure 7.5 Air injector assembly installed in the CFR engine

This configuration allowed minimum modification of the CFR engine while providing secure and flexible access for air injection and data acquisition. This design was tested with the CFR engine, motored and fired for compression ratios ranging from 5:1 to 16:1 and under different operating conditions. The results of these tests indicated the need to incorporate a cooling system into the design of the air injector to prevent the pressure transducer (PT), solenoid valve, and pressure-relief valve from overheating. The air-injector design drawing is displayed in Appendix G.

The first air injector was modified (Figure 7.6) by adding a 1/8" copper water-cooling system and removing the pressure transducer (PT), solenoid valve and pressure-

relief valve NPT ports from the main body of the injector. This was accomplished by eliminating the external steel bushing.

The solenoid and pressure-relief valve were installed in series, and the air was discharged into the CFR combustion chamber through a 1/8”-1000 psig stainless steel tee installed between the air injector and pressure transducer (PT). This new design increased the engine clearance volume by 12 cc. The CFR engine was motored and fired under different operation conditions using the new air injector and air injection system, but it failed to produce auto-ignition. This was attributed to injecting cold compressed air from a bottle instead of high- pressure air, heated by compression as in patent disclosures.

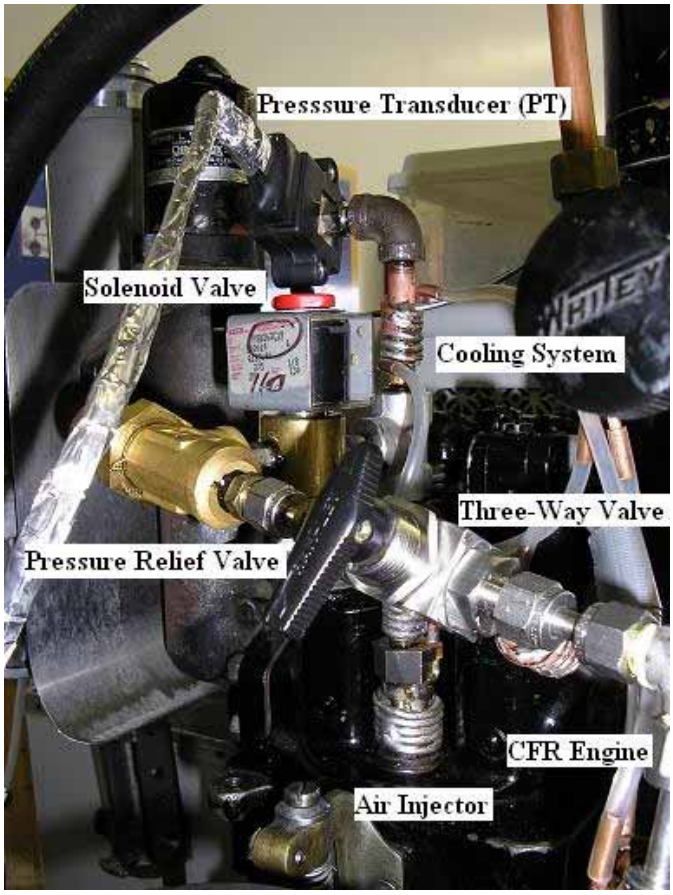

Figure 7.6 Modified air injector with cooling system

Injector Ball-Check Valve

The injector ball-check valve is an important component in the air-injection system. It prevents air from leaking into the cylinder after the air injection. This ball-check valve operates in a difficult environment since it is exposed to extremely high average temperatures (greater than 1000 ^{o}F) and high-pressure variations (0-1000 psig); thus its design requirement is tolerate these conditions.

The ball-check valve consists of a 5/8” NF adjusting screw, a 1-1/8” diameter steel rod of 4” long, a 9/16” OD by 1-5/32” long carbon steel helical spring of 5 windings of 1/8” diameter wire, a 3/8” diameter steel ball, and a 7/8” ID x 1-1/8” OD brass bushing of 3/8” long (Figure 7.7). The steel rod had a centered hole of 3/16” diameter to allow air flow from the solenoid valve to the combustion chamber, and a 1/8” diameter hole centered at 1/4" from the center, and with a 1/8” NPT connection located in its lateral side for the assembly of the water-cooled pressure adapter. The relief-pressure setting can be increased by turning the adjusting screw clockwise.

The adjusting screw has on one end a 1/8” NPT connection to attach the air-injection system, and a machined steel seat to press the steel ball against the helical spring on the other end. The adjusting screw has a 3/16” diameter hole to allow high-pressure hot air to flow from the air heater into the combustion chamber through the steel ball and helical spring when the solenoid has been actuated by the microcontroller, and the opening pressure has been reached.

The function of the brass bushing is to prevent leakage from the combustion chamber into the atmosphere and provide flexibility in assembling the air injection system. The air injection ball-valve check was tested using cold-air injection, while the

engine was motored and fired using different compression ratios. Minor leakage was detected at a 500 psig relief-pressure setting, therefore this was increased to 600 psig at which leakage was almost completely eliminated. The air injector ball-check valve met all the operation requirements during the first set of experiments.

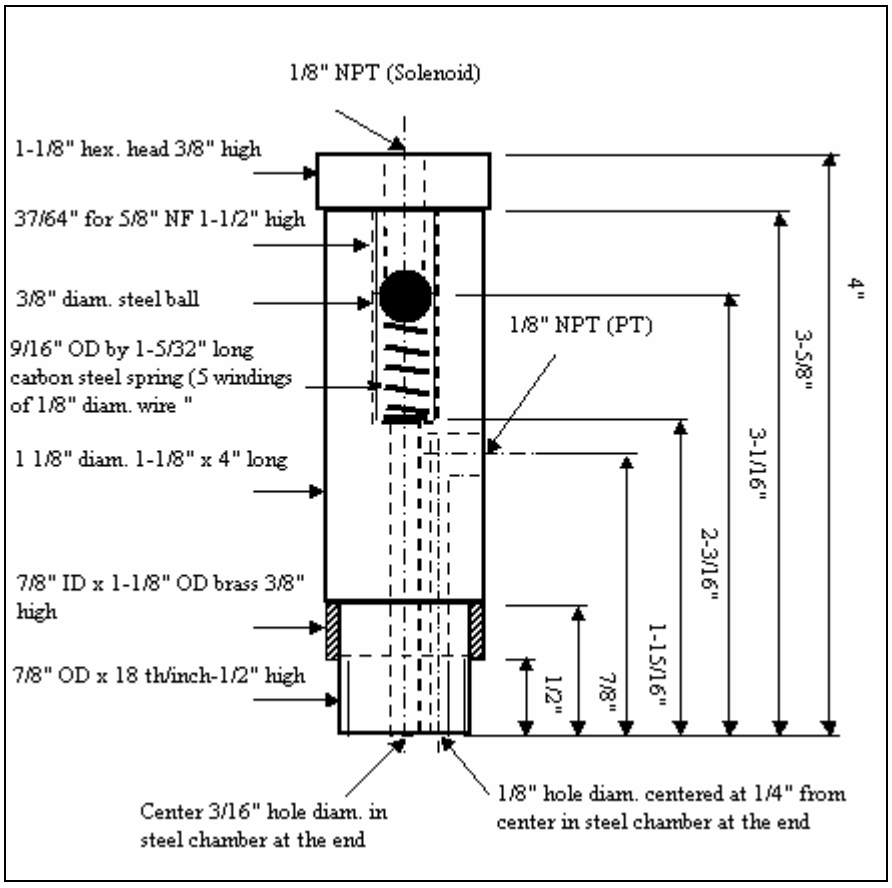

Figure 7.7 Injector ball check valve drawing

Additional details about the design of the cylinder air-injection valve are presented under the experimental set-up and procedures of this dissertation (Chapter 8).

Other mechanical designs done during the course of this research included a spark adapter (Appendix H) used for cold-air-injection tests, and a water-cooled, pressure-transducer adapter (Appendix I) to prevent the pressure transducer (PT) from overheating.

Chapter 8: Experimental Set-Up and Procedures

Overview

The main objective of the experimental work done during the course of this research was to closely simulate a CIBAI engine working under different operation conditions. After designing, building, and evaluating several air-injection systems as presented in Chapter 7, the experimental set-up displayed in Figure 8.1 was selected, and implemented for this study. The engine used for this research was a Cooperative Fuel Research (CFR) engine equipped with a high-pressure air-injection system, and fully instrumented for data acquisition purposes. The engine in-cylinder pressure history with its corresponding crank angle position was recorded while the engine was motored, fired, and operated under the CIBAI principle. The data collected is analyzed in Chapter 9 to provide a better understanding of the CIBAI combustion process. A detailed description of the experimental set-up and procedures are presented next.

Experimental Set-Up

The schematic diagram of the experimental set-up is illustrated in Figure 8.1. The experimental set-up for this research is shown in Figure 8.2. It consisted of five interrelated components: CFR engine, air-injection system, instrumentation, data acquisition system, and microcontroller unit. Each of these components was either modified, designed, built, or assembled during the course of this dissertation and are explained in detail in the following section.

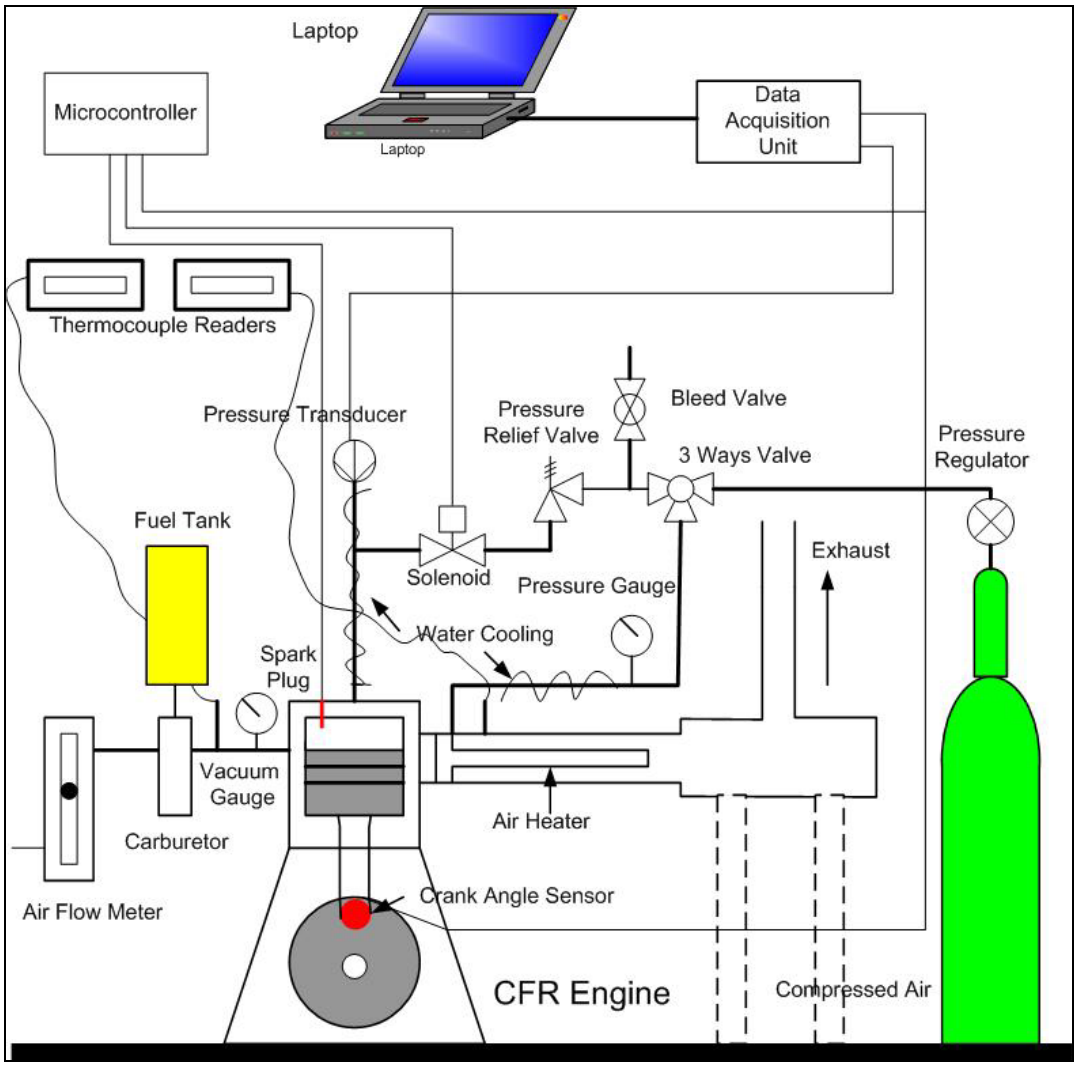

Figure 8.1 Schematic diagram of the experimental set-up

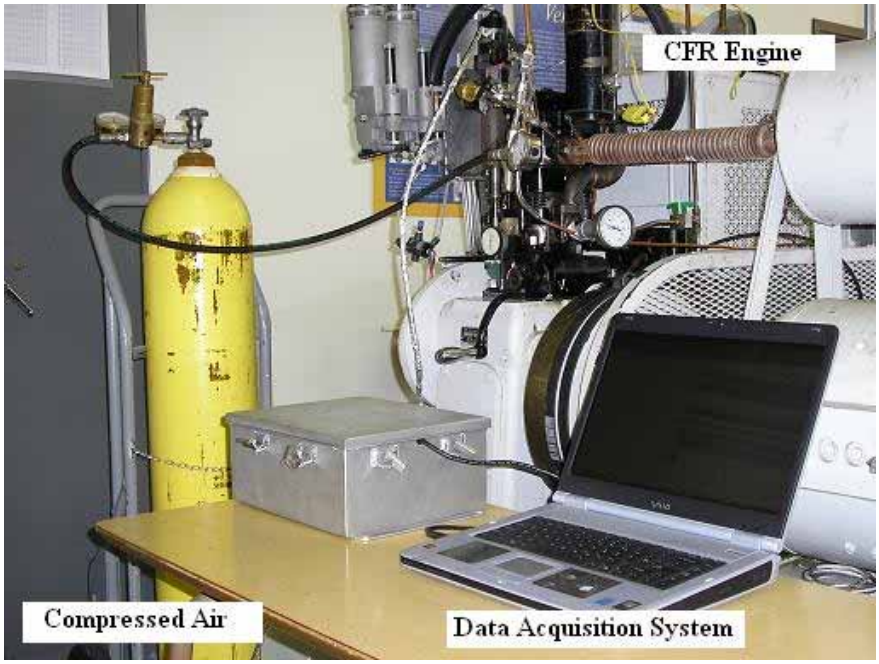

Figure 8.2 Experimental set-up

CFR Engine

The engine used in this project is a standard four-stroke, single-cylinder CFR F-2 (motor method octane rating unit) spark-ignition engine with variable compression ratio, manufactured by Waukesha Motor Company in 1957. The engine flywheel was connected by belt to a special power absorption motor. This motor starts the engine (motoring), absorbs the power output of the engine when the combustion takes place (firing), and maintains a constant engine speed of 900 +/-9 rpm. During firing the absorption motor operates as an alternator and the energy generated is introduced to the AC power system. The engine specifications are given in Table 8.1.

Table 8.1 WVU CFR engine specifications

Specification	English Units	International Units
Model	CFR-48 Crankcase	CFR-48 Crankcase
Octane Method Rating	Motor	Motor
Type	CFR F-2 Rating Unit	CFR F-2 Rating Unit
Engine Speed	900 rpm	900 rpm
Bore	3.25”	82.55 mm
Stroke	4.5”	114.2 mm
Displacement	37.33 cubic inches	612.5 cm^3
Compression Ratio (C.R.)	4:1 to 18:1	4:1 to 18:1
Ignition Timing	Variable	Variable

The main components of the CFR engine are shown in Figure 8.3.

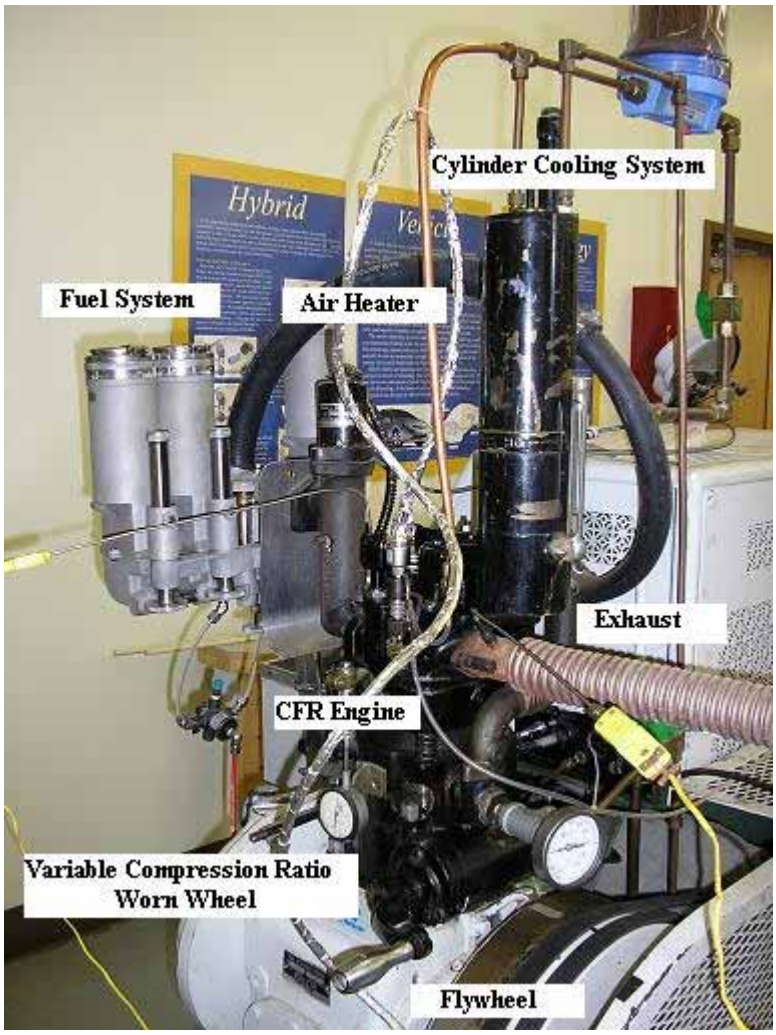

Figure 8.3 CFR engine main components

The CFR engine was equipped with a 1000 watt, 115 VAC, two-element mixture heater that was installed between the carburetor and the engine intake port. The mixture temperature was controlled through the CFR engine temperature controller.

The fuel supply system (Figure 8.4) consisted of three carburetor bowl/float chamber assemblies, mounted on an adjustment screw to increase or reduce the fuel level and thus change the air-fuel ratio. The carburetor assembly consisted of the carburetor body, a 9/16" throat diameter venturi jet, fuel selector, and fuel level sight glasses. The fuel used for all experiments was unleaded gasoline with an anti knock index (AKI) of 87.

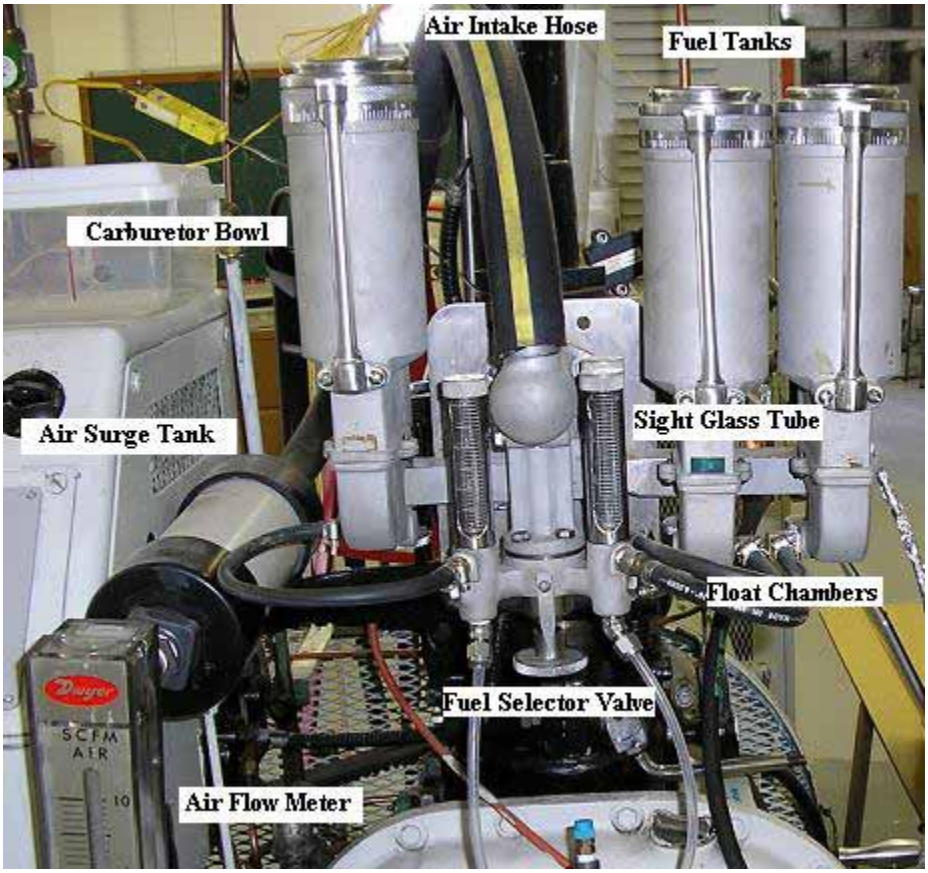

Figure 8.4 Air intake and fuel systems

The CFR cylinder cooling system was of the thermal-syphon, ebullient, recirculating jacket-cooling type. It consisted of a condenser body, condensing coil, coolant baffle, sight glass assembly, return pipe, cooling jacket, and coolant thermometer. Boiling coolant recirculates through the cooling jacket, and when contacted with the condensing coil, condensates and returns to the cylinder jacket creating a continuous loop. During firing operations the cylinder jacket coolant temperature was maintained around 212 ^{o}F.

Several modifications were made to the CFR engine to facilitate air injection into the combustion chamber and allow recording the in-cylinder pressure history. An air surge tank (Figure 8.4) was built using a standard 3" PVC pipe, installed upstream of the carburetor to make the intake-flow rate, steady enough to allow the use of an air-flow meter. The 7/8" diameter detonation pick-up transducer mounted on the top of the cylinder was removed and replaced by a 7/8" diameter, carbon steel, ball-type check valve as shown in Figure 8.5.

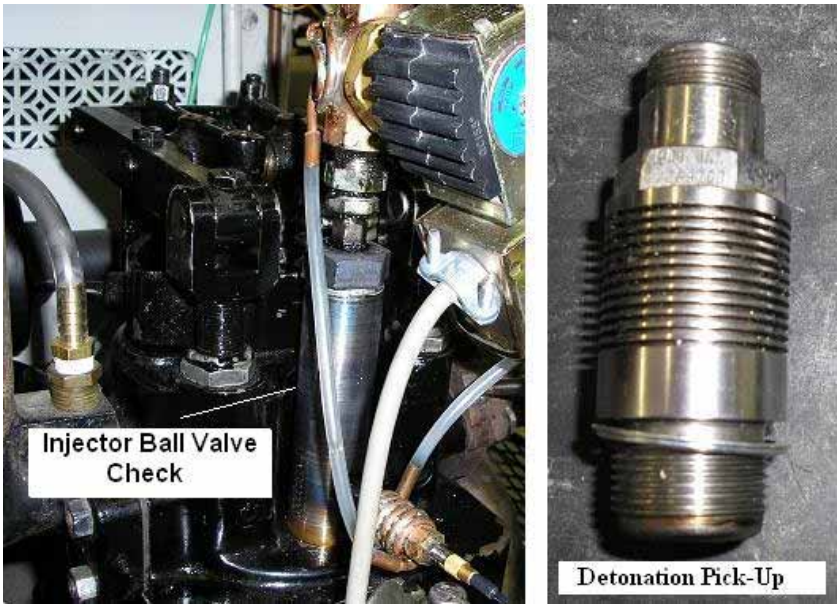

Figure 8.5 Injector ball-check valve and detonation pick-up sensor

Between the exhaust port and the flexible exhaust pipe an air heater was installed to heat the air charge prior to air injection into the cylinder. The air heater was built with a 1/4" by 1 ft long stainless steel schedule 40 pipe as illustrated in Figure 8.6.

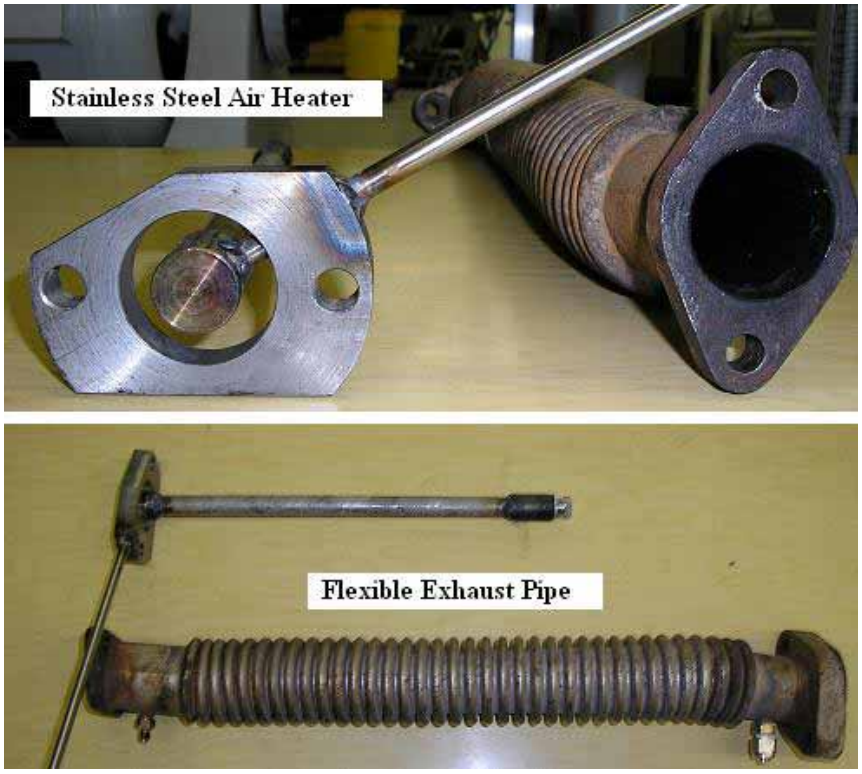

Figure 8.6 Air heater and flexible exhaust pipe

Air-Injection System

The objective of the air-injection system was to simulate the operating conditions of the second parallel cylinder containing air only, which was needed to run the engine under the CIBAI cycle as proposed by Loth and Morris [3,5]. In this research, the air-fuel cylinder was simulated by the CFR engine single cylinder while the air only cylinder was simulated by the air-injection system and its components.

The air-injection system consisted of the following main components: A 2000 psig compressed air bottle (Appendix C) that supplied the high pressure air into the air

heater; A 1/4” by 1ft long stainless steel air heater which contained the correct amount of air mass for injection at high pressure. A water-cooled 1/4”-115V brass solenoid valve (Appendix E) allows high pressure and temperature air to enter the combustion chamber when activated by a microcontroller. A 1/4"- 2500 psig stainless steel three (3) way ball valve (Appendix J) directed the air between the compressed air supply, air heater, and solenoid valve. A 1/8” copper pipe water-cooling system protected all three: ball valve, solenoid valve, and pressure transducer from overheating. A 7/8” carbon steel injector ball-check valve allowed the heated high pressure air to be injected into combustion chamber. The solenoid valve opening timing was controlled by the microcontroller. It was considered to add a 1/8” brass air-pressure-relief valve (Appendix K) with a pressure range 235-450 psig to prevent excess air from entering later in the cycle into the combustion chamber. The air-injection system is shown in Figure 8.7.

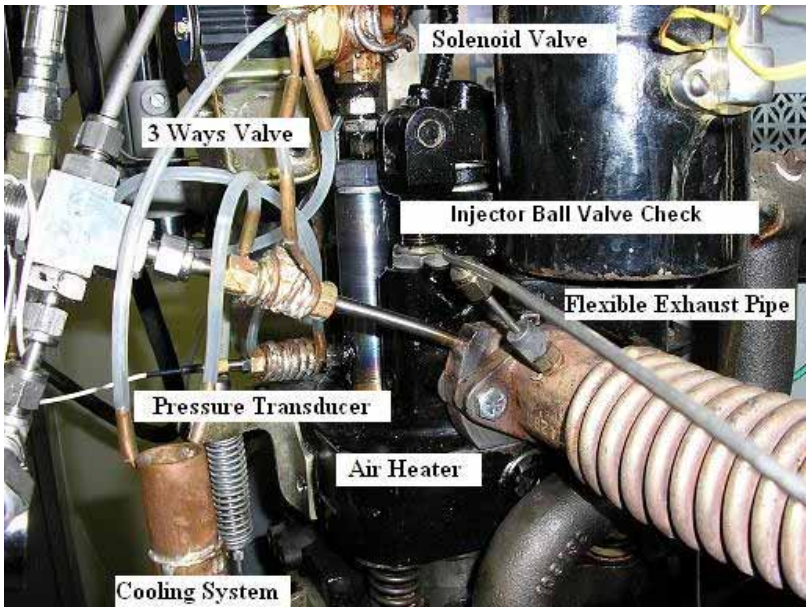

Figure 8.7 Air-injection system

Instrumentation

The CFR engine was fully instrumented so that the engine operating conditions could be monitored, as well as in-cylinder pressure history and crank angle, before and after air injection could be measured. It was essential during the experiments to have repeatability of the engine operations from test to test. Calibration information from all instruments was obtained either from the manufacturer of the particular instrument or generated in the laboratory. Figure 8.8 illustrates the schematic diagram of CFR engine instrumentation used in this research.

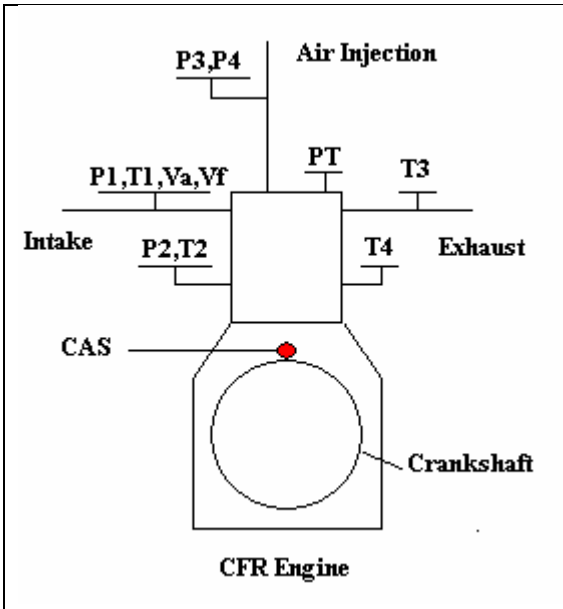

No.	INSTRUMENTATION NAME
P1	Intake Pressure Gauge
P2	Oil Pressure Gauge
P3	Pressure Regulator
P4	Charge Pressure Gauge
PT	In-Cylinder Pressure Transducer
CAS	Crank Angle Sensor
T1	Intake Thermocouple
T2	Oil Temperature Thermocouple
T3	Exhaust Temperature Thermocouple
T4	Coolant Temperature Thermometer
Va	Air Flow Meter
Vf	Fuel Glass Meter

Figure 8.8 Schematic diagram CFR engine instrumentation

Pressure Transducer (PT)

The engine in-cylinder pressure data were obtained with a water-cooled Dytran piezoelectric pressure transducer, mounted on the injector ball-check valve (Figure 8.5). The transducer preparation and calibration procedures described by Lancaster et al. (1975) were followed in this study. The pressure transducer (PT) required a 20 V

excitation, and output 0 V at 0 psig and 5 V at 1000 psig with a minimum rise time of input pressure pulse of 2 microseconds. The pressure transducer (PT) datasheet and calibration certificate are shown in Appendix L. The pressure signal was conditioned using a Kistler Piezotron coupler charge amplifier (Appendix M). The pressure data were acquired with a data acquisition system at a sampling rate of 10 KHz. Significant noise was present in the acquired pressure data despite extensive effort to eliminate it. These included battery power for all sensors, shielding wires, and metallic boxes for the data acquisition unit and microcontroller. Post-processing activities included low pass filters, smoothing techniques, and Fast Fourier Transform (FFT) spectral analysis.

Crank Angle Sensor (CAS)

The instantaneous volume of the cylinder as the piston moves from TDC to BDC was determined with the crank angle data obtained from a 5VDC magnetic switch. The CAS was installed on the left side of the CFR engine and above the ignition-timing shaft as shown in Figure 8.9. The magnetic bar was located at 410^{o} CA bTDC of the compression stroke.

TDC was determined using a dial indicator to indicate the highest point the piston traveled. This was verified with the TDC mark on the flywheel when the piston was at the highest position. The CAS rotated together with the ignition timing shaft, and sent an analog output to the data acquisition system by actuating the normally open (NO) contact when passing in front of the magnetic switch. The CAS required a 5VDC excitation and delivered a square wave with a lower limit of 0 V and an upper limit of 5 V at a rate of 1 pulse per 720^{o} CA degree of rotation. In addition, to determine the crank angle position

with respect to the TDC, the output of the CAS was also used for triggering the data acquisition system and microcontroller unit.

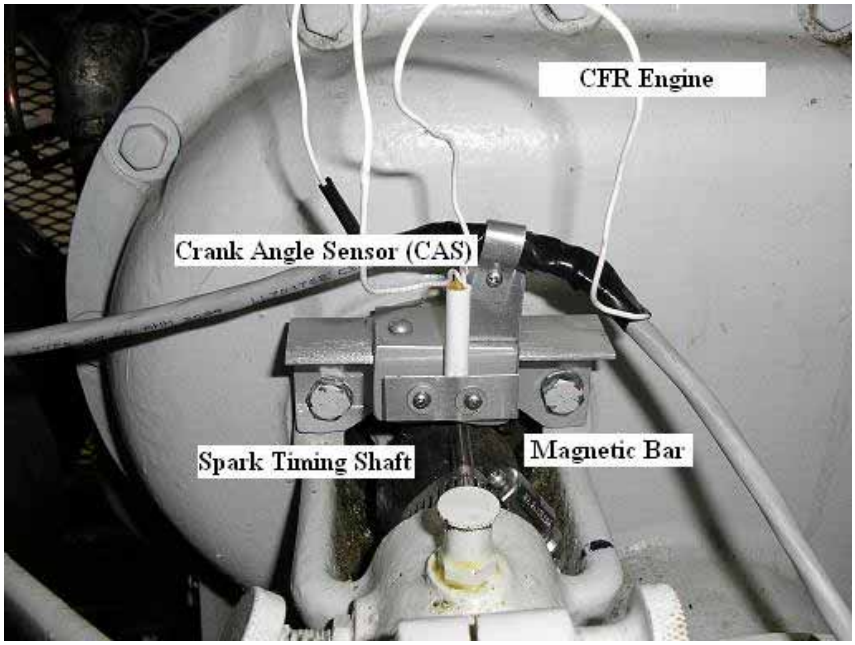

Figure 8.9 Crank angle sensor mounted on CFR engine

Intake Air Flow Rate, Pressure and Temperature

Intake air volumetric flow rate was monitored via a Dwyer float rotameter with a range of 0-10 +/- 0.1 SCFM that was attached to the air surge tank (Figure 8.4). The engine operated at a volumetric air flow rate of 7.0 SCFM. Simultaneously, the pressure and the temperature of the intake were monitored to determine the actual mass flow rate of the intake air using the ideal gas law equation of state.

Intake pressure was displayed on an analog USG vacuum with a range of 0-60 psig +/- 0.1 psig. Intake mixture temperature was monitored with a type K Omega thermocouple with a range of –208 to 2552 ^{o}F +/- 1 ^{o}F. The temperature signal was conditioned and displayed with an Omega 400B thermocouple reader.

Fuel Flow Rate

The fuel flow was measured volumetrically by marking known volumes on the sight glass located in the carburetor bowl (fuel tank). Time was measured using a stopwatch for the consumption of the known volume of fuel. With the known time and volume of the fuel, the volumetric flow rate was calculated.

Coolant and Exhaust Temperature

Exhaust temperature was monitored with a type K Omega thermocouple with a range of –208 to 2552 ^{o}F +/- 1 ^{o}F. The Signal was conditioned and displayed with an Omega 400B thermocouple reader. Cylinder jacket coolant temperature was monitored with a 82F ASTM thermometer with a range of 0-220 ^{o}F +/- 3 ^{o}F. Coolant temperature varied between 160 ^{o}F and 200 ^{o}F during the course of this research.

Oil Temperature and Pressure

Crankcase oil temperature and pressure were displayed on analog gauges mounted on the front of the CFR engine console instrument panel. Crankcase oil temperature was maintained at 135 ^{o}F through the engine temperature controller. Oil pressure was observed at 30 psig during all tests.

Ignition Timing

Ignition timing was monitored using a 12VDC strobe timing light with an inductive pick-up manufactured by Sears Roebuck and Co. The inductive pick-up was wrapped around the spark plug and the strobe light, oriented in front of a scaled plate, mounted on the top of the flywheel. The scaled plate was marked with crank angle degrees with respect to the TDC, and thus the match between the strobe light and the

scaled plate indicated the location of the spark timing when the spark plug was fired. The spark timing varied with the compression ratio.

The basic setting for the CFR engine was 26° CA bTDC at a compression ratio of 5.0. A Champion D-16 spark plug with a 0.020" gap was used for gasoline and spark plug test. The ignition timing of the engine running under normal conditions was employed as a reference to determine the optimal air-injection timing while the engine was running under the CIBAI mode.

Data Acquisition System

A data acquisition system was assembled to acquire and store the air-injection test data. The data acquisition system consisted of hardware and software components. The hardware components included the pressure transducer (PT) sensor, and the crank angle sensor (CAS), the data acquisition (DAQ) unit, the laptop, and data acquisition card. The software components included the DAQ-EZ Professional, V 1.17, and the Signal View, V 1.91 for data collection, and data post-processing techniques, such as signal filtering, smoothing, and FFT spectral analysis. The electric diagram of the data acquisition, and the data acquisition card datasheet are shown in Appendixes N and O respectively.

Microprocessor Unit

A microcontroller unit was developed in order to control the spark timing, injection timing, and injection duration of the CIBAI operation. The schematic diagram of the microcontroller unit is shown in Figure 8.10. The system consists of a Microchip Pic16F72 chip (Appendix P), electric source circuit, the trigger circuit, the air-injection circuit, and the circuit for controlling the spark ignition. The microcontroller unit program (Appendix Q) was written using the PicBasic Pro language. The process in the

microcontroller is described as follows: once the unit is triggered by a push button, it reads the delay time and injection duration signals from a pair of potentiometers installed within the unit and enters into a loop until the spark ignition signal is detected from a normally open (NO) magnetic sensor mounted on the spark-ignition distributor shaft.

Having sensed the spark ignition, the microcontroller outputs the spark-ignition control signal to actuate an external 110VAD/6VDC, normally open (NO) relay, installed between the spark-ignition distributor contact points and ground wire. This relay, when energized, grounds the spark to prevent the air-fuel mixture from igniting by spark ignition. After a programmed time delay has passed, the microcontroller sends an output signal to actuate a second external 110VAD/6VDC, normally open (NO) relay, to energize the normally closed solenoid valve and proceed with the air injection. Once the solenoid is energized, it remains open until the selected injection duration has expired. After this period, the microcontroller outputs a signal to restore the spark ignition and resets itself to wait for a new trigger signal to start the next air-injection cycle.

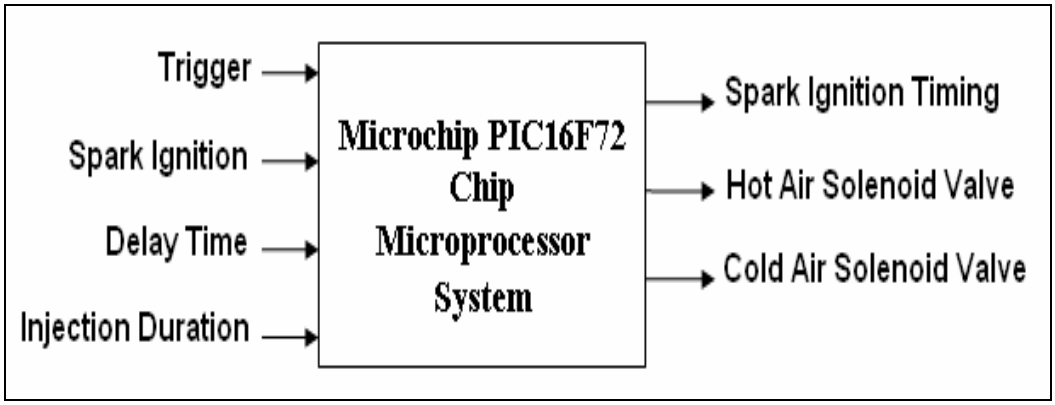

Figure 8.10 Schematic diagram of the microcontroller unit

The air injection strategy discuss above is shown in Figures 8.11, and 8.12.

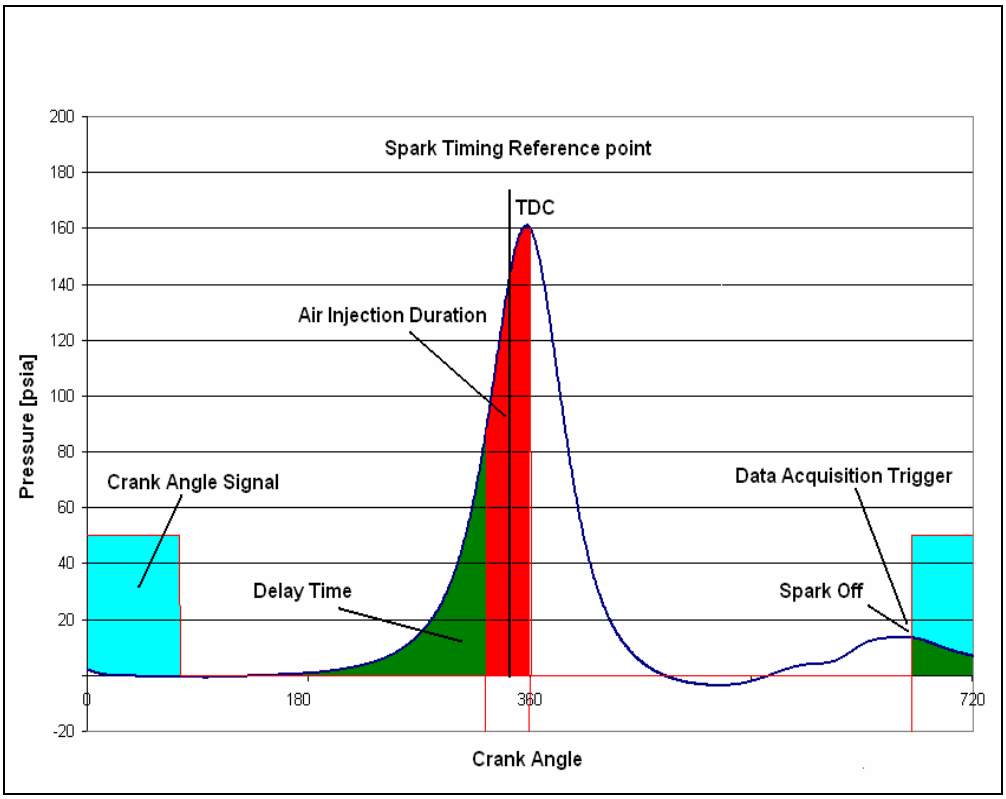

Figure 8.11 Air injection strategy controlled by a microcontroller unit

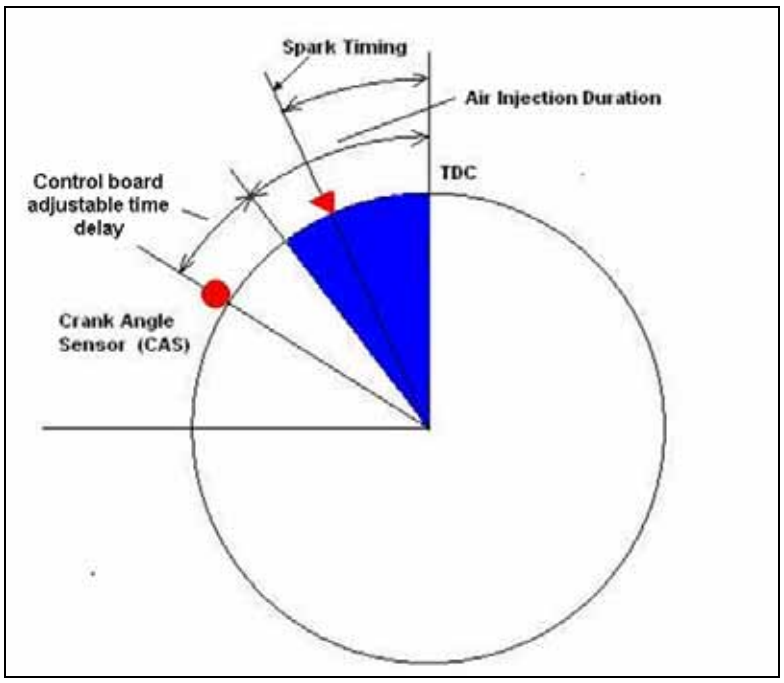

Figure 8.12 Air injection timing crank angle diagram

Engine Preparation

Before the start of the experimental work, the engine was given a complete overhaul, including a thorough cleaning of the carburetor, cylinder head, intake and exhaust manifolds, spark plug, etc. The pressure transducer (PT) and crank angle sensor (CAS) were calibrated, and the TDC was determined following the steps outlined before. A dial indicator was used to find the height between the piston and cylinder head for a given compression ratio. The cylinder-connecting valve (CCV) and pressure transducer (PT) were flush-mounted to the cylinder head (Figure 8.5). The flexible exhaust pipe was removed, and the air heater was inserted between the engine exhaust manifold and the exhaust flexible pipe (Figure 8.6). The solenoid valve, three-way ball valve, cooling system, and their corresponding plumbing were assembled (Figure 8.7), and a hydraulic test was taken to detect possible leakages. Liquid displacement was used to measure the added clearance volume due to the cylinder-connecting valve and pressure-transducer (PT) connection, and consequently the CFR engine variable compression ratio was adjusted to include the new clearance volume.

To conclude the engine preparation, the engine was motored, the pressure transducer (PT) was zeroed, and the in-cylinder pressure taken for compression ratios, ranging between 4.56:1 and 16:1. The intake manifold pressure, specific heat ratio (γ), and P-V diagram were obtained from the motored data.

Experimental Procedures

The experimental procedure is outlined next and corresponds to the actual CIBAI process while the engine was motored with a homogeneous air-fuel mixture. However, extensive experimental work was done prior to it, in which procedures differed

significantly from those presented here. Initial experiments included: Piston-cylinder assembly tests, knock tests, pressure tests without air injection while the engine was motored and fired, cold-air-injection tests with zero back pressure, and cold-air-injection tests while the engine was motored. These initial test results are discussed in the results and discussion section of this paper (Chapter 10).

The experimental procedures for the CIBAI auto-ignition testing are outlined as follows: after the engine preparation and instrumentation calibration were done, the microcontroller unit had been programmed, and the data acquisition system had been properly connected and tested, the CFR engine was motored and fired using the standard procedures outlined by ASTM [67]. While the engine was motored, the compression ratio (C.R) was adjusted to the one selected for the particular test. The carburetor bowl was filled with regular unleaded gasoline with an average knock index (AKI) of 87. The three-way valve was turned to allow regulated air to flow from the 2000 psig compressed air bottle into the air heater. The injection air pre-heater was filled with high-pressure cold air to a predetermined pressure.

The engine was fired by turning the ignition switch on and turning the fuel valve selector to the on-position of the carburetor being used. The fuel sight glass was kept at the level selected for the particular test, and the air flow rate was maintained at 7.0 SCFM. The engine was run at the operating conditions specified in Table 8.2 until the exhaust temperature achieved a steady state.

At this point, the three-way valve was turned to allow pre-heated high-pressure air to become connected to the solenoid valve. The ignition was then shut off and the microcontroller unit and data acquisition triggered. At this moment, the microcontroller

unit had complete control over the engine operation, data acquisition and air-injection processes. With the engine motored with the same operating conditions, a predetermined number of cycles of motored pressures were collected. The microcontroller then used the input data processed from the set of potentiometers installed in its unit to determine the ignition delay and air-injection timing, and proceeded to actuate the solenoid valve to allow high-pressure hot air into the cylinder through the injector ball-check valve.

Table 8.2 CFR engine operating conditions under CIBAI combustion

Fuel	Unleaded Gasoline AKI 87
Fuel Level (in)	0.5, 1.0, 1.5+/- 0.1
Intake Temperature (^{o}F)	70, 150, 250 +/- 5
Oil Temperature (^{o}F)	135 +/- 5
Oil Pressure (psia)	30 +/- 5
Coolant Temperature (^{o}F)	180 +/- 10
Exhaust Temperature (^{o}F)	600 +/- 15
Compression Ratio	7.0, 7.5, 8.0
RPM	900 +/- 9
Air Pre-heater Charging Pressure (psig)	700, 800, 900, 1000 +/- 20
Spark Plug Gap (in.)	0.020-0.025
Spark Timing (Fired)	Variable

If the conditions for self-ignition (e.g. temperature, pressure, and air-fuel ratio, turbulence, density) were met, the air-fuel mixture would auto-ignite, and CIBAI ignition and combustion would take place. After, the auto-ignition was completed, spark ignition was turned back on, and the engine continued to fire at the previous operation conditions. Data from a predetermined number of cycles before and after auto-ignition were collected. Finally, the standard stopping procedures suggested by ASTM [67] were followed to stop the engine. After the experimental work was concluded, the digitized pressure data were scaled, averaged, and analyzed.

This procedure was repeated for air-fuel mixture intake temperatures of 70 ^{o}F, and 250 ^{o}F, at compression ratios of 7.0:1, 7.5:1 and 8.0:1, fuel levels of 0.5 in, 1.0 in, and 1.5

in, air pre-heater charging pressure varied from 700 psig to 900 psig, and air-injection timing from 85°, 75°, and 65° CA bTDC. The experimental matrices for this study are presented next.

Experimental Matrices

The experiments for this research were divided into five matrices. These matrices described the experiments carried out to determine the effect of compression ratio, intake temperature, air pre-heater charging pressure, equivalence ratio, and air-injection timing with CIBAI combustion.

Matrix 1: The Effect of Compression Ratio on CIBAI Combustion

The effect of compression ratio on CIBAI combustion was experimentally studied by increasing the compression ratio from 7.0:1 to 8.0:1 in increments of 0.5, while the engine speed, intake temperature, exhaust temperature, equivalence ratio, air flow rate, and air pre-heater charging pressure were maintained constant. In-cylinder pressure data were recorded and analyzed for motored, fired, and CIBAI combustion. Matrix 1 is shown in Table 8.3.

Matrix 2: The Effect of Intake Temperature on CIBAI Combustion

The effect of intake temperature on CIBAI combustion was experimentally studied by increasing the air-fuel mixture intake temperature from 70 to 250 °F, while the engine speed, compression ratio, exhaust temperature, air flow rate, air pre-heater charging pressure, equivalence ratio, and air-injection timing were maintained constant. In-cylinder pressure data were recorded and analyzed for motored, fired, and CIBAI combustion. Matrix 2 is shown in Table 8.4.

Matrix 3: The Effect of Air Pre-heater Charging Pressure on CIBAI Combustion

The effect of air pre-heater charging pressure on CIBAI combustion was experimentally studied by varying the charging pressure from 700 to 900 psig in increments of 100 psig, while the engine speed, compression ratio, intake temperature, exhaust temperature, fuel level, air flow rate, equivalence ratio, and air-injection timing were maintained constant. In-cylinder pressure data were recorded and analyzed for motored, fired, and CIBAI combustion. Matrix 3 is shown in Table 8.5.

Matrix 4: The Effect of Equivalence Ratio on CIBAI Combustion

The effect of equivalence ratio on CIBAI combustion was experimentally studied by changing the equivalence ratio (Φ) from 0.45 to 0.65 in increments of 0.15, while the engine speed, compression ratio, intake temperature, exhaust temperature, air flow rate, air pre-heater charging pressure, and air-injection timing were maintained constant. In-cylinder pressure data were recorded and analyzed for motored, fired, and CIBAI combustion. Matrix 4 is shown in Table 8.6. A sample calculation for air-fuel and equivalence ratios is shown in Appendix R.

Matrix 5: The Effect of Air-Injection Timing on CIBAI Combustion

The effect of air-injection timing on CIBAI combustion was experimentally studied by changing the air-injection timing from 85 to 65° CA bTDC in decrements of 10°, while the engine speed, compression ratio, intake temperature, exhaust temperature, air flow rate, air pre-heater charging pressure, equivalence ratio, and air-fuel ratio were maintained constant. In-cylinder pressure data were recorded and analyzed for motored, fired, and CIBAI combustion. Matrix 5 is shown in Table 8.7.

Table 8.3 Experimental matrix 1: effect of compression ratio in CIBAI combustion

	Test 1	**Test 2**	**Test 3**
Variable Parameter Compression Ratio	C.R =7.0	C.R =7.5	C.R. =8.0
Fixed Parameters RPM	900 +/- 9	900 +/- 9	900 +/- 9
Intake Temperature (^{o}F)	70 +/- 5	70 +/- 5	70 +/- 5
Exhaust Temperature (^{o}F)	600 +/- 15	600 +/- 15	600 +/- 15
Equivalence Ratio (Φ)	0.50 +/- 0.01	0.50 +/- 0.01	0.50 +/- 0.01
Air Flow Rate (SCFM)	7 +/- 0.1	7 +/- 0.1	7 +/- 0.1
Air Pre-heater Charging Pressure (psig)	800 +/- 10	800 +/- 10	800 +/- 10
Air Injection Timing (° CA bTDC)	75 +/- 0.5	75 +/- 0.5	75 +/- 0.5

Table 8.4 Experimental matrix 2: effect of intake temperature in CIBAI combustion

	Test 4	**Test 5**
Variable Parameter Intake Temperature (^{o}F)	70 +/- 5	150 +/- 5
Fixed Parameters RPM	900 +/- 9	900 +/- 9
Compression Ratio	C.R =8	C.R =8
Exhaust Temperature (^{o}F)	600 +/- 15	600 +/- 15
Equivalence Ratio (Φ)	0.50 +/- 0.01	0.50 +/- 0.01
Air Flow Rate (SCFM)	7 +/- 0.1	7 +/- 0.1
Air Pre-heater Charging Pressure (psig)	800 +/- 10	800 +/- 10
Air Injection Timing (° CA bTDC)	75 +/- 0.5	75 +/- 0.5

Table 8.5 Experimental matrix 3: effect of air charged pressure in CIBAI combustion

	Test 6	**Test 7**	**Test 8**
Variable Parameter Air Pre-Heater Charging Pressure (psig)	700 +/- 10	800 +/- 10	900 +/- 10
Fixed Parameters Compression Ratio	C.R =8	C.R =8	C.R =8
RPM	900 +/- 9	900 +/- 9	900 +/- 9
Intake Temperature (^{o}F)	70 +/- 5	70 +/- 5	70 +/- 5
Exhaust Temperature (^{o}F)	600 +/- 15	600 +/- 15	600 +/- 15
Equivalence Ratio (Φ)	0.50 +/- 0.01	0.50 +/- 0.01	0.50 +/- 0.01
Air Flow Rate (SCFM)	7 +/- 0.1	7 +/- 0.1	7 +/- 0.1
Air Injection Timing (° CA bTDC)	75 +/- 0.5	75 +/- 0.5	75 +/- 0.5

Table 8.6 Experimental matrix 4: effect of equivalence ratio in CIBAI combustion

	Test 9	Test 10	Test 11
Variable Parameter Equivalence Ratio (Φ)	0.65 +/- 0.01	0.50 +/- 0.01	0.45 +/- 0.01
Fixed Parameters Compression Ratio	C.R =8	C.R =8	C.R =8
RPM	900 +/- 9	900 +/- 9	900 +/- 9
Intake Temperature (^{o}F)	70 +/- 5	70 +/- 5	70 +/- 5
Exhaust Temperature (^{o}F)	600 +/- 15	600 +/- 15	600 +/- 15
Air Pre-heater Charging Pressure (psig)	800 +/- 10	900 +/- 10	1000 +/- 10
Air Flow Rate (SCFM)	7 +/- 0.1	7 +/- 0.1	7 +/- 0.1
Air Injection Timing (° CA bTDC)	75 +/- 0.5	75 +/- 0.5	75 +/- 0.5

Table 8.7 Experimental matrix 5: effect of air injection timing in CIBAI combustion

	Test 12	Test 13	Test 14
Variable Parameter Air Injection Timing (° CA bTDC)	85 +/- 1.0	75 +/- 1.0	65 +/- 1.0
Fixed Parameters Compression Ratio	C.R =8	C.R =8	C.R =8
RPM	900 +/- 9	900 +/- 9	900 +/- 9
Intake Temperature (^{o}F)	70 +/- 5	70 +/- 5	70 +/- 5
Exhaust Temperature (^{o}F)	600 +/- 15	600 +/- 15	600 +/- 15
Equivalence Ratio (Φ)	0.50 +/- 0.01	0.50 +/- 0.01	0.50 +/- 0.01
Air Flow Rate (SCFM)	7 +/- 0.1	7 +/- 0.1	7 +/- 0.1
Air Pre-Heater Charging Pressure (psig)	800 +/- 10	800 +/- 10	800 +/- 10

Chapter 9: Data Analysis

Overview

Engine in-cylinder pressure and volume data in combination with thermodynamic principles and ideal gas law are fundamental for a combustion study. In-cylinder pressure data are used to study ignition, auto-ignition, knock phenomena, and cycle-to-cycle variations among others. Pressure measurement data are also used to determine peak pressure, indicated work, engine friction, pumping losses, and to compare experimental pressures with the pressures calculated by combustion models.

In this study, the CFR engine in-cylinder pressure was used to calculate the following parameters: indicated work, indicated mean effective pressure (IMEP), temperature history, heat release rate, mass fraction burned (MFB), ignition delay (ID), and combustion interval. A computer program was developed to carry out the necessary calculations. This computer program used numerical integration methods, thermodynamic principles, and the ideal gas law in order to compute these parameters.

The preparation and calibration of the piezoelectric system used in these experiments were done using the procedure outlined by Lancaster et al. [68]. The combustion characterization of engine pressure data was done using the heat release model, developed by Gatowski et al. [69], and Woschni [70], and the mass fraction burned (MFB) equation, presented by Rassweiler and Withrow [71].

In-Cylinder Pressure History

Most of the pressure data in this research were taken with a water-cooled Dytran pressure transducer Model 2201V1 (Appendix L), and the signal was amplified using a Kistler Piezotron charge amplifier (Appendix M). The correlation between the time-

pressures history with the cylinder volumes was done using an electromagnetic crank-angle sensor (Figure 8.10), as described in the experimental set-up section of this paper. The total cylinder volume associated with each crank angle was calculated by adding the volume, associated with the displacement of the piston, and the clearance volume, associated with the selected compression ratio. The volume generated by the piston motion was calculated from the physical dimensions of the engine, and the crank angle was calculated using Equation 9.1 [72]

$$V = V_c + \frac{\pi b^2}{4}\left[\frac{s}{2}(1-\cos\theta) + l - \sqrt{l^2 - \frac{s^2}{4}\sin^2\theta}\right] \tag{9.1}$$

where:

V = Total volume inside the cylinder
V_c = Clearance volume
B = Engine bore
S = Engine stroke
L = Connecting rod length
θ = Crank angle measured from TDC.

Work

In an internal combustion (IC) engine work is produced by the gas pressure in the combustion chamber, acting on the face of the piston as the engine moves through the entire cycle. The work produced by an IC engine is represented by the following equation:

$$W = \int P dV \tag{9.2}$$

where:

P= Pressure in combustion chamber
dV= Differential volume displaced by the piston.

The net work done by the fluid on the piston (net indicated work) is greater than the work done at the output shaft (brake work). This difference is due to the mechanical friction and parasitic loads, which are not included in the calculation of the net indicated work. The brake work is given by:

$$W_b = Wi - W_f \tag{9.3}$$

where:

W_b = Brake work
W_i = Net indicated work
W_f = Work lost due to friction and parasitic load.

Figure 9.1 shows a typical P-V diagram for the Otto cycle. The upper loop represents the gross indicated work, produced during the compression and expansion strokes while the lower loop represents the pump work, absorbed from the engine during the intake and exhaust strokes. The net indicated work is calculated as follows:

$$Wi = W_{gross} + W_{pumping} \tag{9.4}$$

where:

W_i = Net indicated work
W_{gross} = Gross indicated work
W_{pump} = Pump work.

The pump work is positive when the intake pressure is greater than the exhaust pressure (i.e. supercharged or turbocharged engines), and is negative when the intake pressure is less than the exhaust pressure.

The net indicated work can be obtained through numerical integration using the engine in-cylinder pressure data and its corresponding volume data given by the crank angle during the piston motion.

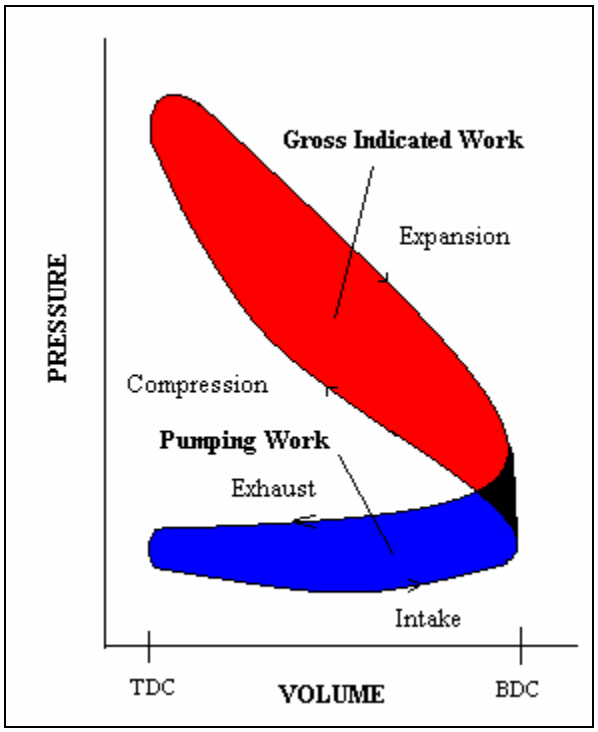

Figure 9.1 Otto cycle p-v diagram

For this study the numerical integration method proposed by Lancaster et al. [68] was used.

By definition:

$$Work = \int_{\theta 1}^{\theta 2} PdV = \int_{\theta 1}^{\theta 2} P\frac{dV}{d\theta}d\theta \tag{9.5}$$

Equation 9.5 can be closely approximated by:

$$Work = \sum_{\theta 1=\theta 1}^{\theta 2} P(\theta)_i \frac{dV}{d\theta}(\theta)_i \Delta\theta \tag{9.6}$$

where:

P(θ)I	= Instantaneous pressure at a given crank angle (θ)
dV(θ)i/d(θ)	= Instantaneous differential volume with respect to the crank angle (θ)
Δθ	= Crank angle sampling variation.

Mean Effective Pressure

The mean effective pressure (MEP) is defined as the theoretical pressure needed to produce a work equal to the type of work done by the gas pressure on the piston per unit, volume per cycle. The MEP is independent of engine size and speed, and thus it is a good parameter to compare engines of different size. The MEP is calculated by integrating the pressure-volume curve inside the cylinder and dividing by the cylinder volume displacement:

$$W = \frac{1}{\pi b^2 s} \int P dV \tag{9.8}$$

or

$$MEP = W / Vd \tag{9.9}$$

where:

MEP = Mean effective pressure
W = Work of one cycle
Vd = Volume displacement.

The mean effective pressure is calculated according to the work segment considered. This gives indicated pumping, brake, and friction mean effective pressures among others. The indicated mean effective pressure (IMEP) was of particular interest for this study. The IMEP represents the net result between the work done by the gases on the piston motion during the expansion stroke and the work absorbed during the compression stroke. The IMEP can be calculated from the in-cylinder pressure data using numerical integration and is given by:

$$IMEP = \frac{1}{\pi B^2 S} \sum_{i}^{j} \frac{1}{2} \left(P(\theta)_{i+1} + P(\theta)_i \right) \left(V(\theta)_{i+1} - V(\theta)_i \right) \tag{9.10}$$

where:

i = Start at BDC before the compression stroke
j = End at BDC after the expansion stroke
$P(\theta)_{i+1}$ = Instantaneous pressure at a crank angle $(\theta)_{i+1}$
$P(\theta)_i$ = Instantaneous pressure at a crank angle $(\theta)_i$
$V(\theta)_{i+1}$ = Instantaneous volume at a crank angle $(\theta)_{i+1}$
$V(\theta)_i$ = Instantaneous volume at a crank angle $(\theta)_I$

Heat Release Rate

The heat release is defined in the literature as the amount of heat that would have to be added to the cylinder contents to produce the measured pressure variations due to combustion of the air-fuel mixture. The heat release rate provides a way to characterize the combustion process within the engine combustion chamber. The heat release rate is obtained using the in-cylinder pressure and crank angle data in combination with the ideal law gas and thermodynamic principles.

The heat release rate is approximated by treating the combustion chamber as a closed system of varying volume and neglecting heat transfer effects to the walls and flows into and out of crevices volumes in the combustion chamber. These assumptions provide significant margin of errors in the final calculation of the heat release rate, and thus analysis based on these results has to be examined in that context. The heat-release rate equation is developed as follows:

The change in pressure during the combustion process is assumed to be the sum of the pressure change due to the piston motion and the pressure change due to the combustion of the air-fuel mixture. This can be calculated using Equation 9.11.

$$\Delta P = \Delta P_M + \Delta P_C \tag{9.11}$$

where:

ΔP = Total change in pressure during the combustion process
ΔP_M = Change in pressure due to the piston motion
ΔP_C = Change in pressure due to the combustion process.

Assuming a constant specific heat ratio (γ) as proposed by Gatowski et al. [69], and using the polytropic process relations, the ideal gas law, the continuity equation, the conservation of energy principle for a closed system, and the in-cylinder pressure and crank angle data, the heat-release rate equation is obtained:

$$\frac{dQ_{HR}}{d\theta} = \frac{V_\theta + \Delta\theta}{(\gamma - 1)\Delta\theta}(P_{\theta+\Delta\theta} - P_\theta\left[\frac{V_\theta}{V_\theta + \Delta_\theta}\right]^\gamma) \tag{9.12}$$

where:

$\frac{dQ_{HR}}{d\theta}$ = The net heat release rate per crank angle degree (θ)
$P_{\theta+\Delta\theta}$ = Pressure at crank angle (θ+Δθ)
P_θ = Pressure at crank angle (θ)
$V_{\theta+\Delta\theta}$ = Volume at crank angle (θ+Δθ)
V_θ = Volume at crank angle (θ)
γ = Specific heat ratio ≈ 1.35 [69].

In this study, the beginning of combustion was set to the crank angle, corresponding to the first negative or zero value for the heat release preceding the maximum release rate. In the same way, the end of combustion was set to the crank angle corresponding to the first negative or zero value for heat release following the maximum heat release.

Mass Fraction Burned (MFB)

The mass fraction burned (MFB) is a measurement of how fast the charge is burned during the combustion process. MFB is obtained from the heat release data by assuming that the heat added to the combustion chamber is proportional to the amount burned. Numerically, it is calculated by integrating the heat release curve up to the point of interest and dividing the result by the total heat release [71], and it is given by:

$$MFB = \frac{\sum_{i=BC}^{P} \left(\frac{dQ_{HR}}{d\theta} \right)}{\sum_{i=BC}^{EC} \left(\frac{dQ_{HR}}{d\theta} \right)} \tag{9.13}$$

where:

BC = Beginning of combustion
EC = End combustion
P = Point of calculation of the MFB.

Typical values for MFB will range from 0% to 100%.

Ignition Delay (ID)

Normally, the ignition delay, $\Delta\theta_{ID}$, for spark ignited (SI) engines is defined as the time between the spark discharge and the time a 10% MFB. In compression ignited (CI) engines the ignition delay, $\Delta\theta_{ID}$, is defined as the time between the start of injection and the onset of combustion. For CIBAI combustion, the ignition delay, $\Delta\theta_{ID}$, has been defined as the crank angle interval between the opening of the cylinder-connecting valve (CCV) and 10% MFB.

Combustion Duration

The combustion duration is an important parameter for the operation of internal combustion (IC) engines. The combustion duration, $\Delta\theta_{CI}$, is defined as the crank angle

required to burn the bulk of the engine charge, and it is usually taken as the difference between crank angles corresponding to 10% MFB and 90% MFB [1]. The ignition delay and combustion interval are also obtained from the heat release data.

Chapter 10: Results and Discussion

Overview

Prior to the actual tests on ignition by air injection (CIBAI) using the CFR engine, preliminary experiments were conducted to create a profile of the operating conditions of the CFR engine, and determine the optimal design for the air-injection system. These experiments were divided into four groups: knock, volumetric, cold-air injection, and compression-pressure tests. These experiments were then followed by the actual ignition by air-injection (CIBAI) tests, using the experimental set-up and procedures outlined in Chapter 8.

After that, the digitized in-cylinder pressure and its corresponding cylinder volume data were scaled to absolute level, and processed using spectral analytical tools. The processed data were then input into a computer program (Appendix A) to be integrated numerically to conduct a parametric study of the ignition by the air-injection (CIBAI) process. The computer program calculated the indicated work, indicated mean effective pressure (IMEP), net heat release, net-heat-release rate, mass fraction burned (MFB), ignition delay (ID), and combustion interval. The results of this experimental work are discussed next.

Experimental Results

Knock Data

The objective of these tests was to determine the onset of the knock to evaluate the incidence of the compression ratio, intake temperature, and spark timing on the appearance of the knock for a particular fuel type and air-fuel mixture. The onset of knock was checked for the CFR engine running under different compression ratios and

operating conditions. The fuel used was unleaded gasoline with an average knock index (AKI) of 87. The engine was run at 900 rpm until the exhaust temperature reached steady state (around 1000 ^{o}F). At that point, the compression ratio gradually increased until audible knock was detected. Using an intake temperature of 120 ^{o}F and a spark timing of 5^{o} CA bTDC, the audible knock was perceived for compression ratios greater than or equal to 12.51:1. When the CFR engine was run with an intake temperature of 400 ^{o}F (using the intake heater) and a spark timing of 15^{o} CA bTDC, the audible knock was detected at a compression ratio of 11:1.

The knock tests showed that increasing the temperature of the engine charge by raising the compression ratio, raising the inlet air temperature, and advancing the spark timing increased the possibility of the knock in the SI engine. The CFR engine operating conditions used during the knock tests are summarized in Table 10.1.

Table 10.1 CFR engine operating conditions during knock testing

Engine Parameter	**Specification**
Fuel	Unleaded Gasoline AKI 87
Fuel Level (in)	1.0 +/- 0.1
Intake Temperature (^{o}F)	70, 150, 250, 400 +/- 5
Oil Temperature (^{o}F)	135 +/- 5
Oil Pressure (psia)	30 +/- 5
Coolant Temperature (^{o}F)	180 +/- 10
Exhaust Temperature (^{o}F)	900 +/- 15
Compression Ratio	Variable from 7.0 to16.0 in increments of 0.5
RPM	900 +/- 15

Volumetric Data

Volumetric tests were conducted using the cylinder-piston arrangement discussed in Chapter 7. The main objectives were to determine the discharged time of the 1/8" solenoid valve and evaluate the mass, injected into the CFR simulator for different charged, amplified, and back pressures. The charged pressure was varied between 30 psig

and 100 psig, and the back pressure from 0 to 150 psig, while the amplified pressure value was kept constant. The amplified pressure was changed from 40 psig to 400 psig. Several important findings were obtained from this experimental work. The maximum pressures for high amplified pressures (200-400 psig) were obtained for a discharged time lasting approximately 40 ms. For low amplified pressures (<200 psig), the maximum pressures were obtained for a discharged time around 150 ms. The discharged time reached with the cylinder-piston assembly was very slow, and thus the system was considered unsuitable to be used as the simulated-air-only cylinder of the CIBAI engine. During the ignition by air-injection (CIBAI) experiment, the CFR engine ran at 900 rpm, and completed a thermodynamic cycle in 133 ms. Air injection was done around 75^{o} CA bTDC for an injection time of 15 ms to achieve maximum compression heating near TDC, and therefore a fast air-injection system was required.

The low response time of the cylinder-piston assembly can be attributed to high friction between the cylinder and piston surface, and/or the large masses of the piston, and solenoid valve actuator.

The volumetric data also indicated the possibility of measuring and injecting a particular amount of air for predetermined initial conditions without affecting the integrity of the engine and/or operator. An average volume fluctuating between 500 and 600 cc of standard air was injected into the measured device for amplified pressures ranging from 80 to 160 psig. These results closely agreed with the initial conditions predicted for the CIBAI combustion test as calculated in Chapter 7.

Cold Injection Data

Cold injection tests were conducted to verify the time response of the actual air-injection system as explained in Chapter 8. For these tests, the spark plug was removed and replaced by a spark plug adaptor (Appendix H), which was used to bleed air into the atmosphere after each test. The compression ratio was then selected, and the air-injection system pressurized for the predetermined air pre-heated charging pressure. After that, the pressure transducer was zeroed and the data acquisition triggered as explained in the experimental set-up (Chapter 8) of this dissertation.

Peak pressure after injection was obtained around 72 ms for all charged pressures tested. This may indicate that the time to reach the maximum pressure does not depend on the charging pressure, but on the response time of the solenoid valve. The information obtained with the cold-injection experiments was fundamental to define the air-injection strategy to control auto-ignition by air injection (CIBAI) using the CFR engine. The air-injection strategy will be discussed later in this chapter.

Compression Pressure Data

In-cylinder pressure data were taken while the CFR engine was motored for different compression ratios and operating conditions. The motored data were then used to check for leakages, verify the calibration of all instruments, determine the intake absolute pressure, estimate the polytropic exponent (n), and check the experimental procedures. The pressure data were also used to verify the phasing of pressure with respect to volume. This was done by verifying the curve pressure-crank near the peak pressure. Normally, the peak pressure occurs near the TDC (1° or 2° CA bTDC) due to irreversibilities mainly by heat transfer [68].

No major leakages were observed during the compression tests. Minor leakages were present in the air-injection system, but they were corrected before the actual air injection. A polytropic exponent (n) between 1.23 and 1.35 was obtained using a logarithmic P-V diagram with the same set of motored data. The numbers obtained closely agreed with the data obtained by previous researchers [68,69]. For this work, a polytropic exponent (n) corresponding to a specific heat ratio (γ) of 1.35 was used for all calculations.

The pressure data did not show a significant shifting with respect to the volume data (<0.5° CA), which were assumed to be acceptable for the current experimental set-up. The intake absolute pressure reading during the compression test was 10.1 psia for the engine running with the flow meter and 11.1 psia without the flow meter. The pressure drop can be attributed to friction and minor losses (pumping losses) due to the flow meter, air surge tank, and intake pipe fittings.

Fired Data

The CFR engine in-cylinder pressure data were digitized and processed for a number of cycles during CIBAI test. This was done in order to compare both, spark ignition, and CIBAI ignition, combustion parameters for the same operating conditions, and determine the net benefits of ignition by air-injection (CIBAI) combustion over sparked ignited combustion. The CFR engine operating conditions used in these experiments are summarized in Table 10.2.

During spark ignition (SI) testing, the CFR engine was fired using a Champion D16 spark plug, and the CFR engine conventional ignition system. This system consisted

of an ignition power supply, an ignition switch, ignition coil, a housing containing the breaker, a spark plug, and high-tension spark wire.

Table 10.2 CFR engine operating conditions during firing testing

Engine Parameter	Specification
Fuel	Unleaded Gasoline AKI 87
Fuel Level (in)	0.5, 1.0, 1.5 +/-0.1
Intake Temperature (^{o}F)	70, 150, 250 +/- 5
Oil Temperature (^{o}F)	135 +/-5
Oil Pressure (psia)	30 +/-5
Coolant Temperature (^{o}F)	180 +/-10
Exhaust Temperature (^{o}F)	600 +/-15
Compression Ratio	7.0 to 12.0
RPM	900 +/- 15
Spark Timing	Variable

The spark timing was automatically adjusted as the compression ratio changed from 4.54:1 to 16:1. The change in spark timing with compression ratio is shown in Table 10.3. These numbers were verified using a strobe light as described in the experimental set-up section of this paper (Chapter 8)

Table 10.3 Change in spark timing with compression ratio

Compression Ratio (Uncompensated)	Micrometer Reading (0.000")	Spark Timing ^{o} CA bTDC
5.00	0.825	26
5.19	0.773	25
5.41	0.721	24
5.64	0.669	23
5.91	0.617	22
6.20	0.565	21
6.54	0.513	20
6.91	0.461	19
7.36	0.408	18
7.86	0.356	17
8.45	0.304	16
9.15	0.252	15
10.00	0.200	14

Using numerical integration techniques as presented in Chapter 9, the indicated net work, indicated mean effective pressure (IMEP), and combustion parameters (net-

heat release, net-heat-release rate, mass fraction burned (MFB), ignition delay (ID), and combustion duration) were obtained from the in-cylinder pressure and crank angle data. These results were then compared with the same parameters obtained during CIBAI combustion to evaluate the benefits of ignition by air injection as a mechanism to control auto-ignition (CAI) and achieve smooth heat release. CIBAI experimental results are discussed next.

CIBAI Experimental Results

The general operating conditions of the CFR engine during the CIBAI Combustion were presented in Table 8.4. The summary of the results for this experimental work for motored, injected, fired, and CIBAI configurations while the CFR engine was run with a compression ratio of 8:1 are summarized in Table 10.4. The air injection strategy was defined in Chapter 8. The indicated net work, indicated mean effective pressure (IMEP), and heat release data were obtained through numerical integration of the pressure and volume data and its combination with thermodynamic principles as detailed in Chapter 9.

Table 10.4 Experimental results summary table for a compression ratio of 8.0:1

	Motored	Injected	Fired	CIBAI
Indicated Net Work (J)	-69.03	9.27	303.54	398.91
IMEP (psia)	-16.37	2.20	71.96	94.58
Ignition Delay (ms)	N/A	N/A	5.00	5.68
Combustion Duration (ms)	N/A	N/A	5.30	4.40
Thermal Efficiency (%)	N/A	N/A	34.97	38.29
Start Combustion (°CA)	N/A	N/A	342.65	344.85
End Combustion (°CA)	N/A	N/A	405.90	403.15
Peak Pressure (psia)	130.49	189.36	291.17	367.66

In-Cylinder Pressure History

The in-cylinder pressure history for motored, cold injection, fired, and CIBAI combustion for a compression ratio of 8.0:1 is plotted in Figure 10.1. Figure 10.1 shows

that the peak pressure obtained through CIBAI combustion was higher than the one obtained for spark ignition, and cold injection, and thus indicated that combustion occurred during air injection. This conclusion is collaborated by the net indicated work, IMEP, and heat release data, obtained through numerical integration as displayed in Table 10.4. The peak pressure for CIBAI combustion was on average twenty six percent higher than the one obtained for spark ignition.

Indicated Net Work, IMEP

The net gain in the indicated net work is calculated as the difference between the curve obtained during CIBAI combustion and the air injected without gasoline, minus the difference between the curve obtained during spark ignition and motored operation for the same compression ratio. An average of 6% net gain in the indicated net work and IMEP was obtained using CIBAI combustion as compared with spark ignition. This may indicate the benefit of using CIBAI combustion as an alternative to conventional spark-ignited (SI) and compression-ignited engines as proposed by Loth and Morris [3,5]. Further research needs to be done to determine the effect of CIBAI combustion on engine power output at full load and the effect on exhaust emissions. Most of the research done on controlled-auto-ignition indicates the need to expand the operational range in which controlled auto-ignition occurs. This is due to difficulty in timing the onset of auto-ignition and combustion duration, and controlling heat-release rate over the entire operational range [56]. An example of an in-cylinder pressure-volume diagram for the CIBAI and spark ignition (SI) engines is shown in Figure 10.2. It clearly illustrates the gain in gross indicated work during CIBAI combustion as described above.

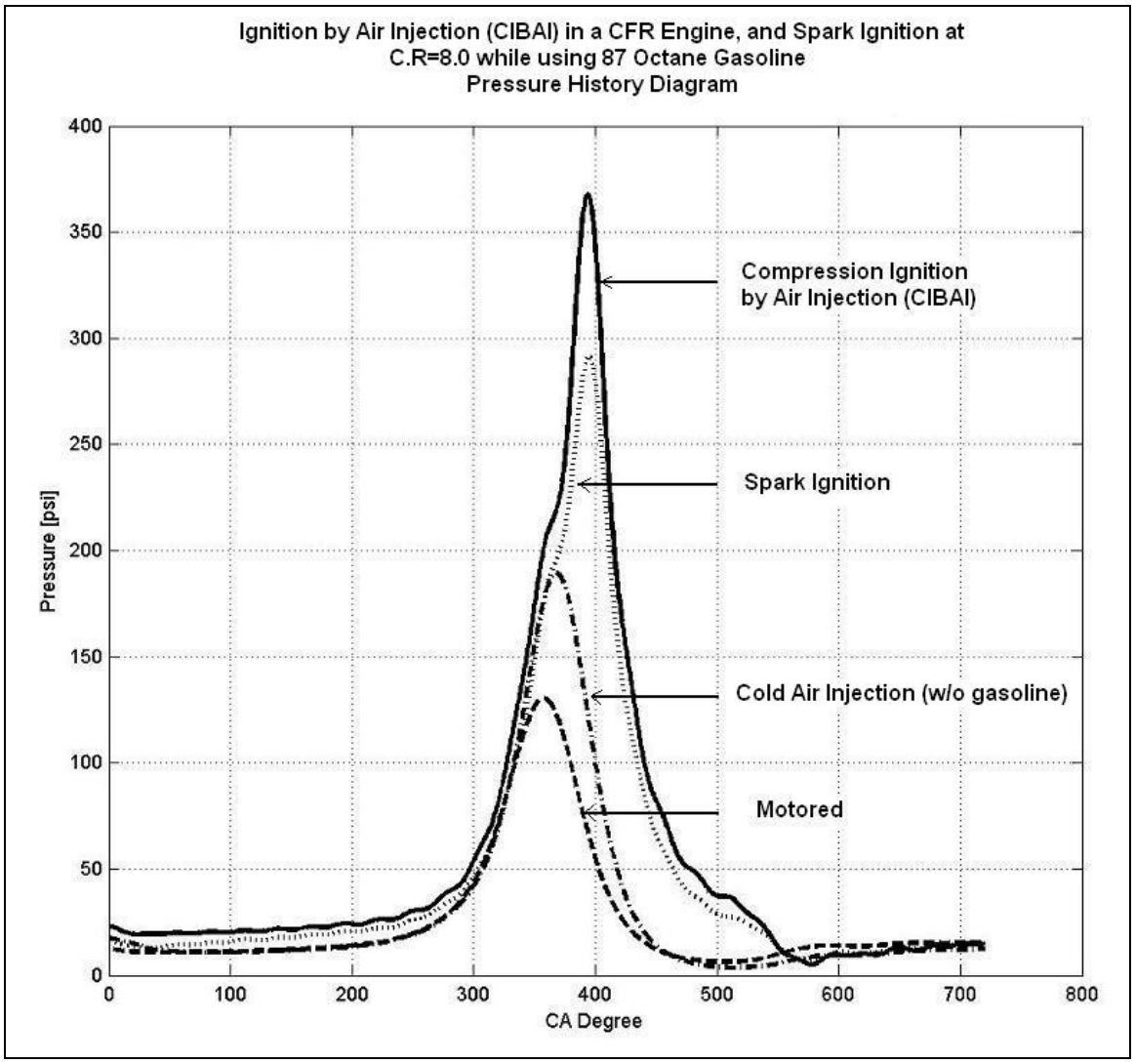

Figure 10.1 Pressure history diagram for motored, cold injection, spark ignition, and CIBAI combustion.

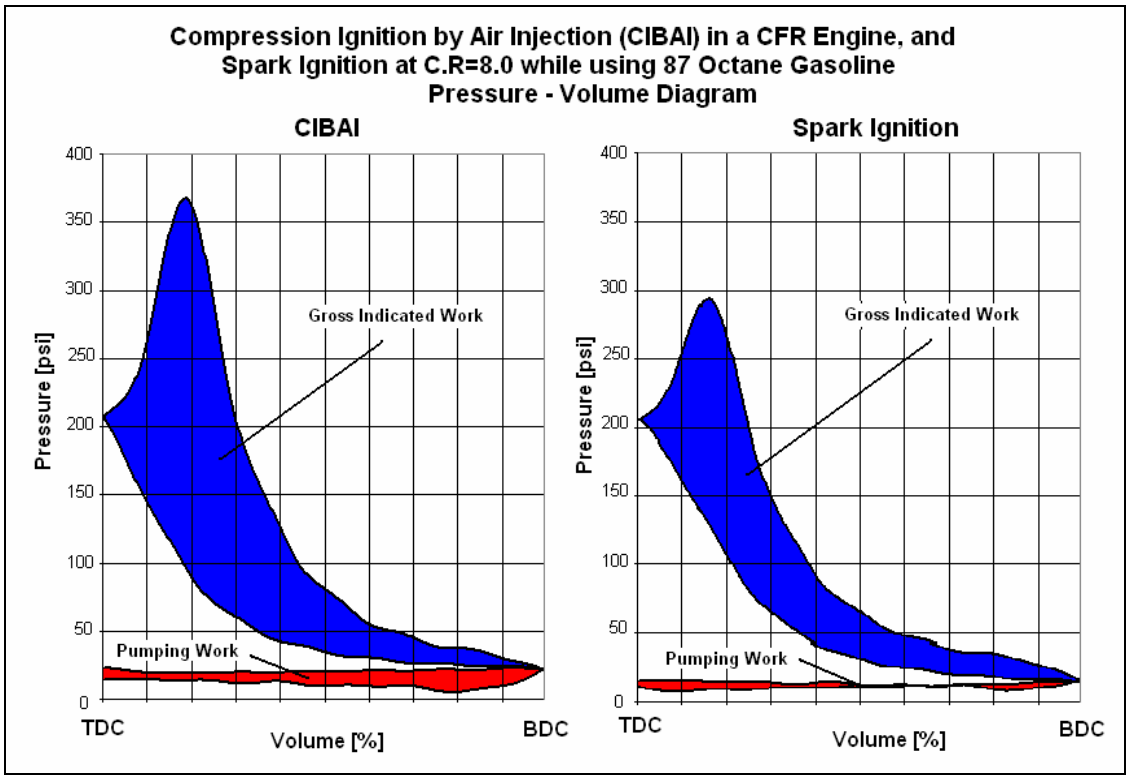

Figure 10.2 In-cylinder pressure-volume diagram for CIBAI and Spark Ignition

In-Cylinder Bulk Mean Temperature History

The in-cylinder bulk mean temperature history for the CIBAI and spark ignition (SI) engines was calculated by combining experimental pressure data, engine geometry, and thermodynamic principles. The air-fuel mixture in the cylinder was treated as air for the entire cycle, and properties values of air were used in the analysis. Air was considered an ideal gas so that the ideal gas relationships could be used to derive the instantaneous in-cylinder bulk mean temperature at each crank angle. During the compression stroke and prior to air injection, the bulk mean temperature (T) was calculated from the total mass air plus fuel (M), using measured data during the stroke intake, the pressure (P) from measured pressure transducer data, volume (V) from piston position. The mass in the cylinder was assumed constant between the intake valve closing (IVC) and the start of

hot-high-pressure air injection. Pressure and volume values are functions of time and were obtained from the pressure and crank angle data, and engine geometry respectively. During air injection the mass inside the cylinder was increased by adding to the initial mass (M_i) the amount of air injected. This is a function of the rate of air injection $(dm/dt)_i$ corresponding to each crank angle (CA) as follows:

$$M = M_i + \sum_{n=SO}^{SC} \left(\frac{dm}{dt} \right) \Delta t \tag{10.1}$$

where:

M= Cylinder total mass
M_i= Cylinder mass before injection
SC= Solenoid Close
SO= Solenoid Opening time
dm/dt= Rate of air injection.

The total mass injected was calculated as the difference between the initial mass of preheated air inside the heat exchanger and the mass remaining after air injection. This was presented in the air-injection model (Chapter 6). The rate of air injection was modeled as a function of time assuming isothermal choked flow independent of the back pressure inside the cylinder. Equation 10.2 was used to calculate the rate of air injection:

$$\frac{dm}{dt} = \frac{0.0406 * P * A^*}{\sqrt{T}} \text{ (Kg/sec)} \tag{10.2}$$

where:

A^*= Effective choked flow area
P = Pressure in Pascal
T = Temperature in degree K
dm/dt= Rate of air injection
Δt = Injection duration

The injection duration (Δt) was assumed equal to the programmed solenoid open time. Initially, the effective orifice area (A^*) was obtained from equation 10.2 by assuming that the pressure (P) drops at steady rate with an average value between the air pre-heater injection pressure and the pressure at which the injector ball-check valve opens, allowing hot-pressure air to flow into the combustion chamber. The exhaust temperature, total mass injected, and solenoid opening time were also used to calculate the effective orifice area (A^*). Finally, the in-cylinder temperature (T) was obtained from equation 10.2 for each pressure reading, corresponding to the duration of the solenoid opening time. The rate of air injection (dm/dt) was integrated numerically to verify that it was equal to the total amount of the air injected into the cylinder. For the remaining part of the power stroke, between the solenoid closing and exhaust valve opening (EVO), the temperature was calculated using the equation of state for known values of pressure (P), and volume (V). In this case the total mass (M) was equal to the initial mass in the cylinder plus the preheated air mass injected. For the first part of the cycle, the temperature (T) was assumed equal to the air inlet temperature. Similarly, the temperature (T) for the last part of the cycle was assumed equal to the exhaust temperature. The resulting in-cylinder bulk mean temperature history is shown in Figure 10.3.

Peak bulk mean temperatures of 1871^o K and 2287^o K were obtained for CIBAI combustion and spark ignition (SI) respectively. The eighteen percent (18%) decline in peak bulk mean temperature for CIBAI combustion is due to the mixture dilution by the injected air. Lean air-fuel mixtures have lower adiabatic flame temperatures. NO_x formation is highly dependent on temperature and time. Significant amounts of NO_x

emission are generated in the 2500-3000^{o} K temperature range [2]. A high expansion ratio produces fast expansion cooling, which also reduces the possibility of NO_x formation [3,5]. Further research needs to be done to be able to evaluate the effect of CIBAI combustion on exhaust emissions. A sample calculation of the in-cylinder bulk mean temperature for both CIBAI and spark ignition (SI) combustion is shown in Appendix S.

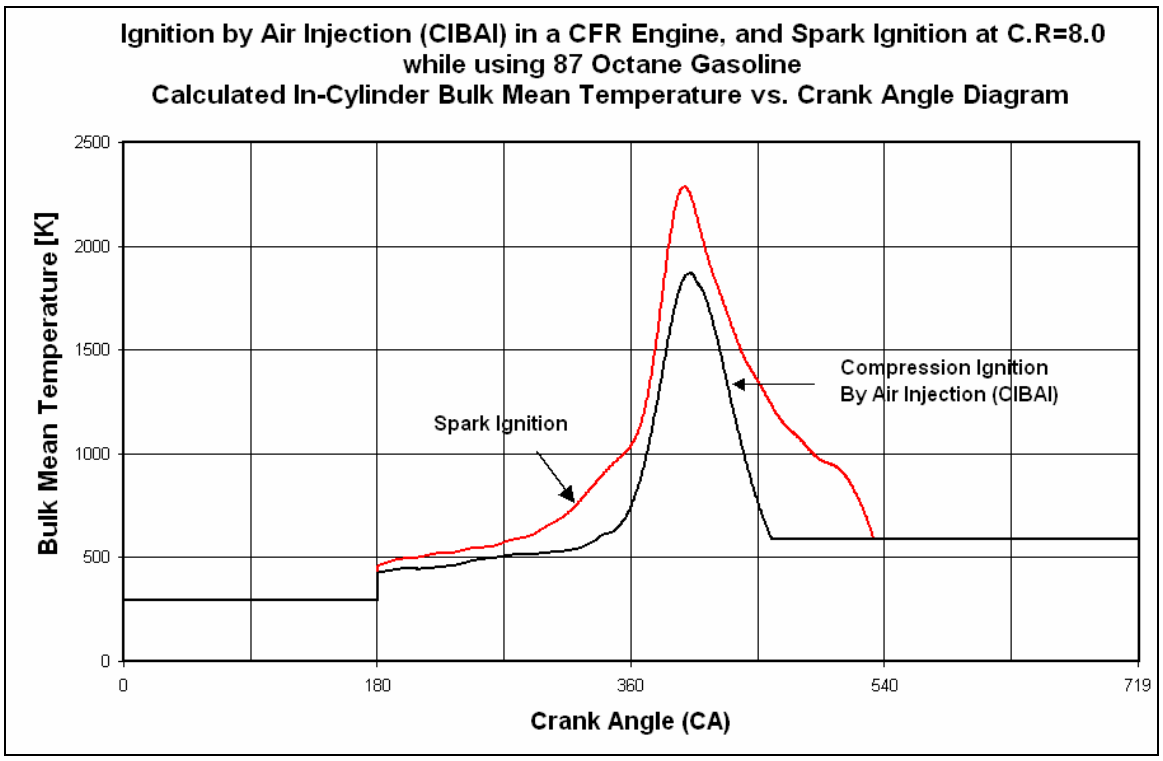

Figure 10.3 Calculated in-cylinder bulk mean temperature history for CIBAI and spark ignition combustion

Heat Release, MFB, Combustion Duration, Ignition Delay (ID)

The heat release data obtained from the methods discussed in Chapter 9 provided a way to determine the heat release rate, mass fraction burned, combustion duration and ignition delay (ID). The heat release is defined as the amount of heat that would have to

be added to cylinder contents to produce the same pressure variations due to combustion of the air-fuel mixture [69].

The net heat release rate curve (Figure 10.4) shows that CIBAI combustion occurred at a faster rate than spark ignition (SI) combustion. This may be attributed to the high temperature achieved at the end of the compression stroke as a result of pre-heating the injected air, increasing the intake temperature, and doubling the compression ratio. The faster heat release rate obtained for CIBAI combustion agreed with earlier researchers who had indicated that auto-ignition occurs almost spontaneously without a presence of flame propagation [14, 20, 23]. However, this result has to be taken in the context of the assumptions involved in the calculation of the net heat release as explained in Chapter 9.

The mass fraction burned (MFB) curves were obtained from the heat release data as described in Chapter 9. Figure 10.5 shows the MFB for both, CIBAI and spark ignition. The air-fuel mixture burned 17 % faster for CIBAI combustion than during spark ignition. This may be attributed to the higher heat release rate after TDC.

Ignition delay and combustion duration data indicate how fast the combustion process occurs. The average ignition delay (ID) obtained for CIBAI combustion was approximately half millisecond longer than the values obtained for spark ignition (SI) combustion. Conversely, the average combustion duration obtained for CIBAI was approximately one millisecond faster than the values obtained for spark ignition. These differences can be attributed to the lower response of the solenoid valve (~20 ms), pressure and crank angle signal shift (<0.5° CA), spark noise in the pressure signal, and higher net heat release rate during CIBAI combustion. Computational fluid dynamics

(CFD) and flow visualization techniques may be helpful in a future CIBAI research to verify or correct the values obtained in this research.

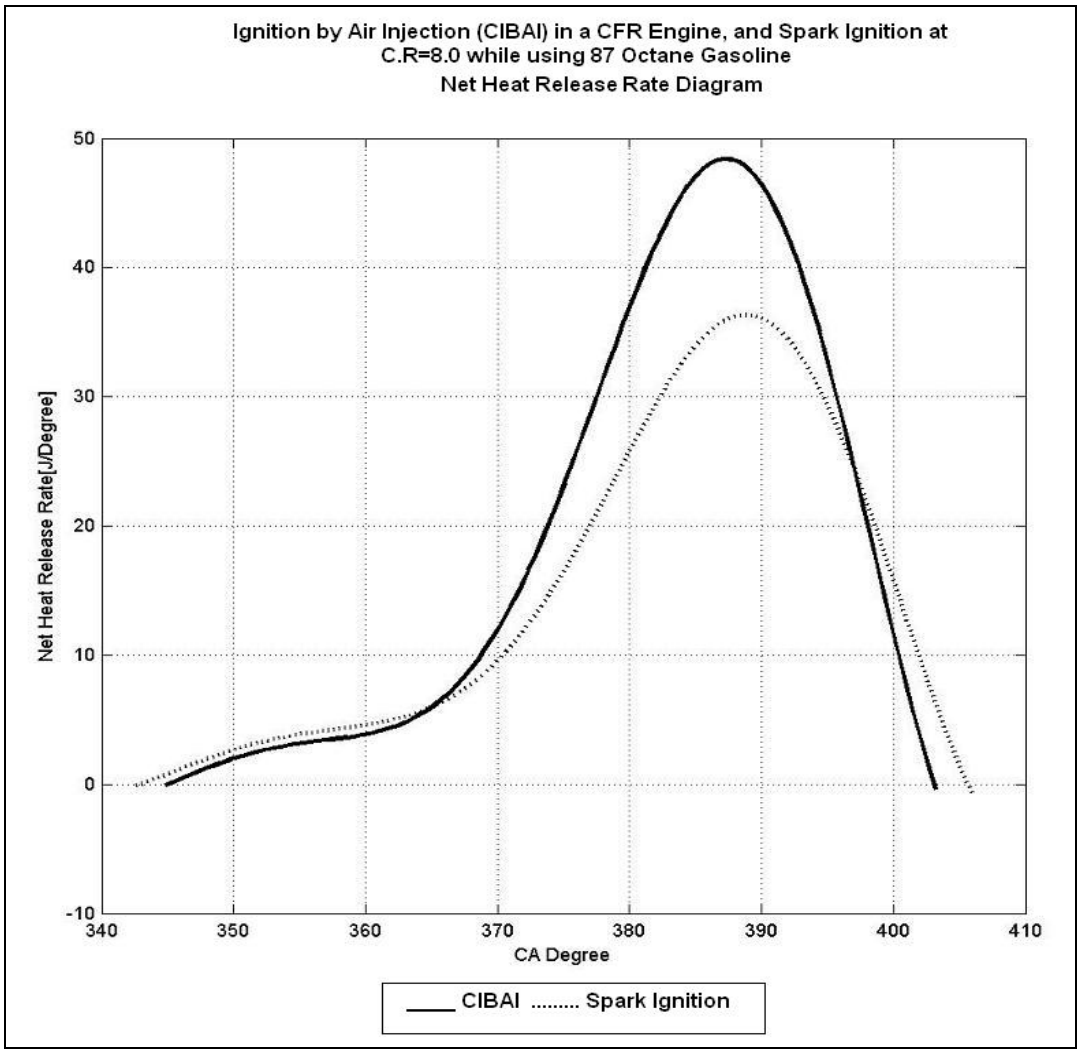

Figure 10.5 Net heat release rate comparison for CIBAI and spark ignition combustion

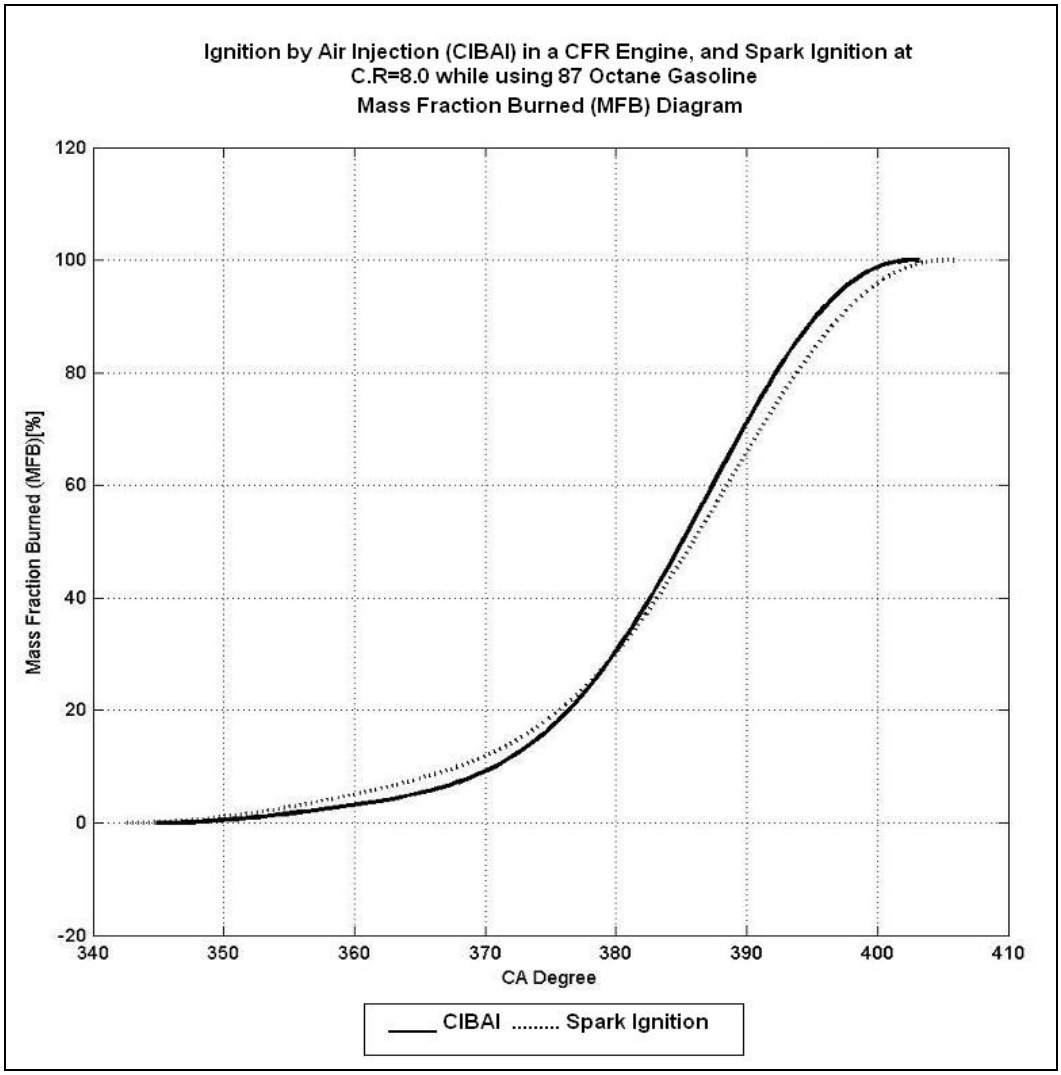

Figure 10.6 Mass fraction burned (MFB) for CIBAI and spark ignition combustion

Chapter 11: Parametric Study

Overview

The objective of the parametric study discussed in this chapter was to determine the effect of the CFR engine operating parameters on CIBAI combustion. The parameters analyzed were the compression ratio, intake temperature, air preheat charging pressure, equivalence ratio, and air-injection timing. To this aim, the analytical, the cold air injection, and thermodynamic models presented in chapters 5 and 6 respectively were incorporated into a computer program written in Matlab version 6.5 (Appendix A).

The computer code contains two main programs. The first subroutine named, CIBAI cycle analysis program, performed a complete CIBAI cycle analysis for different engine configurations. The second subroutine named, CIBAI numerical modeling program, was used to conduct the parametric study for the selected engine parameters. The numerical modeling used the mathematical derivations presented in the data analysis section of this dissertation (Chapter 9). The computer program interacted with the user through a graphical user interface (GUI).

The experimental study conducted during the course of this dissertation provided the empirical data needed as inputs to the analytical model. Multiple experiments were taken for each of the fourteen (14) tests proposed in Chapter 8. Tests producing significant variations in results were repeated until a statistical analysis of their mean performance was accurately established. The sources of error and the experimental uncertainty are discussed at the end of this chapter.

Parametric Matrix

The parametric study involved choosing a compression ratio, volume displacement, air pre-heater charging pressure, equivalence ratio, air flow rate, intake temperature, intake pressure, exhaust temperature, and air-injection timing combination, which offers acceptable CIBAI combustion performance.

The outputs generated by the numerical modeling code included the in-cylinder pressure, net heat release, net heat release rate, and mass fraction burned (MFB) history graphs for a single CIBAI combustion event, and for a particular set the parameters as stated in Chapter 8. In addition, the indicated net work, IMEP, ignition delay (ID), combustion duration, thermal efficiency, and the start and end of combustion were calculated for each simulation.

The parametric matrix for CIBAI combustion consisted of the following cases:

- Three (3) compression ratios: 7.0:1, 7.5:1, and 8.0:1
- Three (3) intake temperatures: 70 °F, 250 °F, and 450 °F
- Three (3) air charged pressures: 700, 800, and 900 psig
- Three (3) equivalence ratios (Φ): 0.45, 0.50, and 0.65
- Three (3) air injection timing: 85°, 75°, and 65° CA bTDC

The results of the parametric study are discussed next.

Parametric Study Results

The objective of the parametric study was to determine the effect of compression ratio, intake temperature, air pre-heated charging pressure, equivalence ratio, and air-injection timing on CIBAI combustion. The understanding of the effect of these engine parameters on the occurrence of CIBAI combustion is vital to specify a CIBAI engine

configuration that would result in maximum power and efficiency. The parametric study results are summarized as follows:

The Effect of Compression Ratio

For the set of initial conditions given in Table 8.3, changes in the compression ratio altered the CIBAI combustion process by increasing the compression temperature. Higher compression ratios and thus expansion ratios significantly increase the net heat release rate, advancing the start of the ignition of the CIBAI combustion, all contributing to increased thermal efficiency. The combustion duration was slightly affected by changes in the compression ratio. The results of this simulation are summarized in Table 11.1, and illustrated in Figure 11.1.

Table 11.1 The effect of compression ratio on CIBAI combustion

RESULTS:	Test 1(C.R=7.0)	Test 2 (C.R=7.5)	Test 3 (C.R=8.0)
Indicated Net Work (J)	283.98	307.55	398.91
IMEP (psia)	67.33	72.92	94.58
Ignition Delay (ms)	6.79	6.69	5.68
Combustion Duration (ms)	4.10	3.90	4.40
Thermal Efficiency (%)	32.21	34.26	38.29
Start Combustion (°CA)	346.50	344.85	344.85
End Combustion (°CA)	402.05	399.85	403.15

The Effect of Intake Temperature

For the set of initial conditions given in Table 8.4, changes in the intake temperature altered the CIBAI combustion process by changing the volumetric efficiency. Higher intake temperature severely increased the net-heat-release rate, considerably advanced the start of the ignition of the CIBAI combustion, significantly reduced the IMEP, and contributed to lower thermal efficiency due to the lower volumetric efficiency. The combustion duration were slightly affected by changes in the intake temperature. The results of this simulation are summarized in Table 11.2, and

illustrated in Figure 11.2. It should be noted that the simulation of the CIBAI combustion using an intake temperature of 450 °F was not conducted due to significant presence of audible knock during the actual experiment.

Table 11.2 The effect of intake temperature on CIBAI combustion

RESULTS:	Test 4 (T=70 °F)	Test 5 (T=250 °F)
Indicated Net Work (J)	398.91	375.49
IMEP (psia)	94.58	89.02
Ignition Delay (ms)	5.68	6.29
Combustion Duration (ms)	4.40	3.80
Thermal Efficiency (%)	38.29	33.93
Start Combustion (°CA)	344.85	339.90
End Combustion (°CA)	403.15	397.65

The Effect of Air Pre-heater Charging Pressure

For the set of initial conditions given in Table 8.3, changes in the air pre-heater charging pressure changed the CIBAI combustion process by changing the air-fuel ratio. Higher pressures drastically retarded the start of the ignition of the CIBAI combustion, significantly decreasing the net-heat-release rate, and considerably reducing the IMEP and combustion duration. This can be attributed to the additional amount of mass of air injected during high air pre-heated charging, which significantly leaned the air-fuel mixture. The results of this simulation are summarized in Table 11.3, and illustrated in Figure 11.3.

Table 11.3 The effect of air pre-heater charging pressure on CIBAI combustion

RESULTS:	Test 6 (P=700 psig)	Test 7 (P=800 psig)	Test 8 (P=900 psig)
Indicated Net Work (J)	355.82	398.91	310.35
IMEP (psia)	84.36	94.58	73.58
Ignition Delay (ms)	3.68	5.68	4.88
Combustion Duration (ms)	5.90	4.40	3.30
Thermal Efficiency (%)	33.41	38.29	33.65
Start Combustion (°CA)	340.45	344.85	357.50
End Combustion (°CA)	404.25	403.15	391.05

The Effect of Equivalence Ratio

For the set of initial conditions given in Table 8.4, changes in the equivalence ratio altered the CIBAI combustion process by varying the amount of compression heating in the charge. Enriching the mixture (Φ=0.65) considerably shortened the ignition delay (ID), retarded the start of the ignition of the CIBAI combustion, and drastically increased the net heat release rate. Leaning the mixture (Φ=0.45) greatly reduced the net heat release, IMEP, and combustion duration. The results of this simulation are summarized in Table 11.4, and illustrated in Figure 11.4.

Table 11.4 The effect of equivalence ratio on CIBAI combustion

RESULTS:	Test 9 (E.R=0.65)	Test 10 (E.R=0.50)	Test 11 (E.R=0.45)
Indicated Net Work (J)	423.04	398.91	244.40
IMEP (psia)	100.30	94.58	57.94
Ignition Delay (ms)	5.38	5.68	4.78
Combustion Duration (ms)	3.10	4.40	3.60
Thermal Efficiency (%)	34.70	38.29	36.78
Start Combustion (°CA)	360.25	344.85	355.30
End Combustion (°CA)	392.70	403.15	393.80

The Effect of Air-Injection Timing

For the set of initial conditions given in Table 8.5, changes in the air-injection timing altered the start of the CIBAI combustion process. Advancing the air-injection timing drastically advanced the start of the combustion process, increased the ignition delay (ID), and substantially, decreased the net-heat-release rate due to the lower compression heating. Conversely, retarding the air-injection timing drastically delayed the start of the combustion process, decreased the ignition delay (ID), increased the peak pressure, reduced the combustion duration, and substantially increased the net-heat-release rate due to the higher compression heating. The results of this simulation are summarized in Table 11.5, and illustrated in Figure 11.5.

Table 11.5 The effect of air injection timing on CIBAI combustion

RESULTS:	Test 12 (100° CA bTDC)	Test 13 (75° CA bTDC)	Test 14 (50° CA bTDC)
Indicated Net Work (J)	418.31	398.91	278.40
IMEP (psia)	99.18	94.58	66.00
Ignition Delay (ms)	8.22	5.68	4.07
Combustion Duration (ms)	7.40	4.40	3.30
Thermal Efficiency (%)	35.66	38.29	33.84
Start Combustion (°CA)	338.25	344.85	356.95
End Combustion (°CA)	419.10	403.15	392.15

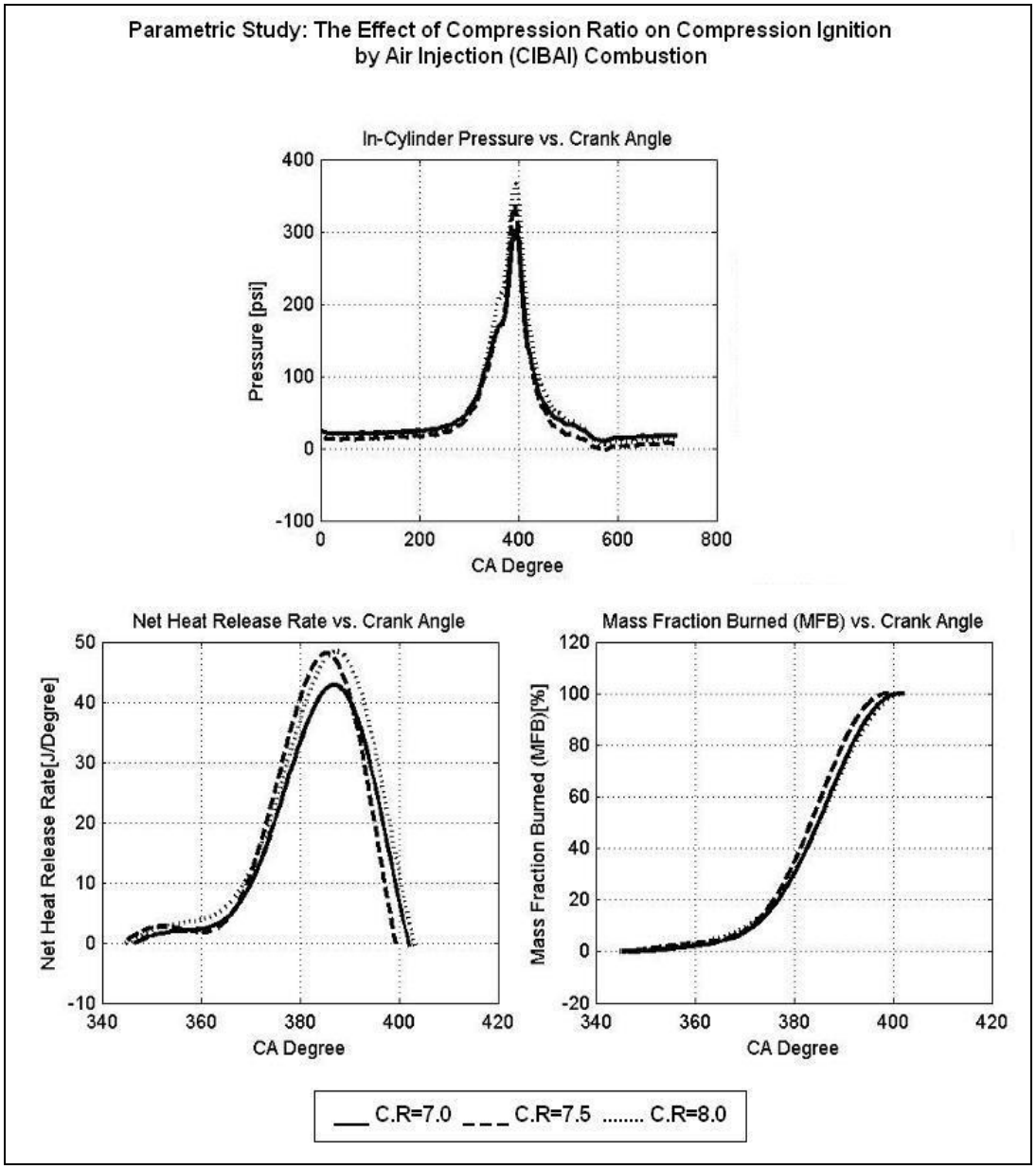

Figure 11.1 Pressure history, net heat release rate, and mass fraction burned (MFB) diagrams for compression ratios of 7.0, 7.5, and 8.0

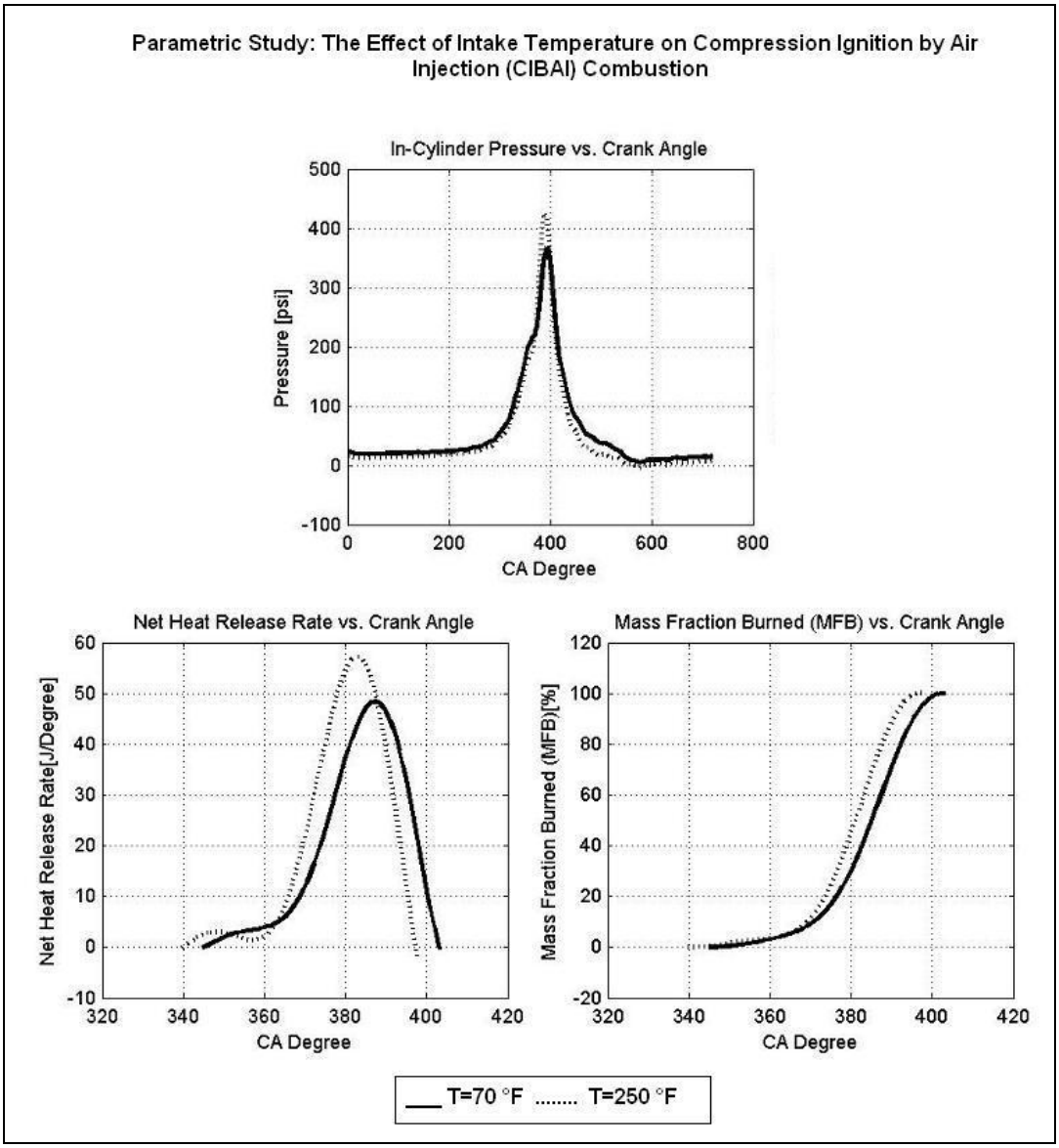

Figure 11.2 Pressure history, net heat release rate, and mass fraction burned (MFB) diagrams for intake temperatures of 70 °F, and 250 °F

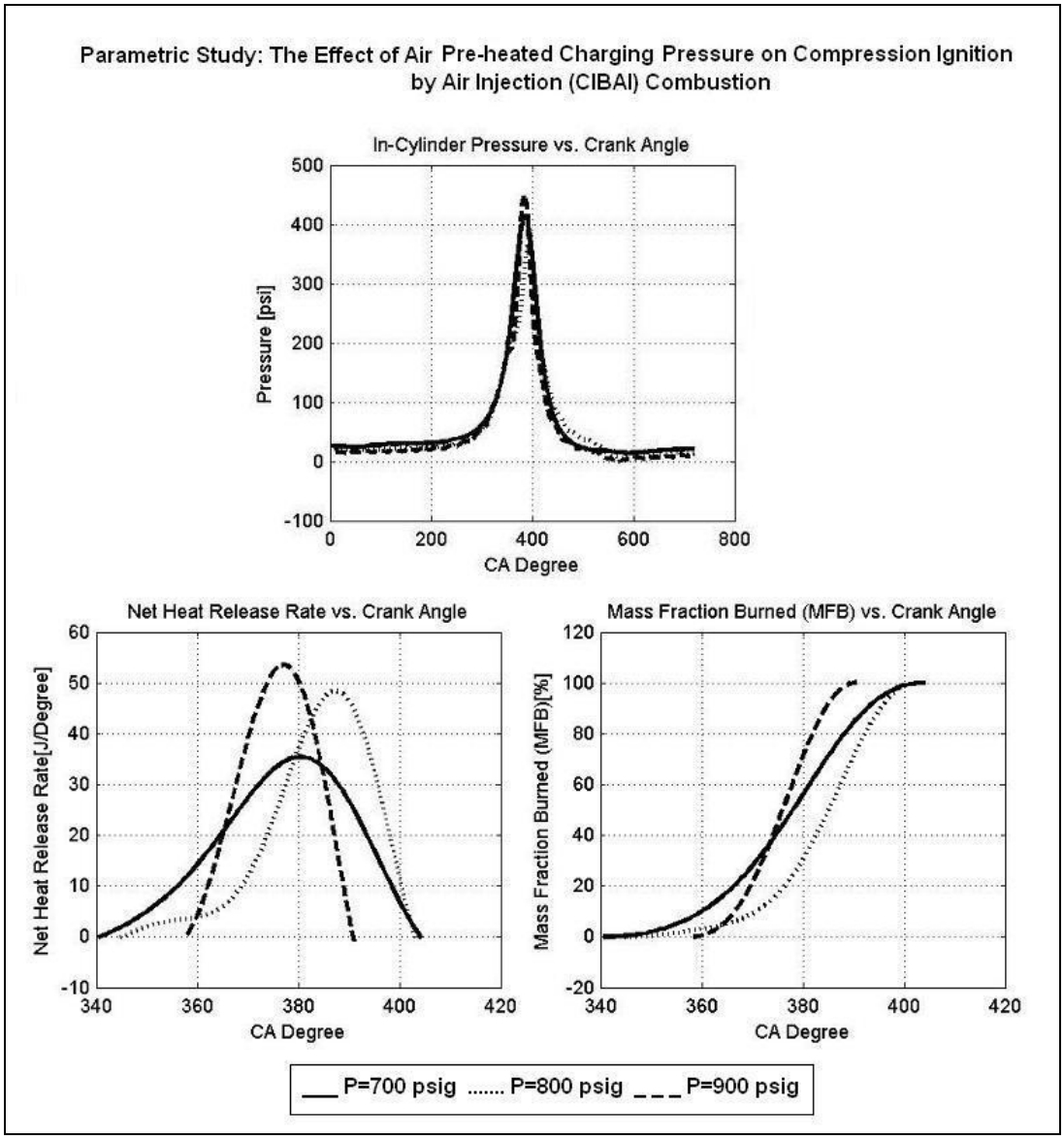

Figure 11.3 Pressure history, net heat release rate, and mass fraction burned (MFB) diagrams for air pre-heated charging pressures of 700, 800, and 900 psig

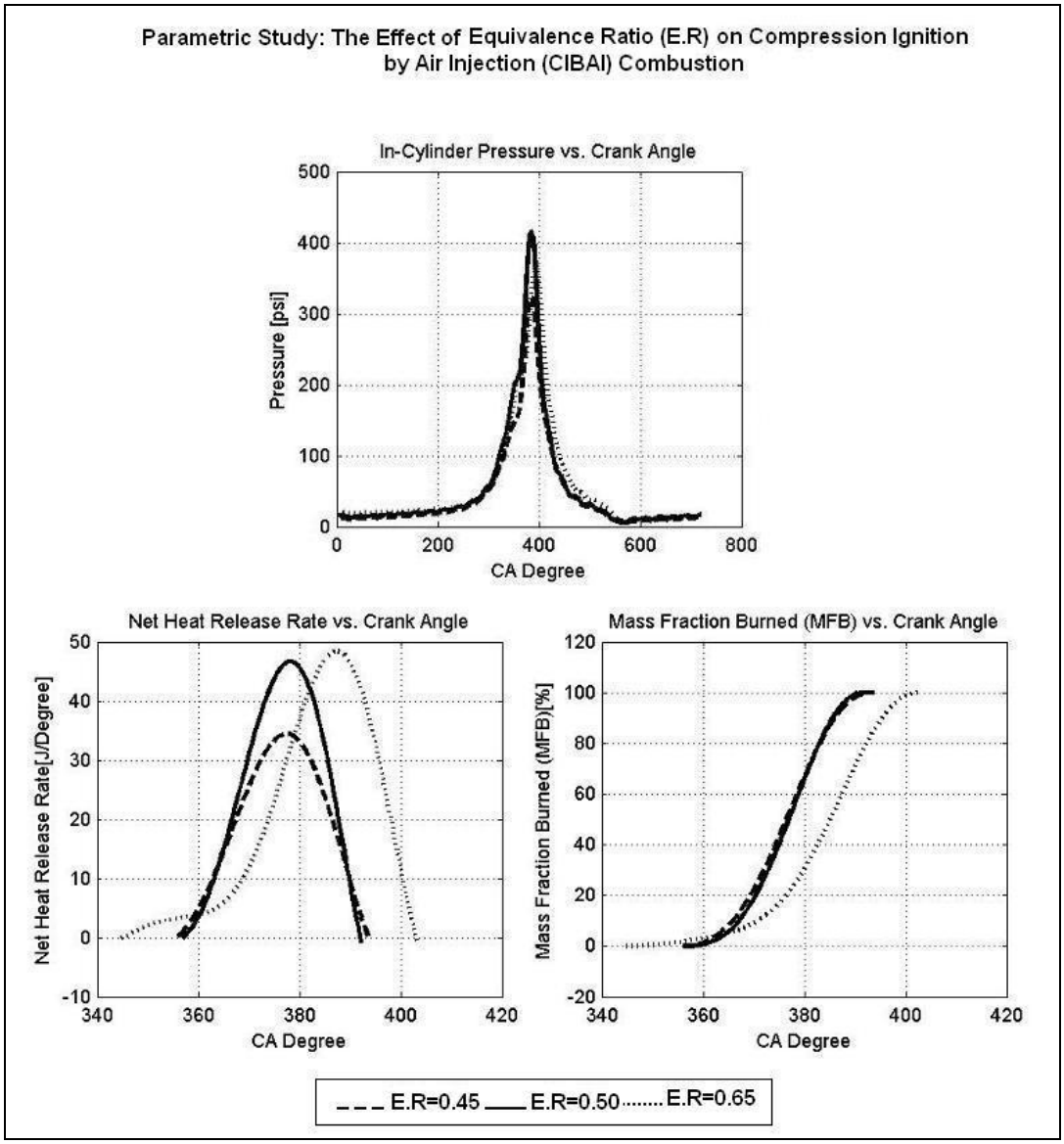

Figure 11.4 Pressure history, net heat release rate, and mass fraction burned (MFB) diagrams for equivalence ratios of 0.45, 0.50, and 0.65

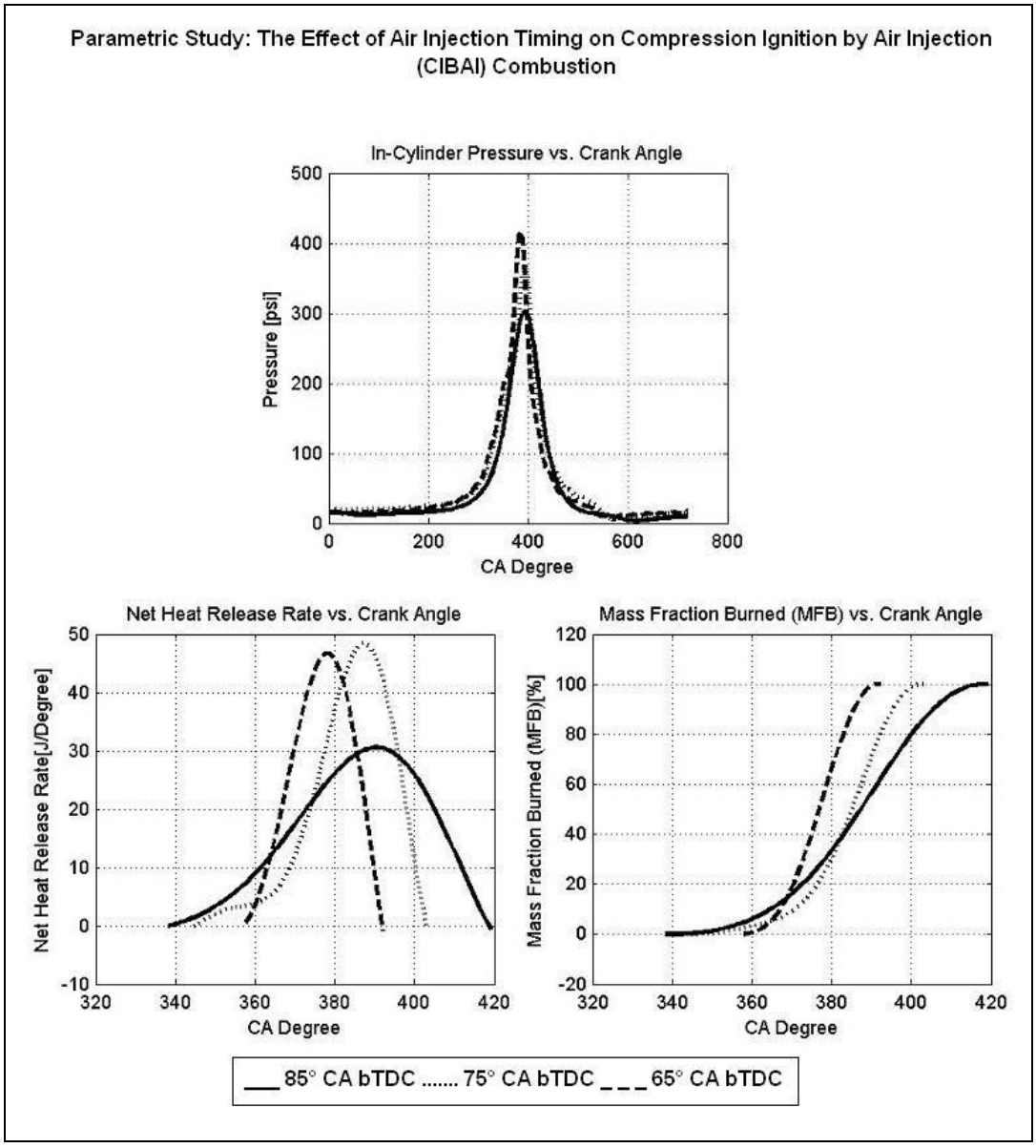

Figure 11.5 Pressure history, net heat release rate, and mass fraction burned (MFB) diagrams for air injection timing of 85°, 75°, and 65° CA bTDC

Sources of Error

Throughout the experimental work, every effort was made to reduce possible sources of error, but as with any experimental procedure, there were some uncertainties with experimental measurements. Possible sources of error and their relative magnitudes are given in Table 11.6.

Table 11.6 Sources of error

Instrument	Error
Intake Pressure Gauge	+/- 0.1 psig
Oil Pressure Gauge	+/- 5 psig
Pressure Regulator	+/- 50 psig
Air Pre-heater Charging Pressure Gauge	+/- 10 psig
In-Cylinder Pressure Transducer	+/- 1 % full scale
Crank Angle Sensor	+/- 0.5° CA
Intake Thermocouple	+/- 1 °F
Oil Temperature Thermocouple	+/- 5 °F
Exhaust Temperature Thermocouple	+/- 1 °F
Coolant Temperature Thermometer	+/- 1 °F
Air Flow Meter	+/- 0.1 SCFM
Fuel Glass Meter	+/- 0.1 in
A/D Converter Data Acquisition Board	+/- 0.0024 V
Compression Ratio Micrometer	+/- 0.0001 in

The results of the numerical model were affected by the experimental data, which were used as inputs into the analytical model. An evaluation of the sensitivity of the numerical results to these errors indicated that the compression ratio, air-injection timing, and scale factor were the mayor contributor to errors in the predicted results. The scale factor is a number used by the numerical code to zero the in-cylinder pressure data to obtain comparable absolute pressure data for multiple simulations. The effects of these three errors in the numerical results are listed in Table 11.7. The ignition delay (ID) was the output with the maximum margin of error (1.31 %).

Table 11.7 Effects of input data on modeling results

	Net Heat Release		Ignition Delay (ID)	
	[J]	Error (%)	[ms]	Error (%)
Case Without Input Errors	844	0.00	6.89	0.00
Compression Ratio Error (+/- 0.1)	841	0.35	6.89	0.00
Air Injection Timing (+/- 0.5° CA)	844	0.00	6.98	1.31
Scale Factor (+/- 25 psig)	848	0.94	6.89	0.00

Uncertainty Analysis

For each experiment the indicated net work was calculated and averaged for a certain number of cycles. The number of cycles used ranged from 20 to 50 depending on the type of operation. This was done for each engine configuration (motored, fired, air injected w/o gasoline, and CIBAI) in order to determine the net gain in the indicated net work as a result of CIBAI combustion. The objective of the uncertainty analysis was to determine the reliability of the average calculations, especially when the fluctuation levels were significant.

Assuming the data were normally distributed, the uncertainty in the mean value was calculated using the following equation [73].

$$\Delta \bar{x} = t_{\alpha/2;v} \frac{s}{\sqrt{N}} \qquad 11.1$$

where the value $t_{\alpha/2;v}$, comes from the t-distribution with 1-α confidence, N= number of samples, v=N-1, and s is the standard deviation of the data. The true sample mean is then $\mu = \bar{x} \pm \Delta \bar{x}$ with the specified level of confidence.

The uncertainty analysis was applied to the indicated net work value obtained during CIBAI Combustion. The true mean value of the indicated net work calculated was 398.91 J +/- 2.14% with 95% confidence for the CFR engine using 87 octane gasoline at

a compression ratio of 8:1, intake temperature of 70 °F, air preheated charging pressure of 800 psig, equivalence ratio (Φ)=0.5, and air-injection timing of 75° CA bTDC.

Chapter 12: Conclusions

The objective of this research was to demonstrate experimentally the viability of achieving ignition by air injection (CIBAI) for controlled auto-ignition in a CFR engine. Experimental work was done on a modified single cylinder, four-stroke, spark ignition cooperative fuel research (CFR) engine, fully instrumented and equipped with a highly specialized air injection and timing system to assure that air injection occurred at the desired crank angle, and the desired amount of air was injected in one step, without additional air entering after ignition started. An air injection model was developed, and a parametric study was conducted to determine the effect of operating parameters on CIBAI combustion. A numerical modeling code was developed and integrated into a graphical user interface (GUI) to analyze the CIBAI combustion process and perform the parametric study.

The following are the main conclusions of this experimental study, and the recommendations for future research work:

- It has been experimentally proven that it is possible to achieve auto-ignition by air injection (CIBAI) with controlled ignition time in a CFR engine by timing a solenoid valve, which simulates the operation of a cylinder-connecting-valve (CCV) in the CIBAI cycle.
- The numerical integration of the pressure- volume diagram of Figure 10.2 shows that the indicated net work and IMEP increased by 31 % using CIBAI like combustion as compared with spark ignition (SI). After subtracting the work done to compress the bottle of air used to simulate CIBAI combustion, a net gain of 6 % in the indicated net work was obtained.

- This parametric study indicated that CIBAI combustion was influenced primarily by the compression ratio, intake temperature, and air-injection timing. Changes in the compression ratio altered the CIBAI combustion process by increasing the compression temperature. Figure 11.1 shows that higher compression ratios and thus expansion ratios significantly increased the net heat release rate, advanced the start of the ignition of the CIBAI combustion, and contributed to increase the indicated thermal efficiency. Changes in the intake temperature altered the CIBAI combustion process by changing the volumetric efficiency. Figure 11.2 shows that higher intake temperature severely increased the net heat release rate, considerably advanced the start of the ignition of the CIBAI combustion, significantly reduced the IMEP, and contributed to lower thermal efficiency due to the lower volumetric efficiency. Changes in the air-injection timing altered the start of the CIBAI combustion process. Figure 11.5 shows that, injecting in a larger volume, drastically slowed the start of the combustion process, increasing ignition delay (ID), and substantially, decreased the net heat release rate due to the reduced compression heating.
- CIBAI like combustion was obtained in a modified CFR engine using unleaded gasoline with an anti knock index (AKI) of 87, compression ratio of 16:1, intake temperature of 70 °F, air pre-heated charging pressure of 800 psig, equivalence ratio (Φ)=0.5, and air-injection timing of 75° CA bTDC.
- The use of an injector ball-check-valve in line with the solenoid valve and electronic injection timing was important to achieve CIBAI cycle like ignition, inside a CFR engine.

Chapter 13: Recommendations for Future Work

The development of a commercial CIBAI engine will be facilitated by the experimental work, numerical modeling, and parametric analysis presented in this dissertation. Future work on CIBAI combustion should include the following activities:

- The development of a detailed chemical kinetics model in order to understand the mechanism of auto-ignition during CIBAI combustion, and predict the composition of CIBAI combustion products.
- The implementation of a computational fluid dynamics (CFD) code in order to predict the effect of CIBAI combustion on NO_X emissions.
- The use of flow visualization techniques such as laser pyrometry, schlieren and shadowgraph photography, and laser Raleigh scattering in order to obtain flow velocity distribution, and temperature and pressure profiles during air injection. This information can be helpful to accurately predict combustion interval and ignition (ID) during CIBAI combustion.
- The implementation and analysis of CIBAI combustion in a production engine.

References

1. Heywood, J. B., Internal Combustion Engine Fundamentals, McGraw-Hill Inc., New York, NY 1988.

2. Pulkrabek, W. W., Engineering Fundamental of the Internal Combustion Engine 2nd Edition, Pearson Prentice-Hall, Upper Saddle River, NJ 2004.

3. Loth, J. L., "Compression Ignition By Air Injection (CIBAI) Cycle and Engine," US Patent No.: 6.899.061, May 31, 2005.

4. Milovanovic, N., and Chen, R., "A Review of Experimental and Simulation Studies on Controlled Auto-Ignition Combustion," SAE Paper No. 2001-01-1890, Warrendale, PA 2001.

5. Loth, J. L., and Morris, G. J., "Compression Ignition Engine by Air Injection from Air-Only Cylinder to Adjacent Air-Fuel Cylinder," US Patent No.: 6.994.057, February 7, 2006.

6. McMillian, M. H., "Laser Spark Ignition for Lean-Burn Natural Gas Reciprocating Engines," National Energy Technology Laboratory (NETL). 2005. <http://www.netl.doe.gov/newsroom/backgrounder/mb-0006.html> (7 Dec. 2005).

7. Ricardo, H. R., "Further Note on Fuel Research. Report of the Empire Motor Fuels Committee," Proceedings of the Institute of Automobile Engineers, London, 1923.

8. Erren, R. A., and Campbell, W. H. "Hydrogen: A Commercial Fuel for Internal Combustion Engines and other Purposes," Journal of the Institute of Fuel, VI, pp. 277-291, 1933.

9. King, R. O., "The Hydrogen Engine and the Nuclear Theory of Ignition," Canadian Journal Research, F.26, p 264, 1948.

10. King, R. O., and Rand, M., "The Oxidation, Decomposition, Ignition and Detonation of Fuel Vapors and Gases," Canadian Journal Technology, pp 445-469, 1955.

11. Obert, E. F., Internal Combustion Engines 3rd Edition, International Textbook Company, Scranton, PA 1968.

12. Miller, C. D., "Roles of Detonation Waves and Auto-Ignition in Spark Ignition Engine Knock," SAE Trans., Vol. 1(1), p. 98, 1947.

13. Hanskell, W.W., "Fuel Ignition in a Rapid Compression Machine," SAE Paper No. 700059, Warrendale, PA 1970.

14. Onishi, S., Jo, S. H., Shoda, K., Jo, P. D., and Kato, S., "Active Thermo-Atmosphere Combustion (ATAC): A New Combustion Process for Internal Combustion Engines," SAE Paper No. 790501, Warrendale, PA 1979.

15. Lavy, J., Dabadie, J. C., Angelberger, C., and Duret, P., "Innovative Ultra-Low NO_x Controlled Auto-Ignition Combustion Process for Gasoline Engines: the 4-SPACE Project," SAE Paper No. 2000-01-1837, Warrendale, PA 2000.

16. Stanglmairer, R. H., and Roberts, C. E., "Homogeneous Charge Compression Ignition (HCCI): Benefits, Compromises, and Future Engine Applications," SAE Paper No. 1999-01-3682, Warrendale, PA 1999.

17. Ishibashi, Y., and Asai, M., "Improving the Exhaust Emissions of Two-Stroke Engines by Applying the Radical Combustion," SAE Paper No. 960742, Warrendale, PA 1996.

18. Duret, P., and Venturi, S., "Automotive Calibration of the IAPAC Fluid Dynamically Controlled Two Stroke Combustion Process," SAE Paper No. 960363, Warrendale, PA 1996.

19. Thring, R. H., "Homogeneous Charge Compression Ignition (HCCI) Engines," SAE Paper No. 892068, Warrendale, PA 1989.

20. Najt, P. M., and Foster, D. E., "Compression-Ignited Homogeneous Charge Combustion," SAE Paper No. 830264, Warrendale, PA 1983.

21. Aoyama, T., Hattori, Y., Mizuta, J., and Sato, Y., "Premixed-Charge Compression Ignition Gasoline Engines," SAE Paper No. 960081, Warrendale, PA 1996.

22. Hanskell, W.W., and Bame, J., "Engine Knock – An End Gas Explosion," SAE Paper No. 650506, Warrendale, PA 1965.

23. Noguchi, M., Tanaka, Y., Tanaka, T., and Takeuchi, Y., "A Study on Gasoline Engine Combustion by Observation of Intermediate Reactive Products During Combustion," SAE Paper No. 790840, Warrendale, PA 1979.

24. Fish, A., "The Cool Flames of Hydrocarbons," Angewandte Chemie International Edition, Vol. 7, pp. 45-60, 1968.

25. Baldwin, R. R., and Walker, R. W., "Problems and Progress in Hydrocarbon Oxidation," 14th Symposium (International) on Combustion. The Combustion Institute, Pittsburgh, PA, pp. 241-257, 1973.

26. Dryer, F. L., and Glassman, I., "Combustion Chemistry of Chain Hydrocarbons," Progress in Astronautics and Aeronautics, Vol. 62, pp. 255-306, 1978.

27. Westbrook, K. C., Pitt, W. J., and Leppard, W. R., "The Auto-Ignition Chemistry of Paraffinic Fuels and Pro-Knock and Anti-Knock Additives: A Detailed Chemical Kinetic Study," SAE Paper No. 912314, Warrendale, PA 1991.

28. Westbrook, K. C., "Chemical Kinetics of Hydrocarbons Ignition in Practical Combustion Systems," 28th Internacional Combustion Symposium, Vol. 28, pp. 1563-1577, Edinburgh, 2000.

29. Halstead, M. P., Kirsch, L. J., and Quinn, C. P., "The Autoignition of Hydrocarbon Fuels at High Temperatures and Pressures, Fitting of a Mathematical Model," Combustion and Flame, Vol. 30, pp. 45-60, 1977.

30. Fiveland, S. B., and Assanis, D. N., "A Four-Stroke Homogeneous Charge Compression Ignition Engine Simulation for Combustion and Performance Studies," SAE Paper No. 2000-01-0332, Warrendale, PA 2000.

31. Goldsborough, S., and Van Blarigan, P., "A numerical Study of a Free Piston IC Engine Operating on Homogeneous Charge Compression Ignition Combustion," SAE Paper No. 1999-01-0609, Warrendale, PA 1999.

32. Xu, H., Fu, H., Williams, H., and Shilling, I., "Modeling Study of Combustion and Gas Exchange in a HCCI (CAI) Engine," SAE Paper No. 2002-01-0114, Warrendale, PA 2002.

33. Dec, J. E., "A Computational Study of the Effects of Low Fuel Loading and EGR on Heat Release Rates and Combustion Limits in HCCI Engines," SAE Paper No. 2002-01-1309, Warrendale, PA 2002.

34. Aceves, S. M., "A Multi-Zone Model for Prediction of HCCI Combustion and Emissions," SAE Paper No. 2000-01-0327, Warrendale, PA 2000.

35. Easley, W. L., Agarwal, A., and Lavole, G., "Modeling of HCCI Combustion and Emissions Using Detailed Chemistry," SAE Paper No. 2001-01-1029, Warrendale, PA 2001.

36. Griffiths, J., Halford-Maw, P. A., and Mohamed, C., "Spontaneous Ignition Delays as a Diagnostic of the Propensity of Alkenes to Cause Engine Knock," Combustion and Flame, Vol. 111, pp.327-337, 1997.

37. Curran, H. J., Gaffuri, P., Pitz, W. J., and Westbrook, C. K., "A Comprehensive Modeling Study of n-Heptane Oxidation," Combustion and Flame, Vol. 114, pp. 149-177, 1998.

38. Christensen, M., Einewall, P., and Johansson, B., "Homogeneous Charge Compression Ignition (HCCI) Using Isoctane, Etanol and Natural Gas: A Comparison with Spark Ignition Operation," SAE Paper No. 972874, Warrendale, PA 1997.

39. Ishibashi, Y., "Basic Understanding of Activated Radical Combustion and its Two-Stroke Engine Application and Benefits," SAE Paper No. 2000-01-1836, Warrendale, PA 2000.

40. Christensen, M., and Johansson, B., "Influence of Mixture Quality on Homogeneous Charge Compression Ignition," SAE Paper No. 982454, Warrendale, PA 1998.

41. Christensen, M., Johansson, B., Amneus, P. J., and Gauss, F., "Supercharged Homogenous Charge Compression Ignition", SAE Paper No. 980787, Warrendale, PA 1998.

42. Flowers, D., Aceves, S. M., Smith, J. R., Torres, J., Girard, J., and Dibble, R. W., "HCCI in a CFR Engine: Experiments and Detailed Kinetic Modeling," SAE Paper No. 2000-01-0328, Warrendale, PA 2000.

43. Law, D., and Allen, J., "On the Mechanism of Controlled Auto-Ignition," SAE Paper No. 2002-01-0421, Warrendale, PA 2002.

44. Law, D., Allen, J., Kemp, D., Kirkpatrick, G., and Copland, T., "Controlled Combustion in an IC Engine with a Fully Variable Valve Train," SAE Paper No. 2001-01-0251, Warrendale, PA 2001.

45. Ryan III, T. W., and Matheaus, A. C., "Fuel Requirements for HCCI Engine Operation," SAE Paper No. 2003-01-1813, Warrendale, PA 2003.

46. Jeuland, N. et al. "Engine and Fuel Related Issues of Gasoline CAI (Controlled Auto-Ignition) Combustion", SAE paper, 2003-01-1856, 2003.

47. Christensen, M., Hultquist, A., Johansson, B., Franke, A., Richter, M., and Alden, M., "A Study of the Homogenous Charge Compression Ignition with Water Injection," SAE Paper No. 1999-01-3680, Warrendale, PA 1999.

48. Lida, N. Y., "Auto-Ignition and Combustion of n-Butane and DME/Air Mixtures in a Homogenous Charge Compression Engine," SAE Paper No. 2000-01-1832, Warrendale, PA 2000.

49. Ryan III, T. W., and Callahan, T. J., "Homogenous Charge Compression Ignition (HCCI) of Diesel Fuel," SAE Paper No. 961160, Warrendale, PA 1996.

50. Chen, Z., and Mitsuru, K., “How to Put the HCCI Engine to Practical Use: Control the Ignition Timing By Compression Ratio and Increase the Power Output by Supercharge,” SAE Paper No. 2003-01-1832, Warrendale, PA 2003.

51. Kontarakis. G., Collings, N., and Ma, T. H, “Demonstration of HCCI Using a Single Cylinder Four-Stroke SI Engine with Modified Valve Timing,” SAE Paper No. 2000-01-2870, Warrendale, PA 2000.

52. Ogura, M., Sasaki, T., and Kawaguchi, Y., “HCCI Combustion Control by Intake and Exhaust Continuous Variable Valve Timing Mechanism in Premixed Gasoline Engine,” SAE Paper No. 2004-32-0096, Warrendale, PA 2004.

53. Yap, D., Wyszynski, M. L., Megaritis, A., Peucheret, S. M., and Xu, H., ”Effect of Hydrogen Addition on Natural Gas HCCI Combustion,” SAE Paper No. 2004-01-1972, Warrendale, PA 2004.

54. Oakley, A., Zhao, H., Ladommatos, N., and Ma, T., “Experimental Studies on Controlled Auto-Ignition (CAI) Combustión of Gasolina in a 4-Stroke Engine,” SAE Paper No. 2001-01-1030, Warrendale, PA 2001.

55. Zhao, H., Li, J., and Ladommatos, N., “Performance and Analysis of a Four-Stroke Multi-Cylinder Gasoline Engine with CAI Combustion,” SAE Paper No. 2002-01-0420, Warrendale, PA 2002.

56. Hiraya, K., Hasegawa, K., Urushihara, T., Liyama, A., and Itoh, T., “A Study on Gasoline Fueled Compression Ignition Engine: A Trial of Operation Region Expansion,” SAE Paper No. 2002-01-0416, Warrendale, PA 2002.

57. Yamaoka, S., Shimada, A., Kihara, Y., Kakuya, H., Nakagawa, S., and Nogi, T., “A Study of Controlling the Auto-Ignition and Combustion in a Gasoline HCCI Engine,” SAE Paper No. 2004-01-0942, Warrendale, PA 2004.

58. Olsson, J. O., Tunestal, P., and Johansson, B, ”Boosting for High Load HCCI,” SAE Paper No. 2004-01-0940, Warrendale, PA 2004.

59. Leach, B., Zhao, H., and Li, Y., “Control of CAI Combustion Through Injection Timing in a GDI Engine with an Air-Assisted Injector,” SAE Paper No. 2005-01-0134, Warrendale, PA 2005.

60. Loth, J. L., Loth, E., and Loth, F., “Isolated Combustion and Diluted Expansion (ICADE) Piston Engine,” United States Patent 5.239.959, Alexandria, VA 1993.

61. El-Messiri, I. A., “The Divided Combustion Chamber Concept and Design For Control of SI Engine Exhaust Air Pollutant Emissions,” Ph.D. Dissertation, University of Wisconsin, 1973.

62. Borman, G. L., "Mathematical Simulation of Internal Combustion Engine Processes and Performance Including Comparison with Experiment," Ph.D. Thesis, University of Wisconsin, 1964.

63. Newhall, H. K., and Starkman, E. S., "Thermodynamic Properties of Octane and Air for Engine Performance Calculations," SAE Paper 633G, Warrendale, PA 1963.

64. JANAF Thermochemical Tables", 2nd Edition., National Bureau of Standards Publications, NSRDS-N35 37, Washington D. C., 1971.

65. Lichty, L. C., Internal Combustion Engines, McGraw Hill Book Company, New York, NY 1951.

66. Moran, M. J., and Shapiro, H. N., Fundamentals of Engineering Thermodynamics 4th Edition, John Wiley & Sons, Inc, New York, NY 2000.

67. ASTM Manual for Rating Motor Fuels by Research and Motor Methods 6th Edition, American Society for Testing and Materials (ASTM), Rahway, NJ 1969.

68. Lancaster, D. R., Krieger, R. B., and Lienesch, J. H., "Measurement and Analysis of Engine Pressure Data," SAE Paper No. 750026, Warrendale, PA 1975.

69. Gatowski, J. A., Balles, E. N., Chun, K. M., Nelson, F. E., Ekchian, J. A., and Heywood, J. B., "Heat Release Analysis of Engine Pressure Data," SAE paper, 841359, Warrendale, PA 1984.

70. Woschni, G., "A Universally Applicable Equation for the Instantaneous Heat Transfer Coefficient in the Internal Combustion Engine," SAE Paper No. 670931, Warrendale, PA 1967.

71. Rassweiler, G. M., and Withrow, L., "Motion Pictures of Engine Frames Correlated with Pressure Cards," SAE Paper No. 970037, Warrendale, PA 1997.

72. Stone, R., Introduction to Internal Combustion Engines, SAE Book, Warrendale, PA, 1994.

73. Lipson, C., and Sheth, N. J., Statistical Design and Analysis of Engineering Experiments, McGraw Hill Book Company, New York, NY 1973.

Appendixes

Appendix A: CIBAI Analytical and Numerical Modeling Program Code

CIBAI Cycle Analysis Code

```
%Name: CIBAI Numerical Model Code
%Institution:West Virginia University
%Developed by: Fernando Echavarria Hidalgo
%Date: February 14, 2006
%Objectives:
%Perform a complete thermodynamic analysis of the CIBAI
%cycle,and compare the results with the ones obtained for the Otto and
%Diesel cycles under comparable parameters.

% --- Executes on button press in clear.
function clear_Callback(hObject, eventdata, handles)
% hObject    handle to clear (see GCBO)
% eventdata  reserved - to be defined in a future version of MATLAB
% handles    structure with handles and user data (see GUIDATA)

set(handles.cibaieff,'string','');%Empty fields
set(handles.ottoeff,'string','');%Empty fields
set(handles.dieseleff,'string','');%Empty fields

cla reset %resets the properties of the current axes.

% --- Executes on button press in plotpressure.
function plotpressure_Callback(hObject, eventdata, handles)
% hObject    handle to plotpressure (see GCBO)
% eventdata  reserved - to be defined in a future version of MATLAB
% handles    structure with handles and user data (see GUIDATA)

%Variable definition

set(gcf, 'name','CIBAI Cycle');
grid; %add grids to current axes

rvastring=get(handles.rva,'string');%get rva string value from screen
rva=str2num(rvastring);%convert rva string value to numeric value

rvafstring=get(handles.rvaf,'string'); %get rvaf string value from screen
rvaf=str2num(rvafstring);%convert rvaf string value to numeric value

nstring=get(handles.n,'string'); %convert n string value to numeric value
```

```
n=str2num(nstring); %convert n string value to numeric value

rcstring=get(handles.rc,'string'); %convert rc string value to numeric value
rc=str2num(rcstring); %convert rc string value to numeric value

stob=1; %input('Stroke-to-Bore Ratio:');
vdo=1; %input('Volume Displacement:');
crtoca=5; %input('Connecting Rod Length to Crank Angle Offset Ratio:');
```

%Initial Calculations

```
vcaftovdo=vdo/(rvaf-1);
%Volume clearance air fuel cylinder to volume displacement
vcatovdo=vdo/(rva-1);
%Volume clearance air only cylinder to volume displacement
bore=(vdo*4/(pi*stob))^(1/3);%Bore
stroke=bore*vdo; %Stroke
co=stroke/2; %Crank offset
crl=co*crtoca; %Connecting rod length
rm=(vdo+vcatovdo)/(vdo+vcaftovdo); %Mass ratio
taft1=rvaf^(n-1);%Taf/T1
tat1=rva^(n-1);%Taf/T1
t2tot1=(1/(1+rm))*(taft1+tat1*rm); %T2/T1
t3tot1=t2tot1*rc; %T3/T1
p2afp1=rvaf^(n); %P2af/P1
p2ap1=rva^(n); %P2a/P1
v2tovdo=vcaftovdo+vcatovdo; %V2/Vdo
p2p1=(t2tot1)/(v2tovdo/(v2tovdo+2*vdo));%P2/P1
p3p1=p2p1*rc;%P3/P1
```

%Overall Efficiency Comparison

```
wintomocvt1=rvaf^(n-1)-1+(rva^(n-1)-1)*rm;  %Work in
wouttomocvt1=rc*(rvaf^(n-1)+rva^(n-1)*rm)*(1-(v2tovdo/(v2tovdo+2))^(n-1));
%Work out
qintomocvt1=(rvaf^(n-1)+rva^(n-1)*rm)*(rc-1);%Heat in
woutoqin=wouttomocvt1/qintomocvt1; %Work out over heat in
wintoqin=wintomocvt1/qintomocvt1; %Work in over heat in
cibaieff=(woutoqin-wintoqin)*100; %CIBAI thermal efficiency
ottoeff=(1-1/rvaf^(n-1))*100; %OTTO thermal efficiency
dieseleff=(1-1/rva^(n-1)*(rc^n-1)/(n*(rc-1)))*100; %DIESEL thermal efficiency
```

%Vector to store P/P1 ratio

```
paftop1=(0:720); %Instantaneous Taf/T1
patop1=(0:720); %Instantaneous Ta/T1
p4top1=(0:720); %Instantaneous T4/T1
detonationlinepressure=(0:720); %Detonation line temperature diagram

for i=1:length(ca)

cpdi=co*cos(ca(i)*pi/180)+(crl^2-co^2*sin(ca(i)*pi/180)^(2))^(1/2);
%Distance between crank axis and wrist pin axis
vdoi=((pi*bore^(2))/4)*(crl+co-cpdi);%Instantaneous volume displacement

if ca(i)>=0 & ca(i)<180

paftop1(i)=1;
patop1(i)=1;
p4top1(i)=0;
detonationlinepressure(i)=0;

elseif ca(i)>=180 & ca(i)<359

paftop1(i)=(((vcaftovdo)/(vcaftovdo+vdoi))^(n))*rvaf^(n);
patop1(i)=(((vcatovdo)/(vcatovdo+vdoi))^(n))*rva^(n);
p4top1(i)=0;
detonationlinepressure(i)=0;
elseif ca(i)==359

detonationlinepressure(i)=(((vcaftovdo)/(vcaftovdo+vdoi))^(n))*rvaf^(n);
paftop1(i)=0;
patop1(i)=0;
p4top1(i)=0;
elseif ca(i)==360

detonationlinepressure(i)=(p3p1)*((vcaftovdo+vcatovdo)/(vcaftovdo+vcatovdo+2*vdoi))
^(n);
paftop1(i)=0;
patop1(i)=0;
p4top1(i)=0;
elseif ca(i)>360 & ca(i)<=540

paftop1(i)=0;
patop1(i)=0;
p4top1(i)=(p3p1)*((vcaftovdo+vcatovdo)/(vcaftovdo+vcatovdo+2*vdoi))^(n);
detonationlinepressure(i)=0;
```

```
elseif ca(i)>540 & ca(i)<=720

paftop1(i)=0;
patop1(i)=0;
p4top1(i)=1;
detonationlinepressure(i)=0;

else
disp('Crank Angle is between 0 and 720 ca degree');
end
end
```

%Plot pressure ratio diagram

```
handle10=plot(ca(1:359),paftop1(1:359),'g-');
set(handle10,'LineWidth',2);
hold on
handle11=plot(ca(1:359),patop1(1:359),'k-');
set(handle11,'LineWidth',2);
hold on
handle12=plot(ca(360:361),detonationlinepressure(360:361),'r-');
set(handle12,'LineWidth',2);
hold on
handle13=plot(ca(362:540),p4top1(362:540),'b-');
set(handle13,'LineWidth',2);
hold on
handle14=plot(ca(541:721),p4top1(541:721),'b-');
set(handle14,'LineWidth',2);
grid %draws a grid over the plot
set(gca,'FontWeight','bold');
title('P/P1 vs. Crank Angle');
xlabel('Crank Angle');
ylabel('P/P1');
legend('Paf/P1', 'Pa/P1', 'Denotation', 'Pprod/P1')
```

%Display results

```
set(handles.cibaieff,'string', cibaieff);       %Cibai efficiency
set(handles.ottoeff,'string', ottoeff);         %Otto efficiency
set(handles.dieseleff,'string', dieseleff);     %Diesel efficiency
```

```
% --- Executes on button press in plottemperature.
function plottemperature_Callback(hObject, eventdata, handles)

% hObject    handle to plottemperature (see GCBO)
% eventdata  reserved - to be defined in a future version of MATLAB
% handles    structure with handles and user data (see GUIDATA)

%Variable definition

set(gcf, 'name','CIBAI Cycle');
grid; %add grids to current axes

rvastring=get(handles.rva,'string'); %get rva string value from screen
rva=str2num(rvastring); %convert rva string value to numeric value

rvafstring=get(handles.rvaf,'string'); %get rvaf string value from screen
rvaf=str2num(rvafstring); %convert rvaf string value to numeric value

nstring=get(handles.n,'string'); %convert n string value to numeric value
n=str2num(nstring); %convert n string value to numeric value

rcstring=get(handles.rc,'string'); %convert rc string value to numeric value
rc=str2num(rcstring); %convert rc string value to numeric value

stob=1; %input('Stroke-to-Bore Ratio:');
vdo=1; %input('Volume Displacement:');
crtoca=5; %input('Connecting Rod Length to Crank Angle Offset Ratio:');

%Initial Calculations

vcaftovdo=vdo/(rvaf-1); %Volume clearance air fuel cylinder to volume displacement
vcatovdo=vdo/(rva-1); %Volume clearance air only cylinder to volume displacement

bore=(vdo*4/(pi*stob))^(1/3); %Bore
stroke=bore*vdo; %Stroke
co=stroke/2; %Crank offset
crl=co*crtoca; %Connecting rod length
rm=(vdo+vcatovdo)/(vdo+vcaftovdo); %Mass ratio
taft1=rvaf^(n-1); %Taf/T1
tat1=rva^(n-1); %Taf/T1
t2tot1=(1/(1+rm))*(taft1+tat1*rm); %T2/T1
t3tot1=t2tot1*rc; %T3/T1
p2afp1=rvaf^(n); %P2af/P1
p2ap1=rva^(n); %P2a/P1
v2tovdo=vcaftovdo+vcatovdo; %V2/Vdo
p2p1=(t2tot1)/(v2tovdo/(v2tovdo+2*vdo));%P2/P1
```

```
p3p1=p2p1*rc; %P3/P1
```

%Overall Efficiency Comparison

```
wintomocvt1=rvaf^(n-1)-1+(rva^(n-1)-1)*rm; %Work in
wouttomocvt1=rc*(rvaf^(n-1)+rva^(n-1)*rm)*(1-(v2tovdo/(v2tovdo+2))^(n-1));
%Work out
qintomocvt1=(rvaf^(n-1)+rva^(n-1)*rm)*(rc-1); %Heat in
woutoqin=wouttomocvt1/qintomocvt1; %Work out over heat in
wintoqin=wintomocvt1/qintomocvt1; %Work in over heat in
cibaieff=(woutoqin-wintoqin)*100; %CIBAI thermal efficiency
ottoeff=(1-1/rvaf^(n-1))*100; %OTTO thermal efficiency
dieseleff=(1-1/rva^(n-1)*(rc^n-1)/(n*(rc-1)))*100; %DIESEL thermal efficiency
```

%Vector to store T/T1 ratio

```
ca=(0:720); %Crank angle vector
length(ca); %Length crank angle vector
taftot1=(0:720); %Instantaneous Taf/T1
tatot1=(0:720); %Instantaneous Ta/T1
t4tot1=(0:720); %Instantaneous T4/T1
detonationlinetemperature=(0:720); %Detonation line temperature diagram

for i=1:length(ca)

cpdi=co*cos(ca(i)*pi/180)+(crl^2-co^2*sin(ca(i)*pi/180)^(2))^(1/2);
%Distance between crank axis and wrist pin axis
vdoi=((pi*bore^(2))/4)*(crl+co-cpdi);%Instantaneous volume displacement

if ca(i)>=0 & ca(i)<180
taftot1(i)=1;
tatot1(i)=1;
t4tot1(i)=0;
detonationlinetemperature(i)=0;

elseif ca(i)>=180 & ca(i)<359
taftot1(i)=(((vcaftovdo)/(vcaftovdo+vdoi))^(n-1))*rvaf^(n-1);
tatot1(i)=(((vcatovdo)/(vcatovdo+vdoi))^(n-1))*rva^(n-1);
t4tot1(i)=0;
detonationlinetemperature(i)=0;

elseif ca(i)==359

detonationlinetemperature(i)=(((vcaftovdo)/(vcaftovdo+vdoi))^(n-1))*rvaf^(n-1);

taftot1(i)=0;
```

```
tatot1(i)=0;
t4tot1(i)=0;

detonationlinetemperature(i)=(t3tot1)*((vcaftovdo+vcatovdo)/(vcaftovdo+vcatovdo+2*v
doi))^(n-1);

taftot1(i)=0;
tatot1(i)=0;
t4tot1(i)=0;
elseif ca(i)>360 & ca(i)<=540
taftot1(i)=0;
tatot1(i)=0;
t4tot1(i)=(t3tot1)*((vcaftovdo+vcatovdo)/(vcaftovdo+vcatovdo+2*vdoi))^(n-1);
detonationlinetemperature(i)=0;

elseif ca(i)>540 & ca(i)<=720
taftot1(i)=0;
tatot1(i)=0;
t4tot1(i)=1;
detonationlinetemperature(i)=0;

else
disp('Crank Angle is between 0 and 720 ca degree');
end
end
```

%Plot Temperature ratio diagram

```
handle5=plot(ca(1:359),taftot1(1:359),'g-');
set(handle5,'LineWidth',2);
hold on
handle6=plot(ca(1:359),tatot1(1:359),'k-');
set(handle6,'LineWidth',2);
hold on
handle7=plot(ca(360:361),detonationlinetemperature(360:361),'r-');
set(handle7,'LineWidth',2);
hold on
handle8=plot(ca(362:540),t4tot1(362:540),'b-');
set(handle8,'LineWidth',2);
hold on
handle9=plot(ca(541:721),t4tot1(541:721),'b-');
set(handle9,'LineWidth',2);
grid %draws a grid over the plot
set(gca,'FontWeight','bold');

title('T/T1 vs. Crank Angle');
```

```
xlabel('Crank Angle');
ylabel('T/T1');
legend('Taf/T1', 'Ta/T1', 'Detonation', 'Tprod/T1')

%Display Results

set(handles.cibaieff,'string', cibaieff);       %Cibai efficiency
set(handles.ottoeff,'string', ottoeff);         %Otto efficiency
set(handles.dieseleff,'string', dieseleff);     %Diesel efficiency

% --------------------------------------------------------------------
function Analysis_Callback(hObject, eventdata, handles)
% hObject    handle to Analysis (see GCBO)
% eventdata  reserved - to be defined in a future version of MATLAB
% handles    structure with handles and user data (see GUIDATA)

gui;%Call cycle analysis program

% --------------------------------------------------------------------
function Numerical_modeling_Callback(hObject, eventdata, handles)
% hObject    handle to Numerical_modeling (see GCBO)
% eventdata  reserved - to be defined in a future version of MATLAB
% handles    structure with handles and user data (see GUIDATA)

gui2;%Call numerical modeling program

% --------------------------------------------------------------------
function raw_data_Callback(hObject, eventdata, handles)
% hObject    handle to raw_data (see GCBO)
% eventdata  reserved - to be defined in a future version of MATLAB
% handles    structure with handles and user data (see GUIDATA)

raw; %Open raw data screen
```

CIBAI Numerical Modeling Code

```
%Institution:West Virginia University
%Developed by: Fernando Echavarria Hidalgo
%Date: February 14, 2006
%Objectives:
%1)Perform numerical integration using in-cylinder pressure
%data to calculate engine power and combustion parameters such as, indicated net work,
%indicated mean effective pressure (IMEP),thermal efficiency, net heat release,
%heat release rate, mass fraction burned (MFB),ignition delay,and combustion duration.
%2)Conduct a parametric study using experimental data as an input to
%predict the effect of compression ratio, air injection pressure, intake
%temperature, air-fuel ratio, and air injection timing on CIBAI combustion.

% --- Executes on button press in pushbutton1.
function pushbutton1_Callback(hObject, eventdata, handles)
% hObject    handle to pushbutton1 (see GCBO)
% eventdata  reserved - to be defined in a future version of MATLAB
% handles    structure with handles and user data (see GUIDATA)

set(gcf, 'name','CIBAI Numerical Modeling');


%Create a get file box

[filename, pathname]=uigetfile('*.m;*.xls',...
  'Open File');

if isequal(filename,0) | isequal(pathname,0)

else

set(gcf, 'name',filename);

%Download test data from excel

%filename=input('Enter File Name: ','fl');%Enter file name

test=xlsread(filename); %Downloading in-cylinder pressure data

%Input variables

crstring=get(handles.cr,'string');%get cr string value from screen
cr=str2num(crstring);%convert cr string value to numeric value

acpstring=get(handles.acp,'string');%get acp string value from screen
```

```
acp=str2num(acpstring);%convert acp string value to numeric value

gammastring=get(handles.n,'string');%convert n string value to numeric value
gamma=str2num(gammastring);%convert n string value to numeric value

flstring=get(handles.fl,'string');%convert fl string value to numeric value
fl=str2num(flstring);%convert fl string value to numeric value

afrstring=get(handles.afr,'string');%convert afr string value to numeric value
afr=str2num(afrstring);%convert afr string value to numeric value
exhtempstring=get(handles.exhtemp,'string'); %convert exhtemp string value to numeric
value
exhtemp=str2num(exhtempstring);%convert exhtemp string value to numeric value

itempstring=get(handles.itemp,'string');%convert itemp string value to numeric value
intemp=str2num(itempstring);%convert itemp string value to numeric value

ipresstring=get(handles.intpre,'string');%convert intpre string value to numeric value
inpres=str2num(ipresstring);%convert intpre string value to numeric value
```

%Calculate combustion duration and injection delay

```
intimstring=get(handles.intim,'string');
%convert air injection timing string value to numeric value
injection_delaystring=get(handles.injection_delay,'string');
%convert spark timing string value to numeric value

if get(handles.checkbox2,'Value')==1
injtiming=360-str2num(injection_delaystring);
%convert spark timing string value to numeric value
else
injtiming=360-str2num(intimstring)+50;
%convert rc string value to numeric value
end

sfstring=get(handles.sf,'string');%convert sf string value to numeric value
scalefactor=str2num(sfstring);%convert sf string value to numeric value
```

%Fixed Variables

```
vd=612.5; %Volume displacement
stroke=4.5;%Stroke
bore=3.25;%Bore
crlength=10;%Connecting Rod Lenght(in)
```

%Initial Calculations

```
tcycle=0.1309;%Duration combustion cycle
disptft=3/12;%Distance pressure transducer
dtheta=0.55;%delta theta
vcin=vd/(cr-1)/(2.54)^3;%Volume clearance in^3
coff=stroke/2;%Crank Offset
crlovercoff=crlength/coff;%Coonecting rod length to crank offset ratio
vdin=0.25*pi*bore^2*stroke;%Volume displacement in^3
vtotal=vcin+vdin;%Total volume
intempr=intemp+460;%Initial temperature in Ranking
temp2=intempr*cr^((gamma-1)/gamma);%Isentropic temperature 2
gasconst=1716;%Gas constant
speedsound=sqrt(gamma*gasconst*temp2);%speed of sound
inprespsig=(inpres/29.92)*14.7;%intake pressure in psig
tlag=disptft/speedsound;%Time lag due to the distance to the PT as a function of speed of
sound
dthetadt=720/tcycle;%Variation of angle with respect time
rpm=dthetadt/6;%RMP
```

%Vector to store pressure and crank angle data

```
global ca2;
global abspressure;
global rawnheatrel;
global rawnheatrat;

ca2=(0:0.55:720);%Crank angle vector
length(ca2);%Length crank angle vector

count = 0;
```

%Adjusted in-cylinder pressure data

```
sigviewfactor=0.3062;%sigview factor 1 sigview unit=0.0003062 volts
ptsens=5;%pressure transducer sensitivity 5 mv = 1 psig
scaletest=test+scalefactor;%Scale pressure
abspressure= inprespsig + scaletest*sigviewfactor/ptsens;%In-cylinder absolute pressure
```

%Change color and line type for the plot

```
value_color=get(handles.listbox1,'value');
value_line=get(handles.listbox2,'value');
```

%Set graph color

```
if value_color==1
color_str='k';
elseif value_color==2
color_str='g';
elseif value_color==3
color_str='r';
elseif value_color==4
color_str='b';
end
```

%Set line type

```
if value_line==1
line_str='-';
elseif value_line==2
line_str=':';
elseif value_line==3
line_str='-.';
elseif value_line==4
line_str='--';
end

style=strcat(color_str,line_str);

if get(handles.checkbox1,'Value')==1 %Proceed for motored pressure graph analysis

for i=1:length(ca2)

ca2rad(i)=ca2(i).*pi/180; %Crank angle vector in radians
vcinst(i)=vdin/(cr-1)+(vdin/2)*(1+crlovercoff-cos(ca2rad(i))-sqrt(crlovercoff^2-
(sin(ca2rad(i)))^2));%Instantaneous volume displacement
crinst(i)=+(vcinst(i)+vdin)/vcinst(i); %Instantaneous compression ratio

end

for i=1:length(ca2)

if ca2rad(i)==0

dvinst(i)=0;%Instantaneous change in volume
workftlb(i)=0;%Indicated work (ft-lb)
powerhp(i)=0;%Power (hp)

else

p=i-1;
```

```
dvinst(i)= vcinst(i)-vcinst(p);%Instantaneous change in volume
workftlb(i)=dvinst(i)*abspressure(i)/12;%Indicated work (ft-lb)

end
end
```

%Plot in-cylinder pressure diagram

```
axes(handles.axes4);
set(handles.axes4,'xgrid','on','ygrid','on');
handle1=plot(ca2,abspressure, style);
set(handle1,'LineWidth',2);
hold on
grid on
```

%Indicated Net Work and IMEP Calculations

```
inetwork=sum(workftlb)*1.35582;%Indicated net work (J)
imep=(sum(workftlb)/vdin)*12; %IMEP(psi)
```

%Display Results

```
set(handles.inw,'string', inetwork);%Cibai efficiency
set(handles.imep,'string', imep);%Otto efficiency
set(handles.nhr,'string', 0);%Diesel efficiency
set(handles.id,'string', 0);%Cibai efficiency
set(handles.cd,'string', 0);%Otto efficiency
set(handles.eff,'string', 0);%Diesel efficiency
set(handles.start_combustion,'string', 0);%Otto efficiency
set(handles.end_combustion,'string', 0);%Diesel efficiency

else
```

%Fill instantaneous vectors

```
for i=1:length(ca2)

ca2rad(i)=ca2(i).*pi/180; %Crank angle vector in radians
vcinst(i)=vdin/(cr-1)+(vdin/2)*(1+crlovercoff-cos(ca2rad(i))-sqrt(crlovercoff^2-
(sin(ca2rad(i)))^2));%Instantaneous volume displacement
crinst(i)=+(vcinst(i)+vdin)/vcinst(i); %Instantaneous compression ratio

end


for i=1:length(ca2)
```

```
if ca2rad(i)==0

dvinst(i)=0;%Instantaneous change in volume
workftlb(i)=0;%Indicated work (ft-lb)
powerhp(i)=0;%Power (hp)

else

p=i-1;
dvinst(i)= vcinst(i)-vcinst(p);%Instantaneous change in volume
workftlb(i)=dvinst(i)*abspressure(i)/12;%Indicated work (ft-lb)
powerhp(i)=workftlb(i)/0.055;%Power (hp)

rawnheatrat(i)=(((vcinst(i)+dtheta)*(abspressure(i)-
abspressure(p)*(vcinst(p)/vcinst(i))^gamma)/((gamma-1)*dtheta))/12)*1.35582; %Net
heat release rate (J/Degree)
rawnheatrel(i)=(((vcinst(i)*(abspressure(i)-
abspressure(p)*(vcinst(p)/vcinst(i))^gamma)/((gamma-1)*dtheta))/12)*1.35582)*dtheta;
%Heat release rate (J/Degree)

end
end
```

%Determine beginning and end of combustion

```
 [maxnheatrel,locmaxnheatrel]=max(rawnheatrel);%Maximum point of heat release

startcomb=0;%Start combustion
endcomb=0;%End combustion
w=0;%Counter

for v=1:length(rawnheatrel)
w=locmaxnheatrel-v;
if w>0
if rawnheatrel(w)<=0

startcomb=w;%determine start combustion
break
end
end
end

for f=1:length(rawnheatrel)
if f>locmaxnheatrel
if rawnheatrel(f)<=0
```

```
endcomb=f;%determine end combustion
break
end
end
end
```

%Fill actual heat release and heat release rate vectors

```
sumheatrel=0; %Summation heat release
count1=0; %Counter for heat release vectors
for i=1:length(rawnheatrel)
if i>=startcomb & i<=endcomb
count1=count1+1; %Counter for heat release vectors
nheatrel(count1)=rawnheatrel(i);%Net heat release
nheatrat(count1)=rawnheatrat(i);%Net heat release
xheat(count1)=ca2(i);%X axis for heat release graph
sumheatrel= sumheatrel + nheatrel(count1);%Summation heat release scalar
sumheatrelvec(count1)=sumheatrel;%Summation heat release vector
end

end
```

%Calculation mass fraction burned (MFB)

```
for k=1:length(sumheatrelvec)
mfb(k)= (sumheatrelvec(k)/sumheatrel)*100;
end
```

%Indicated net work and IMEP

```
inetwork=sum(workftlb)*1.35582;%Indicated net work (J)
imep=(sum(workftlb)/vdin)*12; %IMEP(psi)
thermaleff=(inetwork/sumheatrel)*100;%Thermal efficiency
```

%Calculation ignition delay

```
ignitiondelay=0;
for g=1:length(mfb)
if mfb(g)>=10 %10 percent MFB
tenpercentmark=xheat(g);%Crank angle degree at 10 percent MFB

if ca2(startcomb)>injtiming
ignitiondelay= ((tcycle*(xheat(g)-injtiming))/720)*1000; %Ignition delay

else
disp('Warning: Review Spark-Injection Timing');
```

```
disp('*************************************************');

end
break
end

end
```

%Calculation combustion duration

```
for g=1:length(mfb)
if mfb(g)>=90 %90 percent MFB
ninetypercentmark=xheat(g);%Crank angle degree at 10 percent MFB
break
end
end

combustionduration= ((tcycle*(ninetypercentmark-tenpercentmark))/720)*1000;
```

%Display Results

```
set(handles.inw,'string', inetwork);       %Cibai efficiency
set(handles.imep,'string', imep);         %Otto efficiency
set(handles.nhr,'string', sumheatrel);     %Diesel efficiency
set(handles.id,'string', ignitiondelay);       %Cibai efficiency
set(handles.cd,'string', combustionduration);         %Otto efficiency
set(handles.eff,'string', thermaleff);     %Diesel efficiency
set(handles.start_combustion,'string',ca2(startcomb));%Start combustion
set(handles.end_combustion,'string',ca2(endcomb));%End combustion
```

%Plotting

```
global handle1 handle2 handle3 handle4

%Plot in-cylinder pressure diagram

axes(handles.axes4);
set(handles.axes4,'xgrid','on','ygrid','on');
handle1=plot(ca2,abspressure, style);
hold on
grid on
set(handle1,'LineWidth',2);
title('In-Cylinder Pressure vs. Crank Angle');
xlabel('CA Degree');
ylabel('Pressure [psi]');
```

%Plot net heat release

```
axes(handles.axes2);
handle2=plot(xheat, sumheatrelvec, style);
hold on
grid on
set(handle2,'LineWidth',2);
title('Net Heat Release vs. Crank Angle');
xlabel('CA Degree');
ylabel('Net Heat Release [J]');
```

%Plot net heat release rate

```
axes(handles.axes3);
handle3=plot(xheat,nheatrat, style);
hold on
grid on
set(handle3,'LineWidth',2);
title('Net Heat Release Rate vs. Crank Angle');
xlabel('CA Degree');
ylabel('Net Heat Release Rate[J/Degree]');
```

%Plot mass fraction burned

```
axes(handles.axes1);
handle4=plot(xheat,mfb, style);
hold on
grid on
set(handle4,'LineWidth',2);
title('Mass Fraction Burned (MFB) vs. Crank Angle');
xlabel('CA Degree');
ylabel('Mass Fraction Burned (MFB)[%]');

end
end
```

function pushbutton7_Callback(hObject, eventdata, handles)

```
% hObject    handle to pushbutton7 (see GCBO)
% eventdata  reserved - to be defined in a future version of MATLAB
% handles    structure with handles and user data (see GUIDATA)

global handle1

%Reset axes

reset(handles.axes1);
```

```
set(handles.axes1,'xgrid','on','ygrid','on')
reset(handles.axes2);
set(handles.axes2,'xgrid','on','ygrid','on');
reset(handles.axes3);
set(handles.axes3,'xgrid','on','ygrid','on');
reset(handles.axes4);
set(handles.axes4,'xgrid','on','ygrid','on');
reset(gca);
set(gca,'xgrid','on','ygrid','on');

% --- Executes on button press in save.
function save_Callback(hObject, eventdata, handles)
% hObject    handle to save (see GCBO)
% eventdata  reserved - to be defined in a future version of MATLAB
% handles    structure with handles and user data (see GUIDATA)

%Save results into an excel file
global abspressure;
maxpressure=max(abspressure);

savedata(1)=str2num(get(handles.cr,'string'));%Compression ratio
savedata(2)=str2num(get(handles.acp,'string'));%Air injection pressure
savedata(3)=str2num(get(handles.n,'string'));%Polytropic index
savedata(4)=str2num(get(handles.fl,'string'));%Fuel level
savedata(5)=str2num(get(handles.afr,'string'));%Air fuel rate
savedata(6)=str2num(get(handles.exhtemp,'string'));%Exhaust temperature
savedata(7)=str2num(get(handles.itemp,'string'));%Intake temperature
savedata(8)=str2num(get(handles.intpre,'string'));%Intake pressure
savedata(9)=str2num(get(handles.intim,'string'));%Air injection timing
savedata(10)=str2num(get(handles.injection_delay,'string'));%Spark ignition
savedata(11)=str2num(get(handles.sf,'string'));%Scale factor
savedata(12)=str2num(get(handles.inw,'string'));%Indicated net work
savedata(13)=str2num(get(handles.imep,'string'));%Indicated mean effective pressure
savedata(14)=str2num(get(handles.nhr,'string'));%Net heat release
savedata(15)=str2num(get(handles.id,'string'));%Ignition delay
savedata(16)=str2num(get(handles.cd,'string'));%Combustion duration
savedata(17)=str2num(get(handles.eff,'string'));%Thermal efficiency
savedata(18)=str2num(get(handles.start_combustion,'string'));
%Start combustion crank angle
savedata(19)=str2num(get(handles.end_combustion,'string'));
%End combustion crank angle
savedata(20)=maxpressure;%Peak pressure

coldata= savedata'; %Convert row into column

%Create a save as box
```

```
[filename, pathname] = uiputfile( ...
      {'*.m;*.fig;*.mat;*.mdl', 'All MATLAB Files (*.m, *.fig, *.mat, *.mdl)'; ...
      '*.xls;*.wk1;*.csv',      'Spreadsheet Files(*.xls, *.wk1, *.csv)';...
       '*.*',                   'All Files (*.*)'}, ...
      'Save as');

if isequal(filename,0) | isequal(pathname,0)

else

f='.';
g='xls';

string=strcat(filename,f,g);

wk1write(string,coldata);%Save records into root directory

end

% --- Executes on button press in pushbutton10.
function pushbutton10_Callback(hObject, eventdata, handles)
% hObject    handle to pushbutton10 (see GCBO)
% eventdata  reserved - to be defined in a future version of MATLAB
% handles    structure with handles and user data (see GUIDATA)

global ca2;
global abspressure;
global rawnheatrel;
global rawnheatrat;
global records_plots;

if get(handles.checkbox1,'value')==0

a=ca2';
b=abspressure;
c=rawnheatrel';
d=rawnheatrat';

records_plots=[a b c d]; %Get records into a matrix

%Open save dialog box

[filename, pathname] = uiputfile( ...
      {'*.m;*.fig;*.mat;*.mdl', 'All MATLAB Files (*.m, *.fig, *.mat, *.mdl)'; ...
      '*.xls;*.wk1;*.csv',      'Spreadsheet Files(*.xls, *.wk1, *.csv)';...
       '*.*',                   'All Files (*.*)'}, ...
```

```
      'Save as');

if isequal(filename,0) | isequal(pathname,0)

else
f='.';
g='xls';

string=strcat(filename,f,g);

wk1write(string,records_plots);%Save records into root directory

set(gcf, 'PaperOrientation', 'landscape');%Set landscape orientation
Print(gcf,'-djpeg',filename); % Print Figure with results table
end
else
a=ca2';
b=abspressure;

records_plots=[a b]; %Get records into a matrix
```

%Open save dialog box

```
[filename, pathname] = uiputfile( ...
      {'*.m;*.fig;*.mat;*.mdl', 'All MATLAB Files (*.m, *.fig, *.mat, *.mdl)'; ...
      '*.xls;*.wk1;*.csv',      'Spreadsheet Files(*.xls, *.wk1, *.csv)';...
       '*.*',                   'All Files (*.*)'}, ...
      'Save as');

if isequal(filename,0) | isequal(pathname,0)

else
f='.';
g='xls';

string=strcat(filename,f,g);

wk1write(string,records_plots);%Save records into root directory

set(gcf, 'PaperOrientation', 'landscape');%Set landscape orientation
Print(gcf,'-djpeg',filename); % Print Figure with results table
end
end
```

```
% --- Executes on button press in print.
function print_Callback(hObject, eventdata, handles)
% hObject    handle to print (see GCBO)
% eventdata  reserved - to be defined in a future version of MATLAB
% handles    structure with handles and user data (see GUIDATA)

%global handle1 handle2 handle3 handle4

set(gcf, 'PaperOrientation', 'landscape');%Set landscape orientation
Print(gcf); % Print Figure
```

Appendix B: Cold-Air-Injection-Model Calculations

Calculations

The main specification of the CFR engine used on this experiment is shown in Table A1.1. A detailed description of the CFR engine and its main components will be described in the experimental set-up section of this paper.

Table A1.1 WVU CFR engine specifications

SPECIFICATION	ENGLISH	INTERNATIONAL
Type	CFR single cylinder, four stroke	CFR single cylinder, four stroke
Bore	3.250"	82.55 mm
Stroke	4.5"	114.2 mm
Displacement	37.33 cubic inches	612.5 cm3
Engine Speed	900	900
Compression Ratio	Variable 4:1 to 18:1	Variable 4:1 to 18:1

The displacement volume at sea level of the WVU CFR single cylinder engine can be obtained from equation (6.1) and using the data from Table A.1 as follows

$$Vd = \frac{\pi * b^2 * s}{4} = \frac{\pi * (8.255^2\, cm^2) * 11.42\ \ cm}{4} = 612.5 \text{ cc}$$

Thus at sea level the maximum amount of air-fuel mixture entering is limited to 612.5 cc sea-level conditions (ρair= 1.225 kg/m^3).

The WVU CFR engine runs at 900 RPM with a volumetric air flow rate of 7 SCFM, thus using n=2 (a four-stroke engine takes 2 revolutions per cycle) the actual displacement volume can be calculated with equation (6.2)

$$V_{dact} = \frac{\dot{V}}{\frac{N}{n}} = \frac{7\, ft^3}{\frac{900}{2}} = 0.015\, ft^3 = 439cc$$

The associated volumetric efficiency, (η_{vol}), is given by equation (6.3)

$$\eta_{vol} = V_{dact} / V_d \ \ 439cc / 612.5cc = 71.6\,\%$$

Based on the previous calculations, it was determined that the design of the "air injection" equipment to limit the amount of hot, high-pressure air injection to 439 cc of standard air. A compression ratio limit C.R=8 was selected to be below the design limit of the CFR Engine (C.R=16). When 439 cc of air is injected, all the pressure inside the cylinder is doubled like running with a compression ratio of 2x6=16.

The heater volume, V_{heater}, can be obtained from equation (6.5) for a maximum released pressure of 700 psig, a minimum temperature of 900 degree F, and a cut-off pressure of 200 psig. *Pref* = 14.7 psi and *Tref*= 519 degree R at sea level

$$V_{heater} = \frac{p_{ref} * Vd_{act} * T_{\max}}{[p_{\max} - p_{cutoff}] * T_{ref}} \frac{14.7\,psia * 439cc * (900+460)R}{[(700+14.7)-(200+14.7)]psia * (519R)} = 33.82\ cc$$

The mass injected, m_i, at sea level is

$$m_i = \frac{p_{ref} * V_{dact}}{R * T_{ref}}$$

In SI units

$$m_i = \frac{101325Pa * 0.000439m^3}{(287J/kg*K) * 288K} = 0.00053 \text{ kg}$$

The volume of hot pressure air injected into the cylinder at sea level conditions, V_i, can be calculated from equation (6.6).

$$V_i = \frac{m_i * R * T_{ref}}{p_{ref}}$$

In SI units

$$V_i = \frac{0.00053kg * (287J/kg*K) * 288K * 100^3}{101325Pa} = 432.3 \text{ cc}$$

The temperature, T_2, and pressure, p_2, in the cylinder at TDC before air injection are calculated using equations (6.7) and (6.8) respectively,

where:

C.R=8
k=1.4
p_1=14.7 psi
T_1=298 K.

Thus, p_2 is given by

$$p_2 = p_1 * r^k = 14.7 \text{ psi} * 8^{1.4} = 270 \text{ psi}$$

and T_2 by

$$T_2 = T_1 * r^{(k-1)} = 298 \text{ K} * 8^{(1.4-1)} = 685 \text{ K}$$

The final temperature, T, in the cylinder after injection can be obtained by interpolation using the specific internal energy value, u(T), calculated from equation (6.16)

$$u(T) = \frac{m_C * u(T_c) + m_i * h(T_i)}{m_c + m_i}$$

where:

$m_c = m_i = 0.00053$ kg

$T_c = T_2 = 685$ K

$Ti = T_{max} = 756$ K (900 degree F).

The specific internal energy, $u(T_c)$, is obtained by interpolation as shown in Table A1.2

Table A1.2 Interpolation values for u(Tc)

T(K)	u(kJ/kg)
680	496.62
685	X
690	504.45

$u(T_c) = 500.54$ kJ/kg

The specific enthalpy, *h(Ti),* is obtained by interpolation as shown in Table A1.3

Table A1.3 Interpolation values for h(Ti)

T(K)	h(kJ/kg)
750	767.29
756	X
760	778.18

$h(T_i)$= 773.82 kJ/kg

Replacing the values of $u(T_c)$, and $h(T_i)$ into equations (6.16) and solving for $u(T)$

$$u(T) = \frac{0.00053kg * (500.54 + 773.82)u(T_c)kJ / kg}{2 * 0.00053kg}$$

Thus $u(T)$ = 637.18 kJ/kg.

By interpolation, using the specific internal energy value, *u(T),* the final temperature after the air injection is obtained as shown in Table A1.4

Table A1.4 Interpolation values for u(T)

T(K)	u(kJ/kg)
840	624.95
X	637.18
860	641.4

T = 854.86 K

The final temperature is calculated using 6.19 and the final temperature, T, calculated above and is given by

$$p = pc * \frac{T}{T_c} * \left(\frac{mc + mi}{mc} \right)$$

where:

$p_c = p_2$
$m_c = m_i$

$$p = 270\,psi * \frac{854.86K}{685K} * 2\,.$$

Thus, the final pressure, *p*, after the air injection is 674 psi.

The summary of the results is presented in Table A1.5.

Table A1.5 Summary of air-injection calculations

	Air Heater	Cylinder Before Air Injection	Cylinder After Air Injection
Temperature	756 K (900 F)	685 K (773 F)	855 K (1079 F)
Pressure	714.7 psia	270 psia	674 psia

Volume Heater	33.82 cc	Volume Displacement at Sea Level	612.5 cc
Mass Injected at Sea Level	0.00053 kg	Volume Displacement (actual)	439 cc
Compression Ratio	8	Volumetric Efficiency	71.60%

The value obtained for the final temperature, *T*, after the air injection is well above the auto-ignition temperature of natural, gasoline, and diesel fuels as illustrated in Table A1.6.

Table A1.6 Fuels properties

Property	**Natural Gas**	**Gasoline**	**Diesel**
Flammability Limits (volume % in air)	5.0-15	1.4-7.6	0.6-5.5
Autoignition Temperature (°F)	842	572	446
Minimum Ignition Energy in Air (10-6 BTU)	0.27	0.23	0.23
Peak Flame Temperature (°F)	3423	3591	3729

*Numbers in parentheses refer to References. Source: Properties of Alternative Fuels (Murphy, 1994)

Appendix C: Compressed Air Batch Analysis

Airgas

Airgas Mid America
1 Oregon Street
Charleston, WV 25312
(304) 346-0975 Fax (304) 345-3401
www.airgas.com

Certificate of Batch Analysis
Compressed Air, Breathing, Type 1, Grade D
Cylinder

LOT NUMBER
EU 00 S 298 BA
Cubic Feet 311
Exp Date 10/25/2010

Lot Nu

Serial Number of Cylinder Tested T602975

Test	Specifications	Lot Analysis
Oxygen Contents	19.5-23.5%	20.9%
Moisture Contents (dew point --50 F)	Max. 63 PPM	4 PPM
Condensed Hydrocarbon Contents	Max. 5 mg/m3	N/A
Carbon Monoxide Content	Max. 10 PPM	<5 PPM
Odor	no appreciable odor	NONE
Carbon Dioxide Content	Max. 1000 PPM	<300 PPM

Tested per specifications of Type 1, Grade D according to CGA G – 7.1 – 1989

Suppliers Signature

Date 10-25-05

10-21-03

Appendix D: Omega Pressure Transducer Datasheet

FAST RESPONSE VOLTAGE OUTPUT PRESSURE TRANSDUCER

PRESSURE RANGES FROM 6 TO 2000 psig

PX105 Series
0-6 to 0-2,000 psig

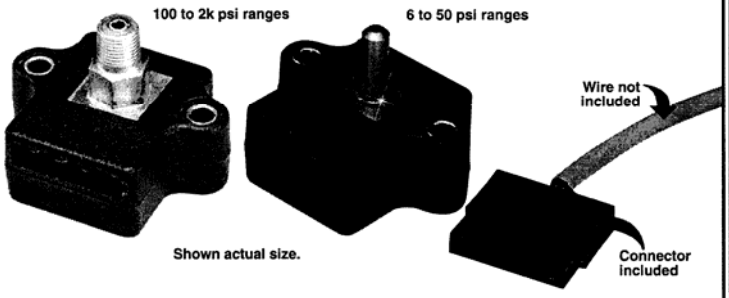

MADE IN USA

- Accuracy: ±0.5% Typ
- Fully Calibrated and Temperature Compensated
- Internal Voltage Regulation
- Interchangeable Unit to Unit ±1%
- Computer Trimmed to Insure Accuracy and Repeatability
- Long Term Stability ±1%
- Operating Temperature Range -55 to 125°C (-66 to 256°F)
- Rugged Temperature Resistant Valox Case and Connector

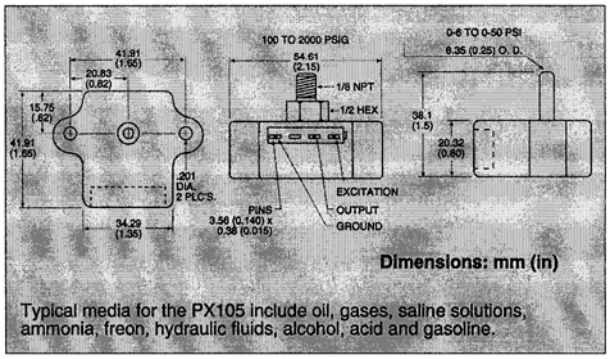

Typical media for the PX105 include oil, gases, saline solutions, ammonia, freon, hydraulic fluids, alcohol, acid and gasoline.

SPECIFICATIONS

Excitation: 8 to 20 Vdc at 15 mA
Output: 1 to 6 Vdc
Accuracy: ±1% full scale maximum
Linearity: <50 psi ±0.5%
≥50 psi ±0.2% FS
Hysteresis: ±0.25% full scale
Zero Balance: ±1% full scale Typ.
±3% full scale max.
Frequency Response: 3 db at 1.5 kHz
Compensated Temperature Range: 0 to 85°C (32 to 185°F)
Thermal Zero Effect: ±0.02% Rdg/°C (±0.01% Rdg/°F)
Proof Pressure: 2 x full scale
Burst Pressure: 5 x full scale Minimum (6, 15, 25, psig = 20 x FS)
Gages: Piezoresistive
Diaphragm/Port Material: 300 Series SS (Silver, Copper, Nickel, Cadmium Brazed)
Electrical Connection: CX106-4
Weight: 114 g (4 oz)

☐ *MOST POPULAR MODELS HIGHLIGHTED!*

To Order *(Specify Model Number)*

RANGE psi	MODEL NO.	PRICE	COMPATIBLE METERS
0 to 6 psig	**PX105-006G5V**	**$335**	DP25-E, DP2000P4, DP3002-E
0 to 15 psig	**PX105-015G5V**	**335**	DP25-E, DP2000P5, DP3002-E
0 to 25 psig	**PX105-025G5V**	**335**	DP25-E, DP2000P4, DP3002-E
0 to 50 psig	**PX105-050G5V**	**335**	DP25-E, DP2000P4, DP3002-E
0 to 200 psig	**PX105-200G5V**	**335**	DP25-E, DP2000P5, DP3002-E
0 to 500 psig	**PX105-500G5V**	**335**	DP25-E, DP2000P4, DP3002-E
0 to 1000 psig	**PX105-1KG5V**	**335**	DP25-E, DP2000P4, DP3002-E
0 to 2000 psig	**PX105-2KG5V**	**335**	DP25-E, DP2000P5, DP3002-E

***Ordering Example:** PX105-006G5V has a range of 0 to 6 psig, $335.*

Appendix E: Solenoid Valve Datasheet

Piston Pilot-Operated Solenoid Valves

For information about solenoid valves, see page 393. For pipe size information, see pages 2-3.

Brass Miniature Solenoid Valves

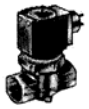

- Normally Closed (valve opens when energized)
- Minimum Differential Pressure: 3 psi
- Maximum Pressure: 150 psi
- Maximum Temperature: 200° F

The answer when vertical installation space is limited. Valve body is brass; seat is stainless steel. Use with air, water, light oil, and low pressure steam (25 psi max.). The enclosed Class F coil operates on 120 VAC, 50/60 Hz, .125 amps. Mount in any position, keeping coil on top. UL listed and CSA certified. **Connections:** NPT female.

Pipe Size	Overall Length	Ht.	Cv Factor	w/18" Leads	Each	w/DIN Connectors	Each
3/8"	2 1/16"	3 3/4"	2.0	7862K38	$76.67	7862K58	$80.52
1/2"	2 5/8"	3 7/8"	3.1	7862K42	84.75	7862K62	88.60
3/4"	3"	4 3/16"	5.0	7862K44	116.63	7862K64	120.48
1"	3 1/2"	4 11/16"	8.0	7862K51	159.12	7862K71	162.96

Stainless Steel Solenoid Valves for Steam

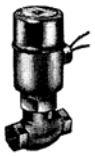

- Normally Closed (valve opens when energized)
- Minimum Differential Pressure: 5 psi
- Maximum Pressure: See table
- Maximum Temperature: 450° F

Great corrosion resistance plus the capability to handle steam and other hot, nonhazardous fluids to 450° F. Body is Type 316 stainless steel with Type 304 and 416 stainless steel internal parts. Seats are EPDM for 5-50 psi valves and PTFE for 5-200 psi valves. Coil is Class H in a NEMA 1 enclosure with 1/2" conduit connection and 18" leads. Coil operates on 120 VAC, 60 Hz, .42 amps. Mount horizontally with coil on top.
Connections: NPT female.

Pipe Size	Overall Length	Cv Factor	Min. Diff. psi: 5 Max. psi: 50	Each	Min. Diff. psi: 5 Max. psi: 200	Each
1/8"	2 5/8"	1.4	4671K71	$347.87	4671K81	$353.89
1/4"	2 5/8"	2.1	4671K72	347.87	4671K82	353.89
3/8"	2 5/8"	2.8	4671K73	347.87	4671K83	353.89
1/2"	3 1/8"	3.0	4671K74	347.17	4671K84	321.72
3/4"	3 3/4"	6.0	4671K75	429.86	4671K85	396.89
1"	4 5/32"	11.0	4671K76	536.49	4671K86	493.82
1 1/4"	6 1/8"	17.0	4671K77	919.90	4671K87	925.79
1 1/2"	6 1/8"	25.0	4671K78	988.09	4671K88	993.99
2"	6 7/16"	45.0	4671K79	1265.20	4671K89	1271.09

Brass Cryogenic Solenoid Valves

- Normally Closed (valve opens when energized)
- Minimum Differential Pressure: 5 psi
- Maximum Pressure: 300 psi
- Temperature Range: −420° to +356° F

Made for temperatures as low as −420° F, these valves are for use with liquid carbon dioxide and cryogenic vapors. Body is brass, internal parts are stainless steel, and the seat is PTFE. Coil is Class H in a NEMA 4/4X enclosure with 1/2" conduit connection and 18" leads; coil operates on 120 VAC, 60 Hz. Mount horizontally with coil on top.
Connections: NPT female.

Pipe Size	Overall Length	Cv Factor	Amps		Each
1/4"	2 5/16"	1	0.2	7902K31	$195.95
3/8"	2 5/16"	2	0.2	7902K32	195.95
1/2"	2 9/16"	3	0.2	7902K33	231.81

Brass High-Pressure Solenoid Valves

90° Angle

- Normally Closed (valve opens when energized)
- Minimum Differential Pressure: 10 psi
- Maximum Pressure: 1200 psi
- Maximum Temperature: 200° F

Don't worry about high pressure, these valves handle up to 1200 psi. Valves have a brass body, brass piston (unless noted), stainless steel seat, and stainless steel sleeve. Coil is Class F in a junction box enclosure with 7" leads. Coil operates on 120 VAC, 60 Hz, .24 amps. Mount horizontally with coil on top.
Connections: NPT female.

Pipe Size	Overall Length	Cv Factor	Flow Direction		Each
3/8"	2 1/16"	1.8	Inline	49895K31	$108.37
3/8"	2 1/16"	1.8	Inline	49895K32★	122.96
1/2"	2 5/8"	3.7	90° Angle	49895K44	158.86
1"	3 3/4"	11.1	90° Angle	49895K51	273.92
1"	3 3/4"	11.1	90° Angle	49895K52★	303.41

★ Stainless steel piston.

Type 304 Stainless Steel Solenoid Valves with Zero Min. Differential Pressure

- Normally Closed (valve opens when energized)
- Minimum Differential Pressure: 0 psi
- Maximum Pressure: See table
- Maximum Temperature: General Service: 400° F; Cryogenic: −320° to +400° F

No minimum pressure necessary—these valves also have a wider temperature range than most of our other solenoid valves and the corrosion resistance of Type 304 stainless steel. Piston is Type 303 stainless steel and seat is PTFE. Coil is Class H in an enclosure with a 1/2" conduit connection, integral junction box, and 18" leads. Coil operates on 120 VAC, 60 Hz. Mount horizontally, coil on top.
Connections: NPT female.

Pipe Size	Max. psi	Overall Length	Cv Factor	Amps	General Service	Each	Cryogenic	Each
1/2"	110	3 1/4"	3.5	0.4	8117K35	$359.09	8117K65	$388.92
1/2"	200	3 1/4"	3.5	0.4	8117K36	391.40	8117K66	421.22
1/2"	300	3 1/4"	3.5	0.8	8117K37	535.53	8117K67	560.90
3/4"	110	3 1/2"	7.5	0.4	8117K45	431.16	8117K75	460.98
3/4"	200	3 1/2"	7.5	0.8	8117K46	547.96	8117K76	573.23
3/4"	300	3 1/2"	7.5	1.2	8117K47	626.24	8117K77	650.90
1"	110	4 1/8"	13.0	0.4	8117K55	495.77	8117K85	525.59
1"	200	4 1/8"	13.0	0.8	8117K56	626.24	8117K86	650.90
1"	300	4 1/8"	13.0	1.2	8117K57	684.64	8117K87	708.83

Stainless Steel Solenoid Valves

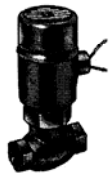

- Choose from Normally Closed (valve opens when energized) and Normally Open (valve closes when energized)
- Minimum Differential Pressure: See table
- Maximum Pressure: See table
- Maximum Temperature: 220° F

A Type 316 stainless steel valve body with Type 304 and 416 stainless steel internal parts provides excellent corrosion resistance. Use with corrosive fluids. *Normally closed valves* with 5-150 psi pressure range have a Buna-N disc and seat screw; valves with 20-1000 psi pressure range have a PTFE seat. For *normally open valves* with a 5-150 psi pressure range, seats are Buna-N and Viton; PTFE for the 10-300 psi range. Coil is Class F in a NEMA 1 enclosure with 1/2" conduit connection and 18" lead wires. Coil operates on 120 VAC, 60 Hz. ***5-150 psi valves** and **10-300 psi valves*** draw .32 amps. ***20-1000 psi valves*** draw .60 amps. Mount horizontally, coil on top. **Connections:** NPT female.

Pipe Size	Overall Length	Cv Factor	NORMALLY CLOSED Min. Diff. psi: 5 Max. psi: 150	Each	NORMALLY CLOSED Min. Diff. psi: 20 Max. psi: 1000	Each	NORMALLY OPEN Min. Diff. psi: 5 Max. psi: 150	Each	NORMALLY OPEN Min. Diff. psi: 10 Max. psi: 300	Each
1/8"	2 5/8"	1.4	4665K11	$347.39	4665K21	$365.40	4665K31	$356.99	4665K41	$374.27
1/4"	2 5/8"	2.1	4665K12	347.39	4665K22	365.40	4665K32	356.99	4665K42	374.27
3/8"	2 5/8"	2.8	4665K13	347.39	4665K23	365.40	4665K33	356.99	4665K43	374.27
1/2"	3 1/8"	3.0	4665K14	347.39	4665K24	364.67	4665K34	356.99	4665K44	374.27
3/4"	3 3/4"	6.0	4665K15	434.22	4665K25	451.50	4665K35	443.82	4665K45	461.10
1"	4 5/32"	11.0	4665K16	546.17	4665K26	562.49	4665K36	555.77	4665K46	573.05
1 1/4"	6 1/8"	17.0	4665K17	950.87	4665K27	965.18	4665K37	959.29	4665K47	974.44
1 1/2"	6 1/8"	25.0	4665K18	1022.46	4665K28	1036.78	4665K38	1030.88	4665K48	1046.04
2"	6 7/16"	45.0	4665K19	1313.42	4665K29	1327.74	4665K39	1321.84	4665K49	1337.00

HIGH PRESSURE SOLENOID VALVES
MODELS 453P, 453S, 454P, 458P, 458PS

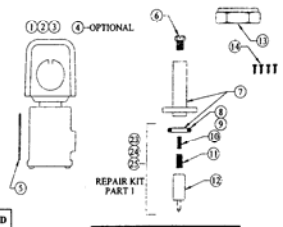

MODEL	PARTS USED
453P	Brass Bore (No SS Sleeve)
	SS Piston
453S	SS Sleeve
	SS Piston
453P	SS Sleeve
	Brass Piston
458P	SS Sleeve
	Brass Piston
458PS	SS Sleeve
	SS Piston

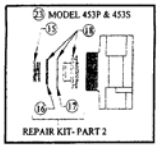

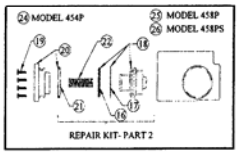

NO.	PART NO.	DESCRIPTRION	VALVE MODEL NUMBER			
			453P/453S	454P	458P	458PS
1	41-9-2	Coil Assembly (Specify Voltage)	*	*	*	*
2	41-9C-2	(Optional) Coil Assembly With Conduit Boss (Specify Voltage)	*	*	*	*
3	41-9D-2	Din Coil (Specify Voltage)	*	*	*	*
4	41-77-100110	(Optional) Din Female Connector	*	*	*	*
5	41-13-6	Nameplate (Specify Model No.)	*	*	*	*
6	41-14-1	Top Plug Screw	*	*	*	*
7	41-7-22	Enclosing Tube With O-Ring	*			
	41-7-23	Enclosing Tube With O-Ring		*		
	41-7-24	Enclosing Tube With O-Ring			*	*
8	41-5-2	O-Ring, Buna-N (1 X 1 1/8 X 1/16)	*			
9	24-3	O-Ring, Buna-N (13/16 X 15/16 X 1/16)		*	*	*
10	41-1-6	Plunger Spring Return	*	*	*	*
11	41-1-7	Plunger Spring Kickoff	*	*	*	*
12	41-10-10	Plunger Assembly		*	*	*
	41-10-12	Plunger Assembly	*			
13	41-17-1	Enclosing Tube Locknut			*	*
	41-17-5	Enclosing Tube Locknut	*			
14	41-16-1	Enclosing Tube Screw (4 Req'd)		*		
15	41-4-1	Closing Spring	*			
16	41-19-2	Piston Ring	*	*		
	41-19-5	Piston Ring			*	*
17	41-20-2	Backup Spring	*	*		
	41-20-6	Backup Spring			*	*
18	41-3-5	Piston Assy, SS With Ring & Backup Spring	*			
	41-3-6	Piston Assy, Brass With Ring & Backup Spring		*		
	41-3-8	Piston Assy, Brass With Ring & Backup Spring			*	
	41-3-9	Piston Assy, Brass With Ring & Backup Spring				*

Appendix F: Double Acting Tie-Rod Hydraulic Cylinder Datasheet

PARTS MANUAL / MANUAL DE PIEZAS / MANUEL DE PIECES DETACHEES

DOUBLE ACTING TIE ROD CYLINDERS / CILINDROSE DE VARILLA DE CONEXION DE ACCIONAMIENTO DOBLE / CYLINDRES A TIGES DE LIAISON, A DOUBLE EFFET

MANUFACTURED BY: / FABRICADA POR: / FABRIQUEE PAR:
PRINCE MANUFACTURING CORP., N. SIOUX CITY, SD 57049

	Parts List (Lista de piezas) (Liste de pieces detachees)										
	4HL38	4HL39	4HL40	4HL41	4HL42	4HL43	4HL44	4HL45	4HL46	4HL47	4HL48
	SAE-32004	SAE-32008	SAE-32020	SAE-32508	SAE-32512	SAE-33008	SAE-33016	SAE-33024	SAE-33508A	SAE-33516A	SAE-33524A
1	010500470	010500472	010500479	010600517	010600519	010700431	010700435	010700438	010700682	010700686	010700689
2	200300040	200300040	200300040	200300040	200300040	200300040	200300040	200300040	200300040	200300040	200300040
3	051100006	051100008	051100014	051300014	051300016	051500007	051500011	051500014	051700009	051700013	051700016
4	141100024	141100024	141100024	141300022	141300022	141500043	141500043	141500043	141700023	141700023	141700023
5	081100177	081100177	081100177	081300248	081300248	081500323	081500323	081500323	081700255	081700255	081700255
6	071100157	071100157	071100157	071300111	071300111	071500244	071500244	071500244	071700174	071700174	071700174
7	220000208	220000208	220000208	220000208	220000208	220000210	220000210	220000210	220000210	220000210	220000210
8	100000423	100000423	100000423	100000423	100000423	100000423	100000423	100000423	100000577	100000577	100000577
9	170103081	170103121	170103241	170201121	170201161	170201122	170201202	170201282	170201123	170201203	170201283
10	190400001	190400001	190400001	190400001	190400001	190400001	190400001	190400001	190400004	190400004	190400004
11	220001504	220001504	220001504	220001504	220001504	220001504	220001504	220001504	220001504	220001504	220001504
12											
13											
14	* THESE ITEMS ARE INCLUDED IN PACKING KIT.										
15	* ESTOS ARTICULOS ESTAN INCLUIDOS EN EL JUEGO DEL PAQUETE.										
16	* CES PIECES SONT COMPRISES DANS LE JEU DE PIECES FOURNI DANS L'EMBALLAGE.										
17											
18											
*	PMCK-32000	PMCK-32000	PMCK-32000	PMCK-32500	PMCK-32500	PMCK-33000	PMCK-33000	PMCK-33000	PMCK-33500	PMCK-33500	PMCK-33500

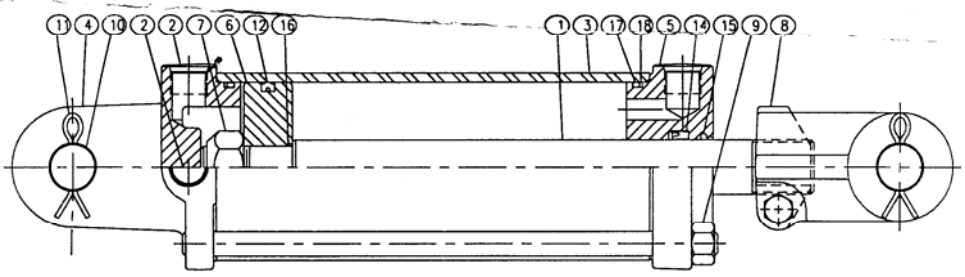

ORDER REPLACEMENT PARTS OR OBTAIN SERVICE THROUGH DEALER FROM WHOM PRODUCT WAS PURCHASED.

If dealer cannot supply, order from:
GRAINGER PARTS OPERATION
1657 Shermer Rd.
Northbrook, IL 60062
TELEPHONE (800)323-0620
FAX (800)PCA-FAX1

Please provide the following information:
* Model number
* Serial number (if any)
* Parts description and number as shown in parts list.

PIDA PIEZAS DE REPUESTO U OBTENGA SERVICIO POR MEDIO DEL COMERCIANTE A QUIEN COMPRO EL PRODUCTO.
Si el comerciante no puede proveer el pedido, dirijase a:
GRAINGER PARTS OPERATION
1657 Shermer Rd.
Northbrook, IL 60062
TELEPHONE (800)323-0620
FAX (800)PCA-FAX1
Por favor, provea la siguiente informacion:
* Numero de modelo
* Numero de serie (si lo tiene)
* Descripcion y numero de las piezas tal como aparecen en la lista de piezas.

Para obtener repuestos en Mexico llame al telefono 95-800-527-2331.
En los EE.UU. llame al telefono 1-800-323-0620

COMMANDER LES PIECES DE RECHANGE DU DEMANDER LE SERVICE SOUS GARANTIE AU REVENDEUR CHEZ QUI LE PRODUIT A ETE ACHETE.
Si le revendeur ne peut pas fournir la commande, s'adresser a:
GRAINGER PARTS OPERATION
1657 Shermer Rd.
Northbrook, IL 60062
TELEPHONE (800)323-0620
FAX (800)PCA-FAX1

Veuillez fournir les renseignements suivants:
* Numero de modele
* Numero de serie (le cas echeant)
* Descriptions et numeros de pieces tels qu'indiques sur la liste de pieces detachees.

graingertierod.dwg 7/31/03 Page 1 of 3

Appendix G: First Air Injector Design Drawing

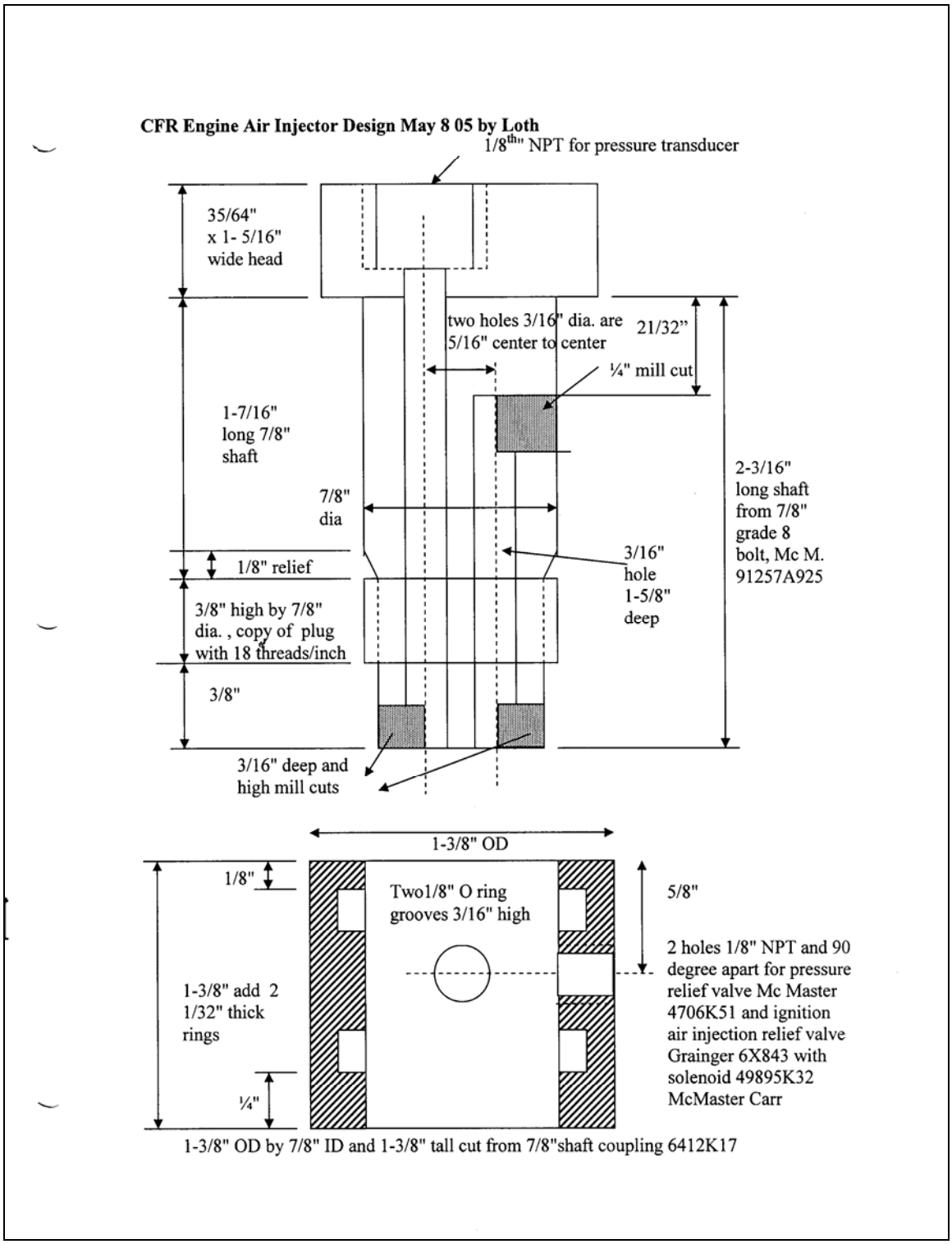

Appendix H: Spark Plug Adapter Drawing

CFR SPARK PLUG ADAPTER

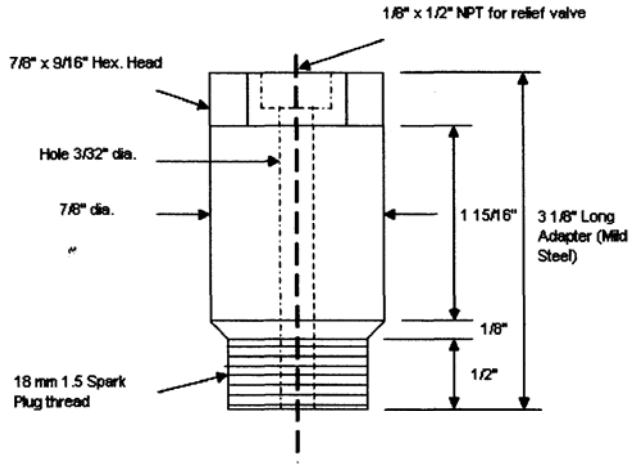

Appendix I: Water Cooled Pressure Transducer Adapter Drawing

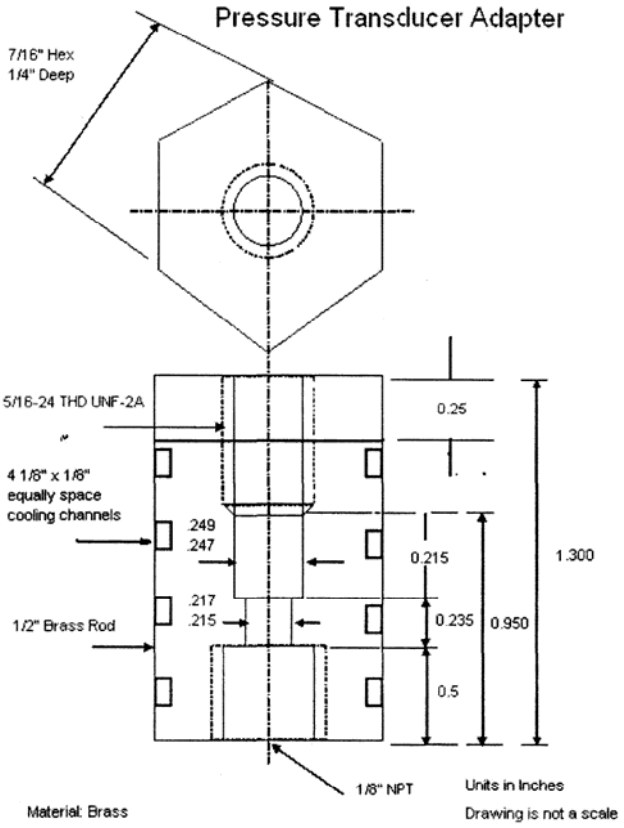

Appendix J: Three (3) Way Ball Valve Datasheet

Type 316 Stainless Steel Ball Valves

For information about ball valves, see page 350. For information about pipe size, see pages 2-3.

Panel-Mount Type 316 Stainless Steel Ball Valves with Yor-Lok Tube Fittings

- Maximum Pressure: W.O.G. (water, oil, inert gas): 6000 psi @ 125° F
  W.S.P. (working steam pressure): Not rated
- Vacuum Rating: 29" Hg
- Temperature Range: −30° to +280° F
- Ports: Standard

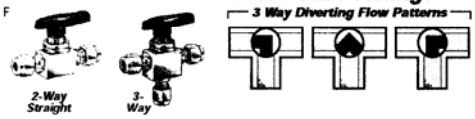

Combine high corrosion resistance with high pressure ratings. Valves include a hex nut for panel mounting in instrumentation applications. Mounting holes are are 13/16" for 1/16"-3/8" tube OD and 1 1/2" for 1/2" tube OD. Use any port as inlet or outlet. Body, ball, and stem are Type 316 stainless steel; seats are Kel-F. Body seals and packing are PTFE. The tee handle is made of nylon. ***2-way*** valves offer leak-tight, positive shutoff; use ***3-way*** valves for diverting flow without full shutoff.

Connections: Yor-Lok double-ferrule compression tube fittings. Can be used with Swagelok, Parker A-Lok, Gyrolok, Bilok, Tylok, and Letlok tube fittings. For Yor-Lok tube fittings, see pages 131-133.

For Tube OD	STRAIGHT End-to-End Lg.	2-Way Each	3-Way	3-Way Each	90° ANGLE End-to-End Lg.	2-Way Each
1/16"	2 3/4"	45775K55	$97.74	45165K29	$112.14	1 3/8"	45775K21	$94.75
1/8"	3 3/32"	45775K56	74.21	45165K31	93.50	1 35/64"	45775K22	90.74
1/4"	3 19/64"	45775K57	82.74	45165K32	116.05	1 21/32"	45775K23	101.62
3/8"	3 13/32"	45775K58	90.89	45165K33	147.68	1 43/64"	45775K24	170.25
1/2"	4 3/64"	45775K59	180.99	45165K34	210.50	2 1/64"	45775K25	236.88

Miniature Type 316 Stainless Steel Ball Valves

- Maximum Pressure:
  W.O.G. (water, oil, inert gas): 500 psi @ 200° F
  W.S.P. (working steam pressure): Not rated
- Vacuum Rating: Not rated
- Temperature Range: 40° to 200° F
- Ports: Full

Great for small spaces and medium pressures, these valves have a corrosion-resistant Type 316 stainless steel body, ball, and stem. Seats and packing are PTFE. The wing handle is made of plated carbon steel. NPSM (National Pipe Straight Mechanical) threads meet SAE J516 fitting recommendations. **Connections:** See below.

Connections	End-to-End Lg.	Each
1/4" NPT Male × 1/4" NPT Male	2 2/32"	4310K11	$42.11
1/4" NPT Male × 3/8" NPSM Male	2 2/32"	4310K13	42.11
3/8" NPT Male × 1/4" NPT Male	2 2/32"	4310K15	39.35
3/8" NPT Male × 3/8" NPT Male	2 2/32"	4310K17	42.11
3/8" NPSM Male × 3/8" NPT Male	2 2/32"	4310K18	42.11
3/8" NPT Female × 3/8" NPT Female	2 2/32"	4310K19	42.11
3/8" NPT Female × 3/8" NPT Male	2 2/32"	4310K23	42.11
3/8" NPT Female × 3/8" NPSM Male	2 2/32"	4310K25	42.11
3/8" ID Tube Stem × 3/8" NPSM Male	3 7/8"	4310K27	42.11
3/8" ID Tube Stem × 3/8" OD Tube Fitting	4 13/64"	4310K37	52.35
3/8" OD Tube Fitting × 3/8" NPT Male	3 15/64"	4310K31	52.35
3/8" OD Tube Fitting × 3/8" NPSM Male	3 15/64"	4310K33	52.35
1/2" OD Tube Fitting × 3/8" NPSM Male	3 29/64"	4310K35	72.48
3/8" OD Tube Fitting × 3/8" OD Tube Fitting	3 35/64"	4310K29	52.35

High-Pressure Miniature Type 316 Stainless Steel Ball Valves

- Maximum Pressure: W.O.G. (water, oil, inert gas): 1000 psi @ 150° F
  W.S.P. (working steam pressure): 150 psi @ 368° F
- Vacuum Rating: 29.9" Hg
- Temperature Range: −36° to +368° F
- Ports: 1/4" × 1/4" and 3/8" × 3/8": Full; 1/2" × 1/2": Reduced

Ideal for limited space and high pressure applications. Either port can be used as inlet or outlet. Body, ball, and stem are Type 316 stainless steel. Seats and seals are PTFE. The wing handle is made of carbon steel. It can be locked in the closed position using a padlock (not included) with shackle dia. up to 5/16". **Connections:** NPT.

Pipe Size	End-to-End Lg.	Each
Male × Male		
1/4"	2 61/64"	45395K101	$65.53
3/8"	2 61/64"	45395K103	66.24
1/2"	3 1/32"	45395K105	92.33
Male × Female		
1/4"	2 49/64"	45395K121	60.23
3/8"	2 49/64"	45395K112	61.64
Male × Female (Cont.)		
1/2"	2 61/64"	45395K114	$92.69
Female × Female		
1/4"	2 49/64"	45395K131	62.06
3/8"	2 49/64"	45395K133	62.88
1/2"	2 61/64"	45395K135	93.10

Type 316 Stainless Steel Ball Valves with Yor-Lok or BSPP Connections

- Maximum Pressure:
  W.O.G. (water, oil, inert gas):
  1000 psi @ 158° F
  W.S.P. (working steam pressure): Not rated
- Vacuum Rating: Not rated
- Temperature Range: −60° to +200° F
- Ports: Standard

Body, ball, and blowout-proof stem are Type 316 stainless steel. Seat and packing are glass-filled PTFE. Lever handles are made of Type 302 stainless steel with a vinyl grip.

Connections: Yor-Lok double-ferrule compression tube fittings or BSPP (British Standard Pipe Parallel) threaded fittings.

Ball Valves with Yor-Lok Tube Fittings— These are ideal for instrumentation applications. Can be used with Yor-Lok, Swagelok, Parker-A-Lok, Gyrolok, Bilok, and Letlok tube fittings. For Yor-Lok tube fittings, see pages 131-133.

Ball Valves with BSPP Threads— Ideal for confined areas where a BSPP connection is required.

For Tube OD	End-to-End Lg.	Each
Yor-Lok Tube Fittings		
1/4"	3 35/64"	4537K11	$51.25
3/8"	3 35/64"	4537K13	59.37
1/2"	3 3/4"	4537K14	75.76
3/4"	4 29/64"	4537K15	97.91
1"	5 5/32"	4537K16	146.08

Pipe Size	End-to-End Lg.	Each
Female × Female BSPP Threads		
1/4"	1 31/32"	4932K32	$35.32
3/8"	2 23/64"	4932K33	39.64
1/2"	2 61/64"	4932K35	44.41
Male × Female BSPP Threads		
1/4"	1 31/32"	4932K62	35.32
1/2"	2 61/64"	4932K65	43.96

Type 316 Stainless Steel Ball Valves with Ratchet-Hole Handle

- Maximum Pressure: W.O.G. (water, oil, inert gas)
  1000 psi @ 100° F
  W.S.P. (working steam pressure): 140 psi @ 360°
- Vacuum Rating: 29" Hg
- Temperature Range: −4° to +392° F
- Ports: Full

A hole in the handle of these valves accommodates a 3/8" square ratchet to provide easier access to tough-to-reach valves. Body, ball, and stem are Type 316 stainless steel. Seats and packing are PTFE. The lever is Type 304 stainless steel and is lockable using a padlock with a shackle diameter up to 5/16".

Connections: NPT female.

Pipe Size	End-to-End Lg.	Each
1"	3 29/64"	5539T15	$56.71
1 1/4"	4"	5539T16	73.33
1 1/2"	4 1/4"	5539T17	94.84
2"	4 7/8"	5539T18	120.00

Appendix K: Air Pressure Relief Valve Datasheet

Adjustable Flow Control Valves

HYDRAULIC SCHEMATIC

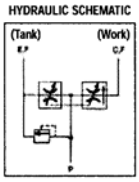

No. 6X842

For Repair Parts Call Your Branch or 1-800-323-0620

Varies speed smoothly over the full range. Once speed is set with the lever, it remains constant regardless of load variation. Comes with built-in ball and spring relief valve with cast-iron seat. Pressure compensated adjustable flow control.

PRINCE THREE-YEAR LIMITED WARRANTY

Text is available upon request. See "Manufacturers' Warranties" on page opposite inside back cover.

Dimensions (In.) L	H	D	Port Size (NPT) (In.)	Max. psi	Flow Range (GPM)	Adjustable Relief	Prince Model	Stock No.	Each	Shpg. Wt.
4.6	4.1	2.9	3/4	3000	0-30	Yes	RDRS-175-30	6X842	$96.95	8.0
4.6	4.1	2.9	1/2	3000	0-16	No	RD-150-16	5PP06	76.75	7.8
4.6	4.1	2.9	3/4	3000	0-30	No	RD-175-30	5PP07	76.75	7.7
4.6	4.1	2.9	1/2	3000	0-16	Yes	RDRS-150-16	5PP08	96.95	8.1

1/2" Adjustable Relief Valve

HYDRAULIC SCHEMATIC

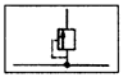

For Repair Parts Call Your Branch or 1-800-323-0620

Compact 1/2" NPT, high pressure relief valve is designed for full flow with low pressure drop. High strength steel bar stock body with replaceable heat treated seat.

Uses: For heavy-duty hydraulic application.

- Pressure adjustable from 1000 to 2500 psi
- 16 GPM max.

PRINCE THREE-YEAR LIMITED WARRANTY

Text is available upon request. See "Manufacturers' Warranties" on page opposite inside back cover.

Description	Prince Model	Stock No.	Each	Shpg. Wt.
1/2" Adjustable Relief Valve	RD1850H	6X843	$36.35	2.2

Adjustable Relief Valves

For Repair Parts Call Your Branch or 1-800-323-0620

No. 4BA48

Controls maximum pressure within a hydraulic circuit. Two-stage, balanced piston design provides fast response and minimizes pressure override. Vent connection allows low pressure venting of system to tank. Remote pressure control capability is achieved by directing flow from vent connection to a separate pressure relief valve. Standard "F3" seals provide multi-fluid capability. Inlet and outlet pressure connections may be used interchangeably when the valve is mounted in the pressure line, or the valve may be teed off the pressure line with one of the inlet pressure connections plugged. 7/8" - 14 UNF-2B thread inlet and outlet connections - CS-03. Max. pressure 3000 psi. 5.6L x 6.6W x 2.1"H.

Adjustable Pressure Range (psi)	Maximum Flow (GPM)	Vickers Model	Stock No.		Each	Shpg. Wt.
125-1000	45	CS-03-B50	4BA48	✓	$293.50	9.0
500-2000	45	CS-03-C50	4BA49	✓	293.50	9.1
1500-3000	45	CS-03-F50	4BA50	✓	293.50	9.0

Flow Dividers

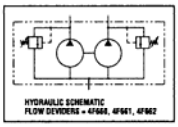

No. 4F660

Hydraulic flow dividers split the flow from a single pump source to a pair of matched cylinders or fluid motors. Gear type rotary flow dividers synchronize two parallel motions hydraulically rather than mechanically.

Both drive gears in 2-section dividers are driven by common shaft, allowing flow equalization to occur in a wide speed range. Speeds in the range of 2000 to 4500 RPM will improve overall efficiency. Up to 4500 psi outer pressure. Max speed up to 4500 RPM.

Integral differential relief valves for each circuit limit pressure intensification and permit cylinders to re-phase at the end of each stroke.

Permanent mold cast-iron body. 11-tooth hardened steel gears.

Inlet Flow GPM Range	Displacement Cu. In./Rev.	Operating Pressure (psi)	SAE Port Sizes (In.) Inlet	Outlet	Dimensions (In.) Length	Width	Height	Barnes Model	Stock No.		Each	Shpg. Wt.
2.4-5	0.129	3000	3/4	3/4 -16	7.55	2.99	3.26	1020075	4F660		$234.50	8.7
5-10	0.258	2300	7/8	3/4 -16	7.55	2.99	3.26	1020076	4F661	✓	234.50	8.6
10-20	0.581	2750	1 5/16	7/8 -14	9.85	4.25	4.00	1100042	4F662	✓	397.50	27.0

⛟ = Shipped Directly from Manufacturer ✓= Extended Warranty Available ★ = New Item

RD-1850-H/6X843

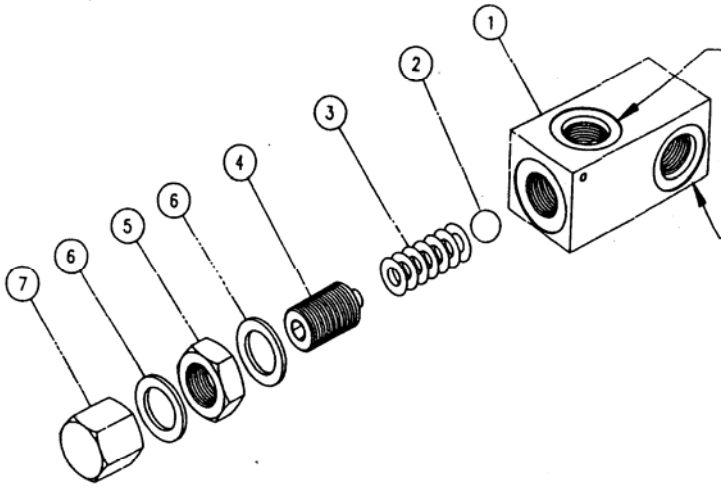

ITEM ARTICULO ÈCE	QTY CANTIDAD QTÉ	PART NO. N° DE PIEZA N° DE PIÈCE	DESCRIPTION/DESCRIPCION/DESCRIPTION
1	1		VALVE BODY/CUERPO DE LA VALVULA/CORPS DE VANNE
2	1	230009014	STEEL BALL/BOLA DE ACERO/BILLE D'ACIER
3	1	670300011	SPRING/RESORTE/RESSORT
4	1	671900001	ADJUSTING SCREW/TORNILLO DE AJUSTE/VIS DE RÉGLAGE
5	1	671800010	JAM NUT/TUERCA DE INMOVILIZACION/CONTRE-ÉCROU
6	2	671500004	WASHER/ARANDELA/RONDELLE
7	1	671800002	ACORN NUT/TUERCA CIEGA/ÉCROU BORGNE

TO ADJUST RELIEF REMOVE ACORN NUT ITEM 7
LOOSEN JAMNUT ITEM 5, TURN ADJUSTING SCREW
ITEM 4 CLOCKWISE TO INCREASE PRESSURE.
COUNTERCLOCKWISE TO DECREASE PRESSURE. DO NOT
BACKOUT ADJUSTING SCREW TO THE POINT IT FALLS OUT.

PARA AJUSTAR LA DESCOMPRESION SAQUE LA TUERCA CIEGA ARTICULO 7 AFLOJANDO LA TUERCA DE INNOVILIZACION ARTICULO 5, LUEGO GIRE EL TORNILLO DE AJUSTE ARTICULO 4 HACIA LA DERECHA PARA AUMENTAR LA PRESION, HACIA LA IZQUIERDA PARA DISMINUIR LA PRESION. NO GIRE EL TORNILLO DE AJUSTE HASTA EL PUNTO EN QUE SE DESPRENDA.

POUR RÉGLER LA DÉCHARGE, DÉVISSER L'ÉCROU BORGNE, PIÈCE 7, DESSERRER LE CONTRE-ÉCROU, PIÈCE 5, TOURNER LA VIS DE RÉGLAGE, PIÈCE 4, DANS LE SENS DES AIGUILLES D'HORLOGE POUR AUGMENTER LA PRESSION ET EN SENS INVERSE POUR DIMINUER LA PRESSION. NE PAS DÉVISSER LA VIS DE RÉGLAGE À FOND JUSQU'AU POINT OU ELLE POURRAIT TOMBER.

WARNING: OVERPRESSURE BAY CAUSE SUDDEN AND UNEXPECTED FAILURE OF A COMPONENT IN THE HYDRAULIC SYSTEM RESULTING IN SERIOUS PERSONAL INJURY. ALWAYS USE A GAUGE WHEN ADJUSTING A RELIEF VALVE.

ADVERTENCIA: LA SOBREPRESION PUEDE CAUSAR UN FALLO REPENTINO E INESPERADO DE UN COMPONENTE EN EL SISTEMA HIDRAULICO PRODUCIENDO LESIONES PERSONALES GRAVES. USE SIEMPRE UN MANOMETRO CUANDO AJUSTE UNA VALVULA DE DESAHOGO.

AVERTISSEMENT: TOUTE SURPRESSION RISQUE DE CAUSER LA DÉFAILLANCE SOUDAINE ET IMPRÉVUE D'UN COMPOSANT DU SYSTÈME HYDRAULIQUE ET PEUT ENTRAÎNER DES DOMMAGES CORPORELS GRAVES. IL FAUT TOUJOURS UTILISER UN MANOMÈTRE POUR RÉGLER UNE SOUPAPE DE SÛRETÉ.

ORDER REPLACEMENT PARTS OR OBTAIN WARRANTY SERVICE THROUGH DEALER FROM WHOM PRODUCT WAS PURCHASED.
Please provide following information:

*Model Number
*Parts Description and Number as shown in Parts List

PIDA PIEZAS DE REPUESTO U OBTENGA SERVICIO DE GARANTIA POR MEDIO DEL COMERCIANTE A QUIEN COMPRO EL PRODUCTO.
Por favor, provea la siguiente información:

*Número de modelo
*Descripción y número de las piezas tal como aparecen en la Lista de Piezas.

COMMANDER LES PIÈCES DE RECHANGE OU DEMANDER LE SERVICE SOUS GARANTIE AU REVENDEUR CHEZ QUI LE PRODUIT A ÉTÉ ACHETÉ.
Veuillez fournir les renseignements suivants:
*Numéro de modèle
*Descriptions et numéros de pièces tels qu'indiqués sur la liste de pièces détachées.

If Dealer Cannot Supply Order From:
Si el comerciante no puede proveer el pedido diríjase a:
Si le revendeur ne peut pas fournir la commande, s'adresser à :

GRAINGER PARTS OPERATION
1657 SHERMER RD.
NORTHBROOK, IL 60062
Telephone 1-800-323-0620
Fax 1-800-PCA-FAX1

3

Appendix L: Dytran Piezoelectric Pressure Transducer Datasheet

Dytran Instruments, Inc.
21592 Marilla St. Chatsworth, CA 91311 Ph: 818-700-7818 Fax 818-700-7880
www.dytran.com email: info@dytran.com

CALIBRATION CERTIFICATE
LIVM DYNAMIC PRESSURE SENSOR

CUSTOMER:	WEST VIRGINIA UNIVERSITY			TEST REPORT #:	1304	11/21/2005	
PURCHASE ORDER #:	M/C - J.LOTH	SALES ORDER #:	121022	PROCEDURE:	TP2002		
MODEL:	2011V	SERIAL #:	1304	TEMP (°C):	21	HUMIDITY (%):	25
NEW UNIT	X	RE-CALIBRATION [1]		AS RECEIVED CODE		AS RETURNED CODE	
BIAS VOLTAGE (VDC):	8.6			DISCHARGE T.C. (sec):	3.4		
CALIBRATION PERFORMED AT	30	Lb-in MOUNTING TORQUE					

PRESSURE (psi)	SENSITIVITY (mV/psi)	PRESSURE (psi)	SENSITIVITY (mV/psi)
1000	5.23		

REMARKS: NONE

TEST EQUIPMENT LIST - CALIBRATION STATION # 5

DII #	MANUFACTURER	MODEL	SERIAL #	DESCRIPTION	CAL DATE	DUE DATE
256	KEITHLEY	179	22129	MULTIMETER	02/12/05	02/12/06
017	NICOLET	310	IAQ9406710	DIGITAL OSCILLOSCOPE	08/18/05	08/18/06
022	AMETEK / MANSFIELD	T-150	15010	DEAD WEIGHT TESTER	10/20/04	10/20/06

[1] AS RECEIVED / AS RETURNED CODES:
1 = IN TOLERANCE, NO ADJUSTMENTS
2 = IN TOLERANCE, BUT ADJUSTED
3 = OUT OF TOLERANCE < 5%
4 = OUT OF TOLERANCE > 5%
5 = REPAIR REQUIRED
6 = REPAIRED AND CALIBRATED
7 = UNIT NON-REPAIRABLE, RECOMMEND REPLACEMENT
8 = UNIT SERVICEABLE WITH CURRENT CALIBRATION DATA

[2] THIS CALIBRATION WAS PERFORMED PER MIL-STD-45662A, ANSI/NCSL Z540-1-1994, ISO 10012-1 AND IS TRACEABLE TO THE NIST THROUGH TEST REPORT NUMBER: 23936.001.
ESTIMATED UNCERTAINTY OF CALIBRATION: 2%.

CALIBRATION TECHNICIAN:	TEST DATE: 11/21/05
	RECALL DATE: 11/21/06

SPECIFICATIONS MODELS 2011V & 2011V1
DYNAMIC PRESSURE SENSOR

SPECIFICATION	VALUE	UNITS
PHYSICAL (BOTH MODELS)		
WEIGHT	13.0	GRAMS
SIZE (HEX X HEIGHT)	.375 X 1.88	INCHES
MOUNTING PROVISION	3/8-24 UNF-2A MALE THREAD	
CONNECTOR, AXIALLY MOUNTED AT TOP	10-32 UNF-2A MICRO-COAXIAL	
BODY/CONNECTOR MATERIAL	STAINLESS STEEL, HARDENED	17-4 PH
DIAPHRAGM MATERIAL	STAINLESS STEEL, ANNEALED	17-4 PH

PERFORMANCE

MODEL	2011V	2011V1	
SENSITIVITY, NOM.	5	1.66	mV/Psi
RANGE F.S. FOR +5 VOLTS OUT	1000	3000	Psi
MAXIMUM PRESSURE	2000	5000	Psi
MOUNTED RESONANT FREQUENCY, NOM.	130	130	kHz
MINIMUM RISE TIME OF INPUT PRESSURE PULSE	2	2	µSEC
EQUIV. ELECTRICAL NOISE FLOOR (RESOLUTION)	.009	.003	Psi
NON-LINEARITY (ZERO BASED BEST FIT ST.LINE) [1]	±1	±1	%F.S.
ACCELERATION SENSITIVITY, AXIAL DIRECTION	.02	.006	Psi/G
DISCHARGE TIME CONSTANT	4.0	4.0	SEC
LOWER -3db FREQUENCY	.04	.04	Hz

ENVIRONMENTAL (BOTH MODELS)		
MAXIMUM VIBRATION	1000	G's RMS
MAXIMUM SHOCK	3,000	G,' s PEAK
TEMPERATURE RANGE	-100 TO +250	°F
MAXIMUM FLASH TEMPERATURE AT DIAPHRAGM	+3000	°F
THERMAL COEFFICIENT OF SENSITIVITY	0.03	%/°F
ENVIRONMENTAL SEAL	HERMETIC	WELDED/GLASS TO METAL
ELECTRICAL (BOTH MODELS)		
EXCITATION (COMPLIANCE) VOLTAGE RANGE	+18 TO +30	VDC
EXCITATION CURRENT RANGE [2]	2 TO 20	mA
OUTPUT IMPEDANCE, NOM.	100	Ohms
OUTPUT BIAS VOLTAGE, NOM	+10	VDC
OUTPUT SIGNAL POLARITY FOR INCREASING PRESSURE	POSITIVE GOING	

SUPPLIED ACCESSORIES

MODEL 6606 SEAL, BRASS, 2 SUPPLIED.

NOTES:

[1] PERCENT FULL SCALE, ZERO BASED BEST FIT STRAIGHT LINE METHOD.
[2] FROM CONSTANT CURRENT TYPE POWER UNIT ONLY. THESE SENSORS **MUST NOT BE CONNECTED** TO A DC POWER SOURCE WITHOUT CURRENT LIMITING, 20 mA MAXIMUM.
3 A CALIBRATION CERTIFICATE TRACEABLE TO NIST IS SUPPLIED WITH EACH INSTRUMENT.

Appendix M: Kistler Piezotron Coupler Charge Amplifier Datasheet

Measure & Analyze - MCP

KISTLER
measure. analyze. innovate.

Piezotron™ Coupler

Type 5118B...

Versatile Voltage Mode Piezoelectric Sensor Power Supply/Coupler

A flexible, simple to use signal conditioner that provides excitation power, signal tailoring and acts as an interface between voltage mode piezoelectric sensors and measuring instruments.

Single channel unit powered by internal AA batteries or an AC/DC adaptor.

- Selectable gain and low pass, plug-in filters
- High pass filtering, panel selectable
- Monitor the condition of the sensors and cables
- Exclusive "Rapid Zero" feature
- AC, DC or battery powered
- Conforming to CE

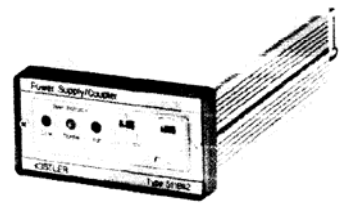

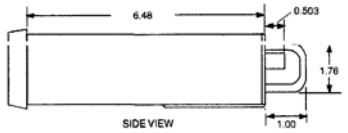

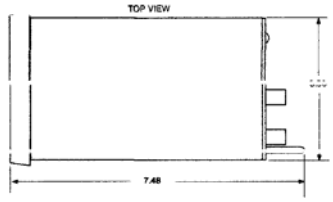

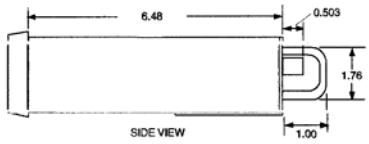

Description

The signal conditioner provides the constant current excitation required by low impedance, voltage mode sensors with built-in electronics (i.e. Piezotron , PiezoBeam™, K-Shear™, and Ceramic Shear) or for high impedance sensors with an external impedance converter. Sensor power is supplied by the same two-wire cable that provides the low impedance output signal. The 5118B2 decouples the DC bias voltage from the output signal and provides a 2mA constant current source which can also be factory adjusted between 2 to 18 mA. Bias indicators display the condition of the sensor and cable. Amplifier gains of 1x, 10x and 100x are selectable from a front panel switch. High-pass filter cutoff frequencies (-3dB) 0.006 and 0.03 Hz are also selectable by a switch on the front panel.

Plug-in, low pass filters are available to limit the frequency response of the amplifier. These low pass filters can be used to attenuate unwanted frequency and/or improve signal to noise ratio. Bias voltage is monitored and displayed with three front panel-mounted LEDs. Bias voltage in the range of 2 to 21V is normal and results in a green "OK" LED indication. Bias voltage below 2V or above 21V results in a red "LOW" or "HIGH" indication. A "LOW" generally indicates a short circuit in the cable or sensor while "HIGH" means an open circuit.

The coupler warns of a low battery audibly, with an intermittent chirping sound. Battery lifetime is about 12 hours at a sensor current of 2mA. Coupler power can be provided from three sources: four AA 1.5 volt batteries, AC-operated from a power line adaptor, or regulated DC source between 6 and 28VDC. A unique "Rapid Zero" feature, allows the coupler to be ready for taking measurements two seconds after powering. When changing gain or filter settings, the 5118B2 is ready to use in two seconds.

Application

The primary use for the 5118B2 is to provide excitation power and signal tailoring for low impedance, voltage mode piezoelectric pressure, force and acceleration sensors. Its small size and rugged construction provides an excellent portable measurement system both in the laboratory or in the field.

000-331a-05.03 (K12.5118)

KISTLER
measure. analyze. innovate.

Technical Data

Type		Units	5118
INPUT:			
Sensor Supply Current		mA	2 (1)
Signal Voltage		V	±5
Gain			1x, 10x, 100x
Bandwidth:			
High Pass (switch selectable)			
Frequency	–3db	Hz	0.03, 0.006
	–5db	Hz	0.10, 0.02
Time Constant		s	5, 25
Low Pass (no filter; @ ± 5V out)			
Gain 1x	–3db	kHz	>100
	–5%	kHz	>40
Gain 10x	–3db	kHz	>100
	–5%	kHz	>20
Gain 100x	–3db	kHz	>30
	–5%	kHz	>12
Noise (without low pass-filter):			
Gain 1x, 10x		mVrms	<2
Gain 100x		mVrms	<5
Output Impedance max.		Ω	100
Voltage Swing max.		V	±10
Connectors input/output		type	BNC neg.
Connector power		type	2.1 x 5.5 mm concentric
Internal Battery (4 each)		type	1.5V AA, alkaline
Temperature Range Operating (alkaline batteries)		°F	–5 ... 125
Storage (w/o batteries)		°F	–20 ...140
External Voltage Source (2)		VDC	6 ... 28
Weight		lb	1.1

(1) Sensor current can be set at factory for any current in the range of 2 ... 18 mA
(2) Optional AC adapter available

1 g = 9.80665 m/s², 1 inch = 25.4 mm, 1 gram = 0.03527 oz, 1 lbf-in = 0.1129 Nm

Mounting

The 5118B2 is a single unit piezoelectric sensor power supply and signal conditioner housed in a extruded aluminum case. It is primarily intended for laboratory bench top use. For permanent installations, the unit can be panel mounted using optional adapters

Ordering Information

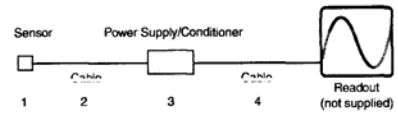

sp = specify cable length in meters

1 - Sensor	low impedance, voltage mode
2 - 1761Bsp	sensor cable, 10-32 pos. to BNC pos.
3 - 5118B2	power/supply coupler
4 - 1511sp	output cable. BNC pos. to BNC pos.

Optional Accessories

5752	power adaptor, 115 VAC, 60 Hz
5757	power adaptor, 230 VAC, 50 Hz, CE certified
5326A	low-pass filter, cut-off frequency; in Hz (10, 20, 50, 100, 200, or 500)
5327A...	low-pass filter, cut-off frequency; in kHz (1, 2, 5, 10, 20)
5324A...	high-pass filter, cut-off frequency; in Hz (1, 10, 100)
5702	panel mounting kit
704-2068-001	power cable (6ft.) with mating plug to pigtails

000-331a-05.0. (K12.5118

Appendix N: Data Acquisition Unit Electric Diagram

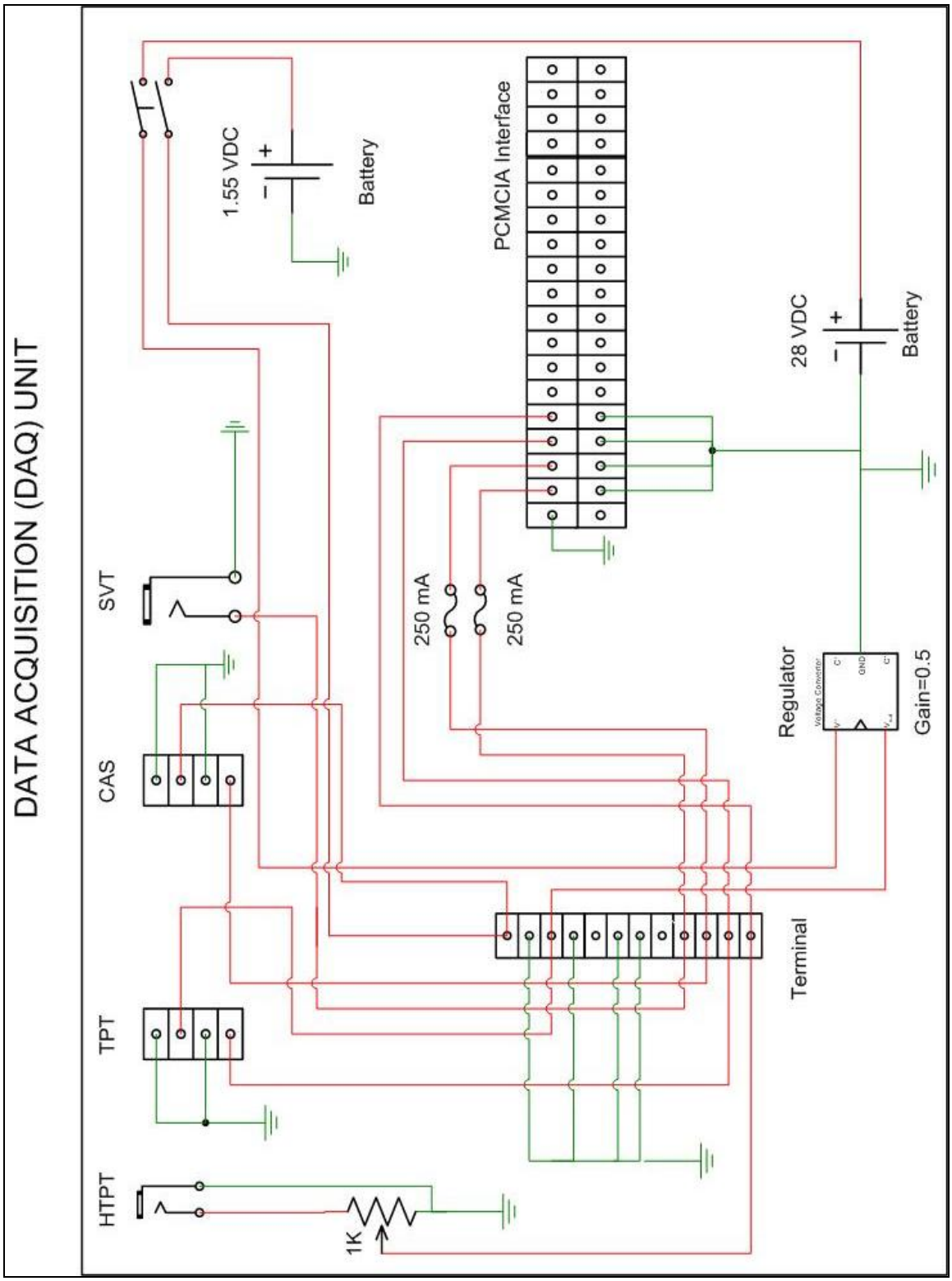

Appendix O: Omega Data Acquisition Card Datasheet

DAQP-208 12 Bit A/D & D/A
PCMCIA Data Acquisition Adaptor

- 12-bit Resolution
- 8 Single Ended or 4 Differential A/D Channels, Expandable to 128
- Two Analog Output Channels
- Four Digital I/O Channels
- 16-bit Timer/Counter with Auto-Reload and Readout Latch
- 100 kHz Sampling Rate
- Bipolar Input Range of ±10 Volts, with Standard Programmable Gain of 1,2,4 and 8
- 1, 10, 100, 1000 High Gain Option
- 2K Data FIFO
- Programmable Scan FIFO with 2048 Entries
- Compatible with SignalPro Series Signal Conditioning Modules
- Drivers Supplied for Dasylab and LabVIEW
- DAQDRIVE and DaqEZ Software Included

Model DAQP-208

The DAQP-208 is a Type II PCMCIA data acquisition card with 4 differential or 8 single ended 12- bit A/D input channels (expandable to 128), with a maximum sampling rate of 100 kHz, and programmable gains of 1,2,4, or 8, which provide ranges of ±1.25 V, ±2.5 V, ±5 V, to ±10 V. A high gain option is also available providing gains of 1, 10, 100 or 1000, for ranges of ±0.01 V, ±0.1 V, ±1 V, to ±10 V The DAQP-208 is also equipped with two 12-bit D/A output channels. The outputs can be updated individually when writing to the corresponding D/A port, or simultaneously when a synchronization signal comes. The DAQP-208 has a 2 K data FIFO which will significantly reduce CPU overhead, and a scan FIFO of 2048 entries, each of which can be specified with an input channel and its associated gain. It has a selectable scan speed of 10 µs to 40 µs per channel. Data acquisition may be initiated by a trigger signal or by using the DAQP-208's pre-trigger capability.

The DAQP-208 has a 24-bit auto-reload pacer clock which generates accurate sampling rates from 0.006 Hz to 100k Hz using an internal or external clock source. The pacer clock is actually a 24-bit auto-reload frequency divider. It contains a 24-bit divisor register, a 24-bit counter, and internal clock pre-scaler and a clock source multiplexer. The DAQP-208 also has a 16-bit timer/counter with an auto-reload and readout latch which provides independent timing for the D/A channels, and operates with internal or external clock source and gate controls.

The DAQP-208 includes OMEGA's DAQDRIVE software driver and DaqEZ user friendly data acquisition application software package. All necessary software is included to install and configure the DAQP-208 for use with Windows 95/98/NT/2000.

Signal Conditioning/Expansion

The DAQP-208 is compatible with the SignalPro line of signal conditioners. These signal conditioners allow the DAQP-208 to read most process sensors and provides channel expansion up to 256 inputs. See the H section of the hand book for detailed information on the SignalPro line.

Software OS Support:

Windows 95/98/NT/2000. DAQDRIVE software drivers support numerous Windows programming languages, including Microsoft C/C++, Borland C/C++ and Visual Basic 5.0 or higher (32 bit version). As part of the DAQDRIVE package, drivers are also included for third-party software packages including DasyLab and LabVIEW.

For implementing a fully integrated data acquisition system, OMEGA's DaqEZ user friendly application software package is included free, and will in many cases be all that is needed.

Appendix P: Microchip Pic16F72 Chip Diagram

MICROCHIP

PIC16F72

28-Pin, 8-Bit CMOS FLASH MCU with A/D Converter

Device Included:

- PIC16F72

High Performance RISC CPU:

- Only 35 single word instructions to learn
- All single cycle instructions except for program branches, which are two-cycle
- Operating speed: DC - 20 MHz clock input
  DC - 200 ns instruction cycle
- 2K x 14 words of Program Memory, 128 x 8 bytes of Data Memory (RAM)
- Pinout compatible to PIC16C72/72A and PIC16F872
- Interrupt capability
- Eight-level deep hardware stack
- Direct, Indirect and Relative Addressing modes

Peripheral Features:

- High Sink/Source Current: 25 mA
- Timer0: 8-bit timer/counter with 8-bit prescaler
- Timer1: 16-bit timer/counter with prescaler, can be incremented during SLEEP via external crystal/clock
- Timer2: 8-bit timer/counter with 8-bit period register, prescaler and postscaler
- Capture, Compare, PWM (CCP) module
  - Capture is 16-bit, max. resolution is 12.5 ns
  - Compare is 16-bit, max. resolution is 200 ns
  - PWM max. resolution is 10-bit
- 8-bit, 5-channel analog-to-digital converter
- Synchronous Serial Port (SSP) with SPI™ (Master/Slave) and I^2C™ (Slave)
- Brown-out detection circuitry for Brown-out Reset (BOR)

CMOS Technology:

- Low power, high speed CMOS FLASH technology
- Fully static design
- Wide operating voltage range: 2.0V to 5.5V
- Industrial temperature range
- Low power consumption:
  - < 0.6 mA typical @ 3V, 4 MHz
  - 20 µA typical @ 3V, 32 kHz
  - < 1 µA typical standby current

Pin Diagrams

PDIP, SOIC, SSOP

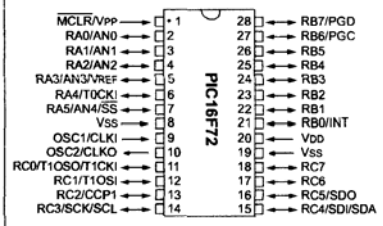

QFN

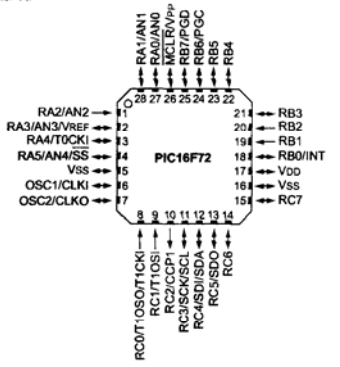

Special Microcontroller Features:

- 1,000 erase/write cycle FLASH program memory typical
- Power-on Reset (POR), Power-up Timer (PWRT) and Oscillator Start-up Timer (OST)
- Watchdog Timer (WDT) with its own on-chip RC oscillator for reliable operation
- Programmable code protection
- Power saving SLEEP mode
- Selectable oscillator options
- In-Circuit Serial Programming™ (ICSP™) via 2 pins
- Processor read access to program memory

Appendix Q: Microcontroller Unit Program

C:\MyProjectspic\cibail.bas

```
        'Modified June 27, 2005

'Set up port A for ADC
        DEFINE ADC_BITS 8        'Set the number of bits in result.
        DEFINE ADC_CLOCK 3       'Set Clock Source (3=RC in ADC)
        DEFINE ADC_SAMPLEUS 50   'Set sampling time in microseconds
        A0 VAR BYTE              'Define A0 varible as byte
        TRISA=255                'Set all PORTA to input
        ADCON1=0                 'PORTA is analog

'Define Variables

        A2DDUMY VAR WORD         'Define ADC Dummy variable.
        DEL1 VAR WORD            'Define delay time in msec from ignition trigger
        DEL2 VAR WORD            'Define delay time in msec from ignition trigger
        butloop VAR byte         'Define start button parameter variable

Starter:Low 3                    'Oscilloscope trigger low
        Low 4                    'Relay 1 off  Ignition Coil power control
        Low 5                    'Relay 2 off  Solenoid to inject cold air.
        Low 6                    'Relay 3 off  Solenoid to inject hot air.

Potloop:
        ADCIN 0,A2DDUMY      'Read in the potentiometer 1 setting.
        DEL1=(255-A2DDUMY)/4
        ADCIN 1,A2DDUMY      'Read in the potentiometer 2 setting.
        DEL2=(255-A2DDUMY)/4
        Button 0,0,255,1,butloop,1,Igloop
        Goto Potloop
Igloop: ADCIN 3,A2DDUMY      'Loop until ignition is sensed.
        IF A2DDUMY<127 THEN Igloop
        High 4           'Open ignition coil and hold when start trigger received and after an
ignition.
        Pause DEL1       'Time delay until air injection,
        High 3           'Trigger Oscilloscope
        High 5           'Inject Cold Air
        Pause DEL2       'Time to hold open air injection solenoid.
        Low 5            'Close Cold Air Injection solenoid
        Pause 2000
        Goto Starter

        END
```

1

Appendix R: Sample Calculations Air-Fuel and Equivalence Ratios

	Intake Temperature= 70 °F			Intake Temperature= 250 °F		
	Fuel Level (F.L)			Fuel Level (F.L)		
Parameters	**0.5 in**	**1 in**	**1.5 in**	**0.5 in**	**1 in**	**1.5 in**
Actual Pressure (in Hg)	30.46	30.46	30.46	30.46	30.46	30.46
Reference Pressure (psi)	14.7	14.7	14.7	14.7	14.7	14.7
Actual Temperature (70 °F)	70	70	70	70	70	70
Reference Temperature (°F)	59	59	59	59	59	59
Density Gasoline at 70 °F (Kg/L)	0.75	0.75	0.75	0.75	0.75	0.75
Volume Gasoline (mL)	50	50	50	50	50	50
Time Recorded Gasoline (sec)	106.34	139.8	155.4	145.67	188.23	210.45
Density Air at 70 F (Kg/m^3)	1.205	1.205	1.205	0.88	0.88	0.88
Air Flow Rate (SCFM)	7	7	7	7	7	7
Time Recorded Air (sec)	60	60	60	60	60	60
Calculations						
Actual Pressure (psi)	14.97	14.97	14.97	14.97	14.97	14.97
Air Flow Rate (CFM)	6.99	6.99	6.99	6.99	6.99	6.99
Mass of Gasoline (Kg)	0.0375	0.0375	0.0375	0.0375	0.0375	0.0375
Mass Flow Rate of Gasoline (Kg/hr)	1.27	0.97	0.87	0.93	0.72	0.64
Mass of Air (Kg)	0.24	0.24	0.24	0.17	0.17	0.17
Mass Flow Rate of Air (Kg/hr)	14.33	14.33	14.33	10.47	10.47	10.47
Actual Air-Fuel Ratio (A/F)	11.29	14.84	16.50	11.29	14.59	16.32
Stoichiometric Air-Fuel Ratio (A/F)	14.70	14.70	14.70	14.70	14.70	14.70
Equivalence Ratio	1.30	0.99	0.89	1.30	1.01	0.90
CIBAI Air-Fuel Ratio	**23**	**30**	**33**	**23**	**29**	**33**
CIBAI Equivalence Ratio	**0.65**	**0.50**	**0.45**	**0.65**	**0.50**	**0.45**

Appendix S: Sample Estimated In-Cylinder Bulk Temperature

Engine Operating Conditions

Cycle Duration (sec)	0.131
Crank Angle Rate (dtheta/dt)	5496.18
RPM	916.03
Crank Angle Differential (dtheta CA)	0.55
Sampling Rate (Hertz)	10000
Air Flow Rate (SCFM)	7
Intake Temperature (K)	294
Air Gas Constant (KJ/kg-K)	0.287
Barometric Pressure (in Hg)	30.14
Barometric Pressure (psia)	14.81
Exhaust Temperature (K)	588.56

Engine Specifications

Displacement Volume (cc)	612.5
Clearance Volume (cc)	111.36
Plumbing Volume (cc)	3.00
Compression Ratio (C.R)	6.5
Adjusted Compression Ratio (C.R)	6.36
Stroke (in)	4.5
Crank Offset (in)	2.25
Bore (in)	3.25

Calculation Volumetric Efficiency

Displacement Volume (in^3)	37.33
Total Volume (in^3)	44.31
Actual Volume Clearance (in^3)	6.98
Cylinder Mass Before Injection (Kg)	0.00052
Volumetric Efficiency	70.7%

Calculation Rate of Injection (dm/dt)

Air Heater Volume (cc)	33
Injector Ball Valve Check Cracking Pressure (psi)	514.7
Air Heater Pressure Before Injection (psi)	814.7
Average Pressure (pa)	4582974
Mass Heater Before Injection (kg)	0.0011
Mass Heater Left After Injection (kg)	0.0007
Mass Injected (kg)	0.0004
Delta t Injected (sec)	0.012
A* (sq. m)	0.00000441
D* (mm)	2.37
dm/dt (kg/s)	3.367E-06

Estimated In-Cylinder Temperature

Start Injection (CA)	340.45
Selected Crank Angle (CA)	400.95
Pressure at CA (Psia)	342.47
Volume at CA (in^3)	12.45
Mass Injected (Kg)	3.703E-04
Cylinder Mass After Injection at CA (Kg)	0.0009
Estimated In-Cylinder Temperature (K)	1866.9